The Optimisation of Flexible Impact-Protection Systems for Varying Strain Rates and Energies.

DANIEL JAMES PLANT

March 2014

Mechanics of Materials
Department of Mechanical Engineering
Imperial College London

A thesis submitted for the degree of Doctor of Philosophy of
Imperial College London and the Diploma of Imperial College

Declaration of Originality:

All of the work in the thesis is the original work of Daniel James Plant. All work is referenced accordingly.

Copyright Declaration:

Abstract

The need for smarter and active, energy absorbing systems designed especially for human protection applications has sparked interest in highly strain rate sensitive compounds. This thesis describes the iterative design, development and optimisation of a novel form of energy absorbing, body worn protection.

The original contribution to knowledge is the development of a novel strain rate sensitive protection system incorporating synergetic internal architecture. Co-continuous blends of silicone based dilatant and thermoplastic elastomer have been developed through a recursive design process to develop a new material specifically optimised for body worn protection.

Failure mechanisms were analysed, and from these results techniques have been developed to mitigate internal fracture mechanisms. This enabled the development of a strain rate sensitive material utilised with an internal architecture.

The novel material properties were examined and developed using monolithic samples, tested at a variety of energies, speed and environmental conditions. Methods for designing and developing auxetic structures that work synergistically with the new material have been developed.

The novel system has also been combined with textiles, and the merit of this combination explored.

An improvement in performance has been validated, as well as a design improvement through being able to attach parts directly to garments.

The resulting impact protectors are applicable over a range of strain rates. Systems have been designed to incorporate this novel technology in pre-production prototypes in three selected market areas, which typify low, medium and high impact speeds. The work also explores the systems ability

to manage multiple impacts at the same location with a surprisingly low loss in performance, effectively making a protector that can withstand repeat impacts.

This work has contributed to the methods previously used in testing personal protective equipment. The techniques developed in this work have enabled new revision of these PPE standards, as well as directly contributing to two new standards.

Acknowledgements

Thanks for always being there for the business support line over the last decade.

Lastly, I must thank my wife, Vashti, for putting up with the multitude of strange chemicals and silicones that all to often found there way onto the kitchen table and for always being there. Thank you

Contents

List of Figures

List of Tables

List of Published works and papers

Papers

Hip protectors: recommendations for biomechanical testing--an international consensus statement (part I). Osteoporosis international vol. 20 (12) p. 1977-88

Hip protectors: recommendations for conducting clinical trials--an international consensus statement (part II). Osteoporosis vol. 21 (1) p. 1-10

Standards

Efficiency of Head Protection Equipment for two mainstream sports – a comparison.
Helmet Performance and Design. Imperial College London 15th February 2013 p.11-1
Helmet Performance and Design Conference Presentation. Imperial College London 15th February 2013.
Use of Dilatant in Ballistics poster competition winner The Royal British Legion Centre for Blast Injury Studies. Network Event. Friday 21st September 2012

BSI 8575 Medical Hip protectors –final draft.

BS 6366:2011 Specification for studs for rugby football boots.

BS EN 1621-2:2014 Motorcyclists' protective clothing against mechanical impact. Motorcyclists' back protectors. Requirements and test methods
BS EN 1621-1:2012
Motorcyclists' protective clothing against mechanical impact. Motorcyclists' limb joint impact protectors. Requirements and test methods

Patents

Energy absorbing system :EP2361023A2, EP2361023B1, US20120021167, WO2010076257A2
Energy absorbing protective member :CA2373535A1, DE60010069D1, DE60010069T2
Flexible energy absorbing material and methods of manufacture thereof :EP1178743A1, EP1178743B1, US6913802, WO2000069293A1, DE60236548D1, EP1489934A2, EP1489934B1, US7608314, US20040171321, WO2003022085A2, WO2003022085A3

Glossary

Energy Shunting -An energy shunting protector attempts to distribute the force over a large area reducing the peak pressure to the wearer, less energy is absorbed at the point of impact.

Energy Absorbing - The energy absorbing systems look to ameliorate the impact by absorbing the impact energy, utilising energy absorbing materials and structures.

Reticulated Foam - Reticulation is a post process that removes the window membranes of the cell, leaving only the skeletal structure intact.

Bingham Plastic. A material that behaves as a rigid body at low stress, but flows as a viscous fluid at high stress.

Dilatant Fluids: The viscosity increases as the shear rate increases

IMDS - Injection mouldable dilatant silicone. New material developed to allow dilatant silicone to be injection mouldable at ratios of up to 90% Dilatant Silicone

1 <u>Introduction.</u>

Body armour has been in use in one form or another since biblical times. Classically, armour was made from hard materials such as metal as this was able to resist the high-energy impacts used on medieval battlefields. However, soft armour, typically made from leather, was also used where greater flexibility was needed. In modern times though, ballistic protection has become an important application and other uses of body armour have also developed; specifically, the protection against orthopaedic injury in vulnerable patients and in sportswear [1]. In all of these applications, just as on the battlefields of the past, body armour must meet seemingly conflicting requirements. On the one hand it must resist impact and lower the force applied to the wearer to acceptable levels. On the other hand it must be light and comfortable – specifically, armour needs to be flexible. Developing a novel of body armour that is flexible, light and able to resist high impact loads is the subject of this thesis.

Elastomeric foam polymers are the most common energy absorbing materials used in flexible body-worn sporting applications [2]. Under impact loading, the foam initially compresses through an elastic region and then follows a plateau to final densification [3], as shown in Figure 1 below. Catastrophic failure ultimately occurs in the cell walls, and the material fractures. When the cell walls fail the elastomeric foam is free to move out of the high impact zone, leaving no material in the area where it is most needed. The materials fail and moving away from the impact site ultimately give poor high load performance.
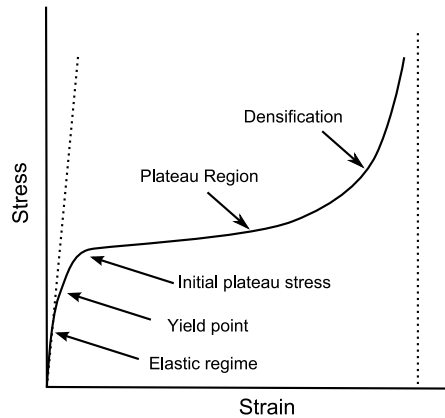
Figure 1 Typical stress versus strain curve of a foam material.

One way to improve this limit of performance is to use thicker layers of material, but there are practical limitations. A second method of increasing performance of elastomeric foam materials is to make the cell walls thicker (reticulation), or to add more cell walls. There is also a practical limitation to this methodology as it increases mass and also reduces flexibility. An increase in performance can be obtained by changing the polymer composition, but the same trends are still observed for densification and cell wall strength.

More recently, shear thickening fluids (STF) have generated much interest in the area of flexible body-worn protection, especially within the military/armed forces [4]. They have been widely studied because of their unique ability to change from a low to a high viscosity fluid under impact loading. Most recent research work has been on the effects of STF coatings applied to ballistic panels [4], and STF combined fluid filled reticulated foams [5].

Commercialisation of these STF systems has not occurred, predominantly due to difficulties in manufacture, and also the necessity for the STF to be contained within the foam, usually sealed in a polymeric container. This has required complicated sealing processes and reduced the breathability of the final products – a clear drawback for body-worn applications. The long term durability of such a system has not yet been proven.

There has also been some interest in using silicone dilatant compounds in conjunction with Polyurethane (PU) foams. These materials have a similar behaviour to STF, but are primarily modelled on silicone based products that are currently commercially available. These have been compounded with PU foams in low volume fractions (<5%), with some success. The underlying fracture mechanics for foams still limits the system's ultimate performance. It is difficult to see a true impact performance benefit with such a small volume fraction as that of the parent PU foam, and there is little published experimental data.

Auxetic foams have also shown some benefit for flexible body-worn protection. These materials tackle the issue of material moving away from the impact site with a macro scale negative Poisson's ratio. Here, performance is improved by the negative Poisson's ratio, effectively dragging more material into the impact site. Performance improvement can be shown, but the production methods are complex and no known commercial examples have been successfully commercialised. Once again, there is little published experimental data.

The benefit of using a silicone based dilatant or strain rate sensitive material is appealing [6], as they are stable at different temperatures, easy to produce in quantity, self-amalgamating, and have been in commercial use since 1960.

Lastly, additional constraints should be considered when designing an efficient system for flexible body-worn protection. In fact some requirements may not be directly related to the level of protection - for example, weight requirements, breathability, manufacturability, and the comfort and flexibility of the final product [1].

1.1.1 Aims

In this work, we explore methods for utilising silicone dilatants as part of a novel energy absorbing system.

1. The primary aim was to determine whether it was possible to develop a highly strain rate sensitive material incorporating silicone based dilatants and thermo plastic elastomer that could be used as 'soft armour' to protect the human body against impact.

2. The secondary aim was to determine if a co-continuous blend could be designed that would be suited to the injection moulding process; allowing repetitive reproduction of samples and parts.

3. The third aim was to establish whether different architecture and internal geometries could be designed and developed to further the performance of the highly strain rate sensitive material. Of particular interest were auxetic structures, and exploring the benefit from designing an anisotropic architecture that could work in synergy with a strain rate sensitive material.

4. The final aim was to establish if the strain rate sensitive materials could be combined with a tensile layer and form a basic composite that could further benefit performance, but also lead to an improved method of incorporating such armour into everyday clothing.

1.1.2 Objectives

The objectives for this work are detailed below, each objective is reviewed as a chapters of this thesis.

Chapter 2 is a high level review of literature that is relevant to this research. This section introduces strain rate sensitive materials in the form of shear thickening fluids. Internal foamed structures are reviewed along side auxetic structures, with examples of documented uses in the field of personal protective equipment (PPE).

Chapter 3 introduces the equations that can be used to review impact mechanics and the fundamental physics behind them, in order to develop an understanding of how these principles could be applied to body-worn protection. The forces and loading that a human body might be able to withstand are discussed. Typical industry standards and techniques are reviewed in this section and an introduction into transmitted force versus time data and how best to practically measure this data. The type of test data collected from these standards is considered; and reviewed in light of how an optimised material might behave using these techniques.

Current test methods for Conformité Européenne (CE) certification were reviewed along with the relevant British Standards Institute (BSI) standards. A set of techniques and standardised tests have been developed that have been used to rank and quantify the protective properties of armour systems which are used to help develop and design novel energy absorbing materials of this thesis. Finally, the concept of developing a novel strain rate sensitive material is introduced.

The development of a specific test technique is covered in Chapter 4. In order to conduct this work, a highly accurate drop tower was designed and built, that exceeds the specifications of traditional certification standards. During this research over 8000 impact tests were carried out. This machine was utilised in the development of a number of new standards.

Chapter 5 looks to validate the second aim of the thesis, through the design and development of homogeneous blends, which can be easily processed. Using the developed techniques of this thesis samples are tested at multiple impact speeds and energies as well as a variety of environmental conditions. This chapter is split into two sections; the first is a wide screen used to validate the first and second aim of this work, and the second section is a further round of samples to optimise the co-continuous morphologies with different polymer blends. This is an iterative approach taking the merits of the first set of experiments and further developing these in the second.

The third aim of designing and developing the internal architecture through simple changes in geometry and addition of a simple tensile layer to make a primitive composite is explored as a final piece of Chapter 5.

The best ranking materials were then further developed in Chapter 6 with more advanced architecture. This development path included the design of internal geometries and auxetic structures. Further development of designs incorporated textiles to form a composite protection system. Research continued to develop and optimise geometry using these standardised techniques at different material thicknesses for two different loading conditions (point impact and Hertzian line impact). Layering, density and thickness of these auxetic structures and composite samples are reviewed, with a view to validating the concept hypothesised in Chapter 3 and answer the third aim of the project, to produce a synergy between an auxetic structure and an active material.

Chapter 7 looks to optimise these novel systems at three different strain rates. Applications were selected at low, medium and high strain rate, with a specific commercial focus. Design and development of these energy absorbing systems are reviewed and validated against test methods typically used for personal protective equipment at these strain rates.

For the low strain rate design and development, the focus of medical hip protector was chosen as the end application area. The research contributed to developing a new biofidelic test method for medical hip protection, which contributed to a BSI draft standard. Optimisation of the co-continuous blend and auxetic geometry for this specific application, at lower strain rate was developed and validated against existing products.

The medium strain application selected was to design and develop finished parts for sporting equipment particularly the motorcycle PPE industry. This area continued the development of the samples generated in chapter 6 at a medium strain rate and follows the design from the samples of

chapter 6 to finished products. These have since been manufactured and externally accredited by UKAS approved test house as part of the validation at this strain rate.

Ballistics applications were chosen for the high strain rate application. A modified gas gun was developed to test systems for energy absorption at high speed using a 9mm round. Existing ballistic packs were impregnated in strain rate sensitive materials and the effects on back face signature were measured. Composite panels were developed for improving energy dissipation. These were compared against pack area density of a control pack. Finally a hybrid composite panel was developed.

1.1.3 Test Strain rates, Energy Density and Apparatus.

The final task was to see if the system could be optimised over a speed range and Impact energy density of two magnitudes, below is a overview of these test speeds, impact energy density and strain rate for these three chosen areas, and a brief description of which equipments was used.

The low strain rate application, as a medical hip protector device, has an impact speed in the range 1-2.3m/s, and a strain rate of 10^2 s^{-1}. The medium rate is for sports protection, specifically motorcycle protection with an impact speed of between 5-10 m/s, with a strain rate of 10^3 s^{-1} and the high rate area is ballistic protection at 100m/s and over, giving a strain rate of 10^4 s^{-1}. These impact speeds typically increase by an order of magnitude between the application areas and provide a broad scope and range for these focused research areas.

Experiments were completed on the drop tower for the low and medium strain rate developments. The impact kinetic energies for these tests have ranged from 10^2 to 10^5 J/m^3; The Hip fractures standard is at about 3 x 10^3 J/m^3; while motorcycle sporting goods PPE protection is 6x10^6 J/m^3 ; for comparison the impact energies resultant from a football tackle are reported to be around 5x10^4 J/m^3.

For the high strain rate development experiments a pneumatic gas gun was used. The samples were subjected to tests using a 9mm full metal jacket at speed of 360m/s. The impact energy densities from these tests were in the region of 6×10^6 J/m^3.

2 <u>Literature Review</u>

2.1.1 *Personal Protective Equipment (PPE).*

There is a wide range of equipment for protecting the user against the rigours of everyday working life. A plethora of products exist for protecting all parts of the human body.

The British Standards Institute controls the standards for many of these products in the UK, and the views expounded by British Standards feed into Europe through the European Committee for Standardisation (CEN). The standards are split into areas of expertise according to the threat and also the body area. Technical Committee 192 TC192 covers all body worn PPE and sporting goods in the UK and Europe, except for helmets and footwear.

Whilst conducting his PhD research, the writer became a technical member of TC192 and eventually Conveyor of the Technical Committee, reporting into Europe for all PPE and sporting goods. There are many outcomes from this work, but BSI 6366 [7] was redrafted and updated, the martial arts standard EN13277 [8] was set up and the writer pursued an active role in future development of motorcycle standards, namely EN1621-1 [9]and EN1621-2 [10]. The Author also took an active role in developing a new standard for hip protection for the elderly, which is now in draft form and out for public comment. Technical advice was also provided for two Home Office standards (HOSBD).

The testing methodology in this research was based on EN1621-1 and EN1621-2 tests and the newly developed Medical Device Hip Protector test. These standards are not simplistic and are being used to advance these products globally.

2.1.2 *Materials and Methodologies for Armour.*

There are two main methodologies for protecting the human body. These are typically based on the energy shunting or the energy absorbing method, or more recently a mixture of the two. [1]

Typical hard-shelled devices use the energy shunting method [11]. Here a hard inflexible shell is placed above a soft comfort foam. The hard shell spreads the load over a large area in an attempt to ensure that the pressure is evenly distributed as far as possible. This load spreading is intended to alleviate the peak pressure that causes damage to the skin's surface and also to direct forces away from critical areas. An energy shunting protector attempts to distribute the force over a large area reducing the peak pressure to the wearer, less energy is absorbed at the point of impact.

These products are typically 'one size fits all' and do not really adapt to body movement. Other major limitations are that these are usually non breathable and uncomfortable to wear, especially in the highly flexibly joint areas of the knee and elbow.

The energy absorbing systems look to ameliorate the impact by absorbing the impact energy, utilising energy absorbing materials and structures. There are a number of common protectors that use EPS and these are typically used in cycling helmets. These are invariably of single event usage as is the case with European bicycle helmets.

There are also soft protectors that use Polypropylene (PP) and Polyethylene (PE) foams. These can be flexible and have multi hit capability, such as boxing helmets and gloves and also karate body protectors, but are often not suitable for higher energy impacts.

There are many other materials that can be used to absorb energy in different ways, such as the good use of honeycombed structures that crush to absorb significant energy. Honeycomb structures are very good at absorbing the energy of a single impact event and are also breathable, they are typically used in conjunction with a load spreader. The most commonly used materials are polymers such as PP honeycomb or thin walled aluminium honeycomb [12]. In addition, a combination of energy shunting and energy absorbing systems are sometimes deployed.

There are many foam materials that have been used in energy absorbing pads; open cell, closed cell reticulated, and re-entrant, to name but a few. These are manufactured from a multitude of materials but Polyurethane (PU) is the most common in body worn protection.

Foams and cellular structures can be engineered to crush at an almost constant force, which is seen as a plateau region on the 'stress strain curve' for the material. The limitations of foam systems are that ultimately they bottom out and the materials start to fracture at the impact site. In this event there is no material left to absorb any energy, and so foams and cellular structures are not very good when loaded over their design point i.e. in an over-load situation.

The EPS systems can absorb a great deal of energy for a single impact, but for high energy impacts such as cycle helmets they are not flexible [12]. For lower energy impacts, they do not start to crush, absorbing very little energy, and not reaching the plateau stress.

Dual density foams are now being deployed where the higher density foam is near the external surface and the lower density (more comfortable foam) is adjacent to the wearer. In a dual system like this the harder foam almost acts as a load spreading device [13].

2.2   Dilatants and Shear Thickening Fluids (STFs).

An interesting category of fluids are those called **Non-Newtonian Fluids**. These substances, unlike their counterpart and namesake, Newtonian Fluids, do not possess viscosities that are of a single-value constant. A fluid is said to be Newtonian if the viscous stresses that arise from its flow, at every point, are proportional to the strain rate at a constant temperature [14].

The word dilatant has many different meanings and is frequently used arbitrarily.

Some published definitions:

Dilatant is an Adjective:

'Increasing in viscosity and setting to a solid as a result of deformation by expansion, pressure, or agitation', is an early description from the Encyclopaedia Britannica after its first known use in 1885. 'Encyclopaedia Britannica', published in 1885.

'A dilatant material (also termed 'shear-thickening') is one in which viscosity increases with the rate of shear', comes from 'An Introduction to Rheology' published in 1989 by Howard A. Barnes, John Fletcher Hutton, Kenneth Walters [15].

'Dilatant Fluids: The viscosity increases as the shear rate increases' as described more recently, in 'Basic Orthopaedic Sciences' written by Ramachandran in 2006 [16].

For Newtonian fluids, the viscosity is a constant that usually only varies with temperature and pressure, a viscosity versus shear rate relationship can been seen in

Figure 2 for Polyethylene glycol (PEG) with four different molecular lengths. Fluids whose shear stress does not vary linearly with deformation or shear rate are called non-Newtonian fluids. There are shear thinning and shear thickening fluids and in recent publications it has transpired that these fluids are actually both, shear thinning at some lower strain rates and shear thickening at higher rates [17][18][19].
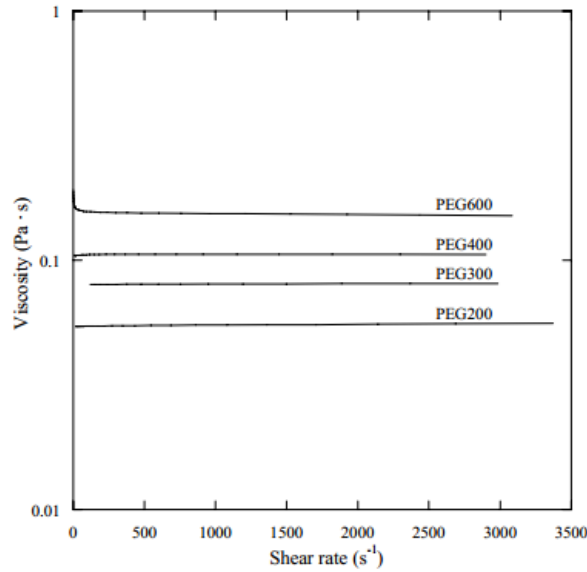
Figure 2 Viscosity as a function of shear rate for PEGs of various molecular weights [19]

2.2.1   The shear-thickening non-Newtonian liquid

It is possible that the very act of deforming a material can cause rearrangement of its microstructure, such that the resistance to flow increases with shear rate. Typical examples of the shear-thickening phenomenon are given in Figure 3. It can be observed that the shear-thickening region extends over only about a decade of shear rate [15]. The common misconception which causes confusion, and which most literature fails to mention, is that in almost all known cases of shear-thickening, there is a region of shear-thinning at lower shear rates. This causes unusual rheological behaviour, as can be seen in Figure 3. This shows viscosity verses shear rates at different fill fractions, expressed as the ratio of solid over solvent. The suspension that gives the largest change in increasing shear rate has a particle loading of 46%, and typically very high volume fractions give the largest change in viscosity with shear rate. The viscosity of this suspension is initially large at over 10^4 Pa·s and falls to 10 Pa·s as the shear rate approaches 10s^{-1}. This actually is shear thinning. Then the viscosity rapidly increases, as shown by the 0.46 curve in Figure 3. A better description for these materials therefore would be 'non-Newtonian'. This particular one is shear thinning and then highly shear thickening.

13
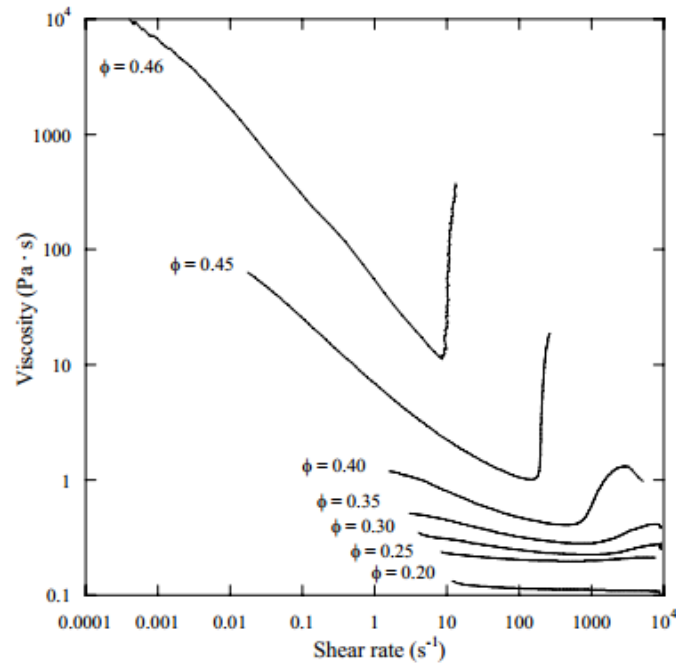
Figure 3 Viscosity as a function of shear rate for a STF of 2:1 aspect ratio CaCO$_3$ STF at various particle loadings[19].

There are many common materials that exhibit this behaviour, and most authorities refer only to the shear thickening phenomenon found for:

- Borosiloxane
- Silica-glycol blends
- Corn starch & water
- Quicksand
- Soil, rocks, geo-materials

The graph in Figure 4 will give the reader an idea how various non-Newtonian fluids behave compared to Newtonian fluids, in very simple ideal terms. In more recent online based literature, the axes are inverted and this can lead to further confusion [20]. It is more helpful to plot this as shown in Figure 4, with shear rate on the x-axis and shear stress on the y-axis, as this can be more easily compared with common literature on these materials.
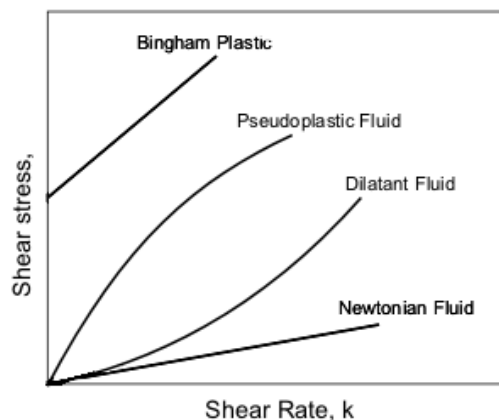
Figure 4 Behaviour of various fluids.

Much has been written about printing inks as dilatants, and most of the research in this field was carried out in the late 20th century, concerned with the rheology of printing inks and rheology of pastes and paints.

In the past decade most research in this field has been carried out to look at improved body armour, utilising shear thickening fluids. Wagner describes the use of a shear thickening fluid (STF), primarily as a colloidal shear thickening fluid in his patent #US2006234577 within paragraph 4, page 1,:

"It has been demonstrated that reversible shear thickening in concentrated colloidal suspensions is due to the formation of jamming clusters resulting from hydrodynamic lubrication forces between (colloidal) particles, often called hydro clusters."

The dilatant used here is a non-Newtonian fluid, made from a solvent with colloidal dispersions. The rheological properties of which, rely on the suspension of colloidal shapes suspended in a dispersion. These colloidal dispersions are well known and numerous papers and references describe them. The patent further clarifies the use of STF in paragraph 30. *'The particles are suspended in the solvent and should produce a fluid that has the shear thickening property'*. Therefore it is the use of the particles in a solvent that give this colloidal STF its properties.

15

Colloidal suspensions are found in a number of different, simple, liquids;

- o Printing ink in a suspension.
- o Corn starch and water

The literature refers to these materials as STFs and they are more often than not described as colloidal dispersions, which can be thought of as mechanical dilatants. In effect, these colloidal dispersions are all mechanical STFs. They rely on mechanical interactions between the colloidal shapes to obstruct one another. When moved slowly, they behave like a liquid and flow past each other. When required to move quickly, they 'lock up' by mechanically hitting each other, giving the colloidal dispersion its mechanical dilatant properties.

In contrast, there is another group of materials that are silicone based dilatants, and these have been used over the years for many applications. The most common silicone based dilatant is 'Silly Putty'. This is a material produced by Dow Corning Corporation and sold under the catalogue number 3179 Dilatant Compound. This is a mixture of compounds where the active material is Polyborodimethylsiloxane (PBDMS). Silly putty contains 65% PBDMS. These materials form the basis of this research and these have been extensively characterised and tested. This work is reported in Chapter 3.

There is another type of fluid that is worthy of mention, also shown in Figure 4, and that is a Bingham Plastic. These materials behave as a rigid body at low stress, but flows as a viscous fluid at high stress. It is named after Eugene C. Bingham who proposed its mathematical description. A common example is Mayonnaise.

2.2.2 Auxetic Structures and Re-entrant Geometry

Most engineering materials, when subject to uniaxial tension, contract in the other two directions. Similarly, when under uniaxial compression, they tend to expand in the transverse direction. This relationship is defined as the Poisson's ratio, this being defined as:

$$v_{yx} = -\frac{\varepsilon_x}{\varepsilon_y} \qquad [21]$$

Where v_{yx} is the resulting Poisson's ratio after compression along the axial direction, ε_x is transverse strain and ε_y is axial strain. This effect is shown in Figure 5, where the material expands laterally as it is compressed.

R.S. Lakes discovered the first material to possess a Poisson's ratio smaller than zero; a modified form of polyurethane (PU) foam [22]. This class of materials is now known as an 'auxetic'. When you stretch a negative Poisson ratio material in uniaxial tension, they expand in the transverse direction. Conversely, if you were to compress it longitudinally, it would get thinner in the lateral direction.
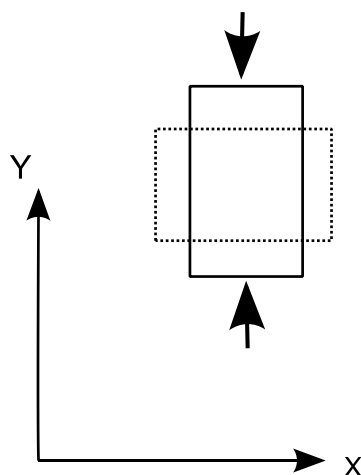
Figure 5 demonstration of Poisson's ratio effect
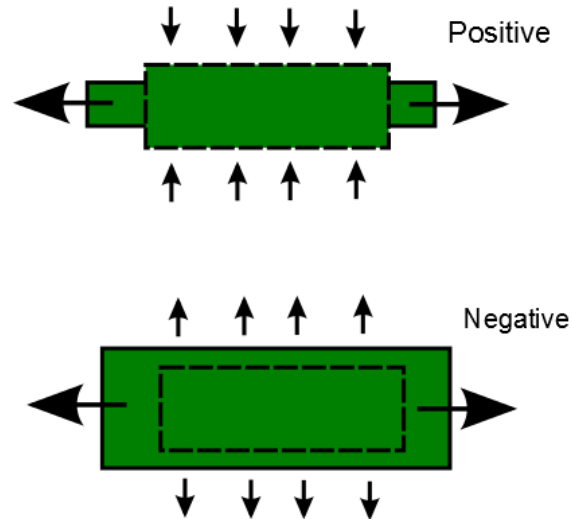
Figure 6 Graphic of an auxetic material.

Since Lakes' discovery, much research has been carried out into this class of materials. In general, auxetic materials posses enhanced properties, greater resistance to indentation, increased fracture toughness or increased shear modulus [22].

Auxetic materials do occur naturally. Examples of these are single crystals of arsenic and cadmium, α-cristobalite, cat skin, salamander skin, cow teat skin and also load-bearing cancellous bone [23].

A variety of different auxetic materials have been discovered, manufactured and theoretically modelled and predicted.

These fall into all the different classes of materials, but all these structures have a similar mechanism in the way that they achieve a negative Poisson's ratio. This basic mechanism, as reviewed by Qianchu Liu in 2006, is shown in Figure 7. As the geometry is stretched it grows in width, non-auxetic materials would shrink or neck.
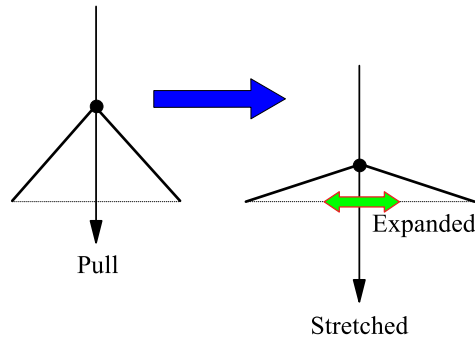
Figure 7 Deformation mechanism in auxetic materials.

2.2.3 Classification

Figure 8 shows the different classifications of types of auxetic materials, including ceramics, polymers, metals and composites. These materials can exhibit several orders of magnitude of stiffness. Two main classes of the auxetic solids that have been heavily researched in the recent years are honeycombs and foams (cellular solids).
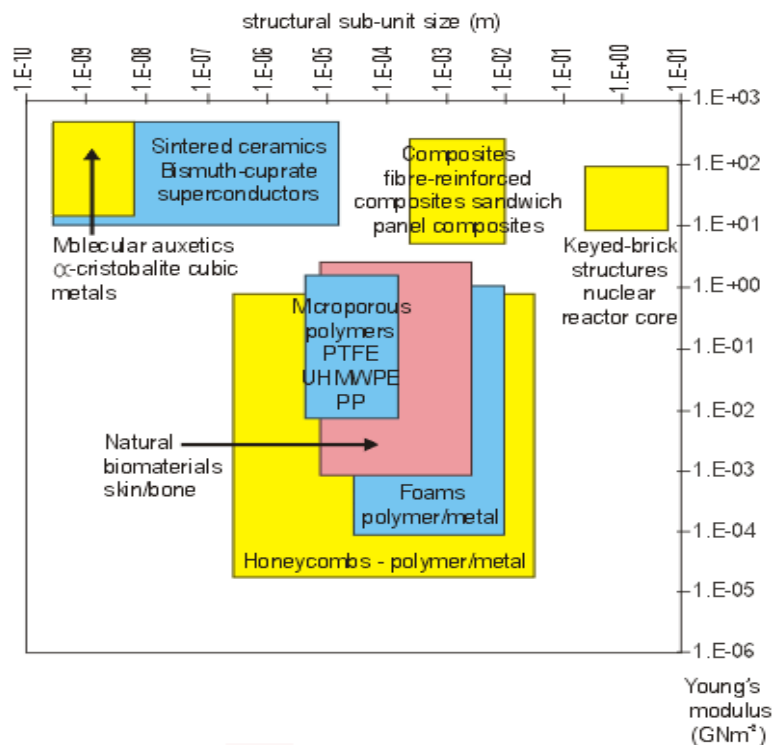
Figure 8 Different classes of materials available in Auxetic form [24]

19

2.2.4 Honeycombs

Auxetic honeycomb structures can give a material a negative Poisson's ratio, the earliest example being the tessellating re-entrant hexagon topology, shown schematically in Figure 8 [25].
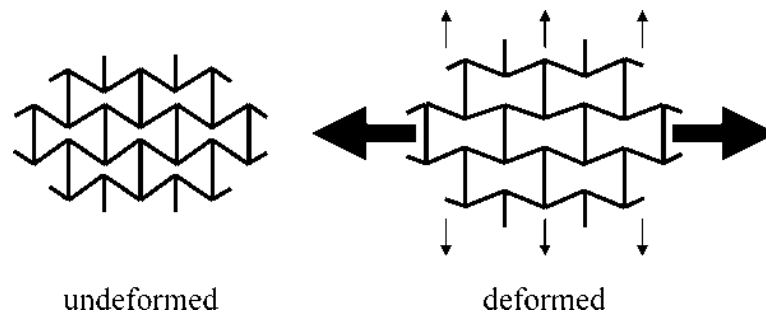
Figure 9 Undeformed and deformed re-entrant honeycomb structure.

Figure 9 shows how the application of a uniaxial load causes the diagonal ribs to be aligned along the horizontal direction of the applied force. In turn, this causes the vertical ribs to move apart from each other, resulting in the sample material expanding, because of this stretch.

There are alternative more efficient topologies of this type of re-entrant honeycomb structure presented in Figure 10 [23].
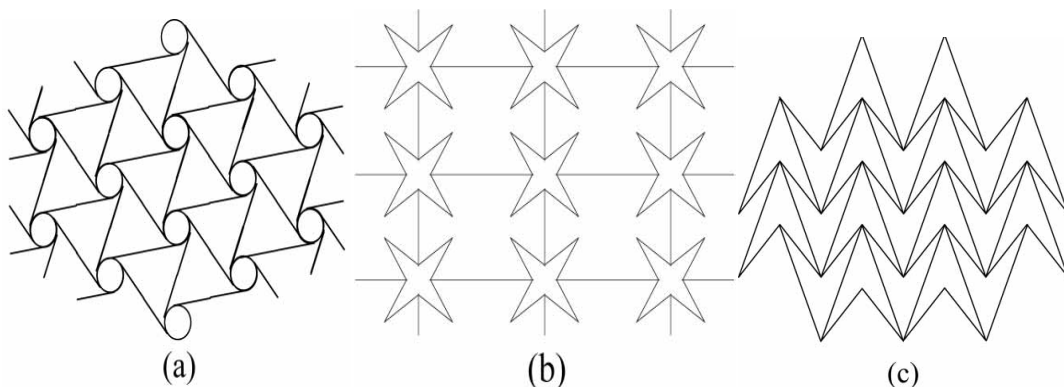
Figure 10 (a) Chiral honeycomb (b) Star honeycomb (c) Double arrow-head honeycomb

The auxetic effect is achieved in these structures in a similar way to the conventional re-entrant honeycomb alignment. In Figure 10 (b) and (c), again the hinging of the diagonal ribs, in response to an applied force, cause the stars and arrow-heads respectively to open or close. The chiral honeycomb (Figure 10 (a)) responds by unwrapping or wrapping the ligaments around circular cross-section nodes.

2.2.5   Cellular Solids - Foams

A method of converting thermoplastic polyurethane foam, with a positive Poisson's ratio, into an auxetic form was reported in 1987 [26]. Since then, different methods have been developed to produce thermoplastic (silicone rubber) and metallic (copper) auxetic foams [27].

In order to achieve the auxetic effect in foams, convex polyhedral cell shape characteristics of a conventional foam are converted to a re-entrant and a much more complicated cell structure. Figure 11 shows micrographs of polyurethane (PU) foam before and after the conversion and Figure 12 shows the idealised model of foam before and after the transformation.

Positive Poisson's ratio PU foam   Auxetic PU foam
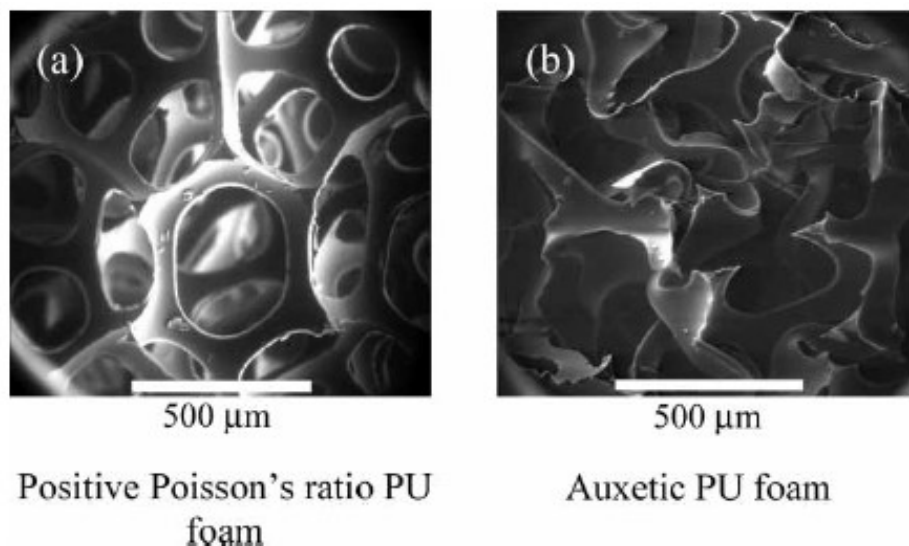
Figure 11 PU foams: (a) unconverted (i.e. positive), (b) converted (auxetic with negative) [23]
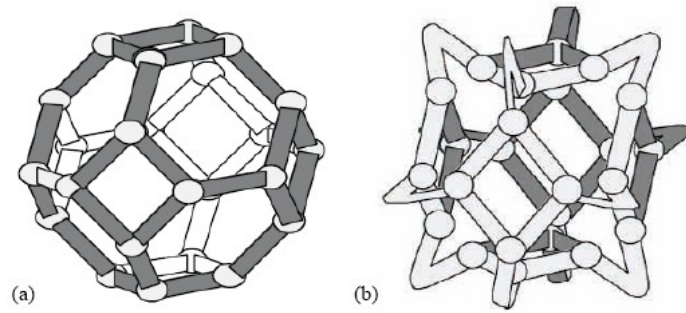
Figure 12 Idealised model - (a) conventional cell, (b) re-entrant cell

The physical effect of a negative Poisson's ratio can be utilised in different applications. One such example is illustrated in Figure 13. An out-of-plane bending moment is applied on a normal material, e.g. to form a wing panel, which displays an anticlastic curvature with a saddle point. Whereas an auxetic material will show synclastic curvature resulting in a dome shape. This means that auxetic materials don't require unnecessary machining or bending to take up a desired shape, which could deteriorate the material properties [26].
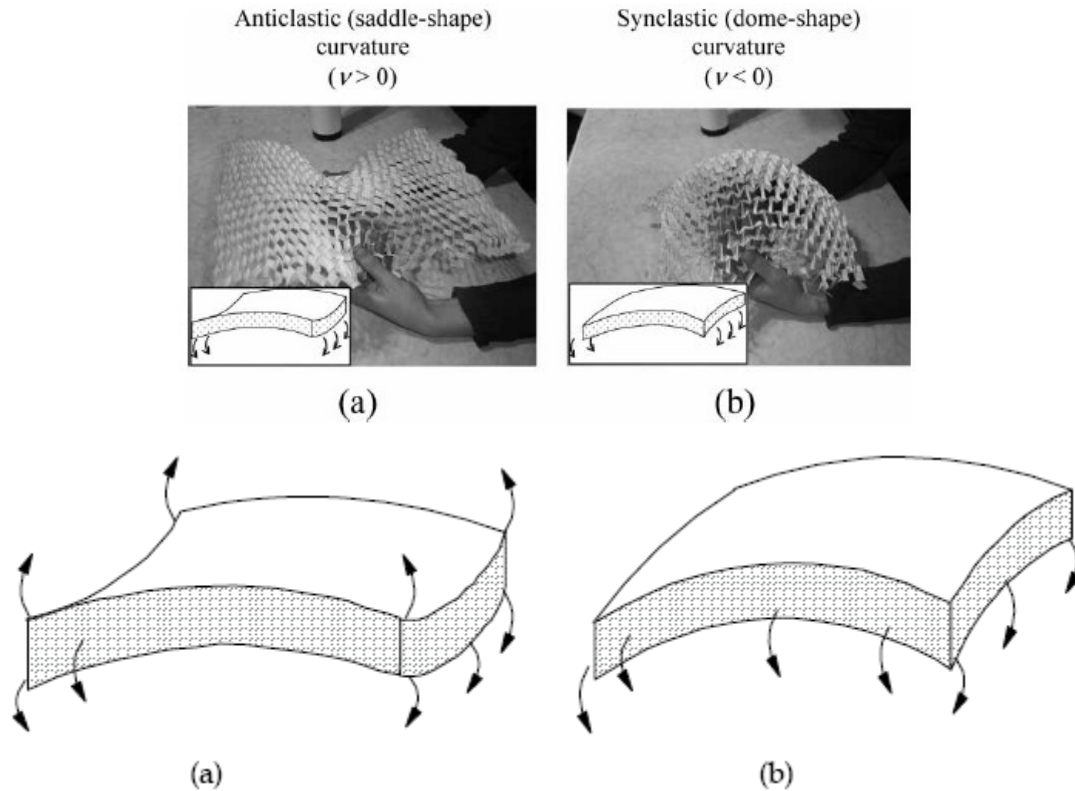
Figure 13 (a) Anticlastic (saddle shape).

(b) Synclastic (dome shape) curvature shown by auxetics materials.

Auxetic honeycombs have the potential to be used to produce curved parts of an aeroplane e.g. the nose cone. Not only can they take up a curved shape without needing to be machined , but also the stiffness is increased, since the ribs of the honeycomb are always perpendicular to the curved surface and therefore giving out-of-plane strength. Curved sandwich panels, with an auxetic honeycomb core in the centre with two outer coverings, have been successfully produced [23].

2.3 Ballistics

2.3.1 Introduction

Ballistic armour worn or carried by the owner has been in demand since the very advent of handheld projectile-firing weaponry. It was a very obvious addition to plate armour, which probably began in the 16th century, as observed in an engraving, drawing attention to a dent on a breastplate, which was probably an indication that they had been "ballistically" proof tested for resistance, before sale. Subsequent advances in firearms technology eventually rendered plate armour largely ineffective, unless they were thick enough to resist impact, but this in turn made the armour extremely heavy and expensive. Lightweight silk bullet resistant armour was developed in the late 19th century, but the quantity of silk required, again made this too expensive. Later, in the 1920s and 30s, thick cotton outfits were worn by criminals which shielded them against a number of commonly issued police weapons of the time, however minor changes in weaponry rendered this effort obsolete. It was not until the 1970s with the discovery of para-aramid, namely 'Kevlar' fibre that advances in materials made effective and lightweight bullet-resistant armour viable for general use.

The bulk of ballistic armours are made from multiple layers of woven textile cloth composed of high tenacity yarns, compiled into multilayer packs and often post quilted. These soft ballistic packs can absorb a considerable amount of energy from a ballistic impact, before parting. Additional ceramic or composite plates can also be inserted into pockets to further protect vital points, with different

plates available to provide protection against a variety of threats. This review will consider only 'soft' armour and not inserted ceramic coatings, or plates.

2.3.2   Soft Armour

A number of standards exist by which to classify ballistic armour. These rate armour on how capable it is of protecting against ballistic threats, ranging from low velocity handguns to armour piercing rifles. Each region and occupation generally requires its own system, as the most commonly encountered threats vary by location. For example, the British Police force will not usually expect to encounter weaponry more powerful than pistols and shotguns, while assault rifles and submachine guns are commonplace throughout the USA. Furthermore, boarder patrol guards and prison wardens will be more likely to require vests capable of stab resistance than protection against high velocity rounds. However, the general literature will usually refer to the more widely recognised standards from North America and Britain.

Each armour sample is tested for penetration, back face signature (BFS) and ballistic limit. The armour is fitted over a calibrated backing material and shot at specific points, generally not close to a previously tested point of impact or an edge of the material.

Penetration is defined as the bullet, any fragment of the bullet or any fragment of the armour, penetrating through to the back of the armour.

Back face signature is the depth of impression created into the backing material by the bullet impact, which is representative of the amount of energy that would be transferred to the body of the wearer. If the energy is not sufficiently absorbed or spread out by the fabric, deep impressions can indicate that the armour would still allow the bullet to cause significant blunt trauma. The limit for the depth of this impression in the relevant American standard is 44mm, whereas the relevant

British police standard specifies 25mm as a maximum depth. [28][29]. These standards are detailed in Chapter 7.4.4 and 7.4.5.

Ballistic limit will refer to a bullet velocity that can reasonably be expected to defeat the armour. Testing for the velocity of bullet that a vest will always defeat (the so called V0) is problematic due to variations in armour samples. A better limit is the V50, the velocity at which half of the bullets will completely penetrate the armour and the other half will only partially penetrate, as this to some extent accounts for the presence of product and testing variability [30].

2.3.3 Fibres

Both soft and hard bullet resistant armours employ high strength fibres in their construction. These fibres are stronger and lighter than steel wires of the same thickness, but are generally more expensive to produce. Common ballistic fibres are para-aramid and ultra high molecular weight polyethylene.

2.3.4 Shear Thickening Fluids in Armour

These materials have been discussed in section 2.2. This section reviews their specific use in ballistic armour as opposed to their bulk mechanical properties previously discussed.

Shear thickening fluids, have considerable potential in ballistic armour, as an STF can be used to create armour that is soft and flexible until it is hit, at which point it instantly hardens up – in effect, a comfortable armour that reacts of its own accord to protect the wearer against threats.

STFs can be as simple as cornstarch in water, but for ballistic use, a number of different STFs have been developed. One is a polyethylene gel with silica particles dispersed throughout. The silica forms approximately half of the mass fraction of the STF, which is then dissolved in ethanol and line coated onto a woven para-aramid. The solvent is evaporated to leave the textile coated in the STF [31].

However, the silica particles have been observed as causing pitting and damage to the Kevlar fibres over time, making the effective life of treated Kevlar armour questionable [32].

Other STFs are under research, for example a PMMA suspension in polyethylene glycol, these were initially thought to show shear thickening properties, but is was discovered during testing to exhibit shear thinning at high shear rates [32]. Also a Kaolinite clay suspension was found to produce similar protection against stabbing and similar puncture threats, though it only produced a third of the improvement in ballistic testing as compared to silicone coating [33].

The benefits of using STFs in combination with conventional armour are considerable [34]. For example, four layers of Kevlar painted with STFs was found to provide greater protection than that of 10 untreated layers. The overall weight was similar but the treated Kevlar still had the distinct advantage of being as flexible as four layers of Kevlar as shown in Table 1. In addition, it did not increase the bulk, as Kevlar has around 50% void space into which the STFs are absorbed.

Table 1 Comparison of ballistic performance for shear thickening fluid impregnated in 4 layers of Kevlar and pure Kevlar with varying target weights [4].

Description	Sample Weight (g)	Penetration Depth (cm)	Dissipated Energy (Joule)	Bending Angle, θ (°)	Sample Thickness (mm)
4 layers of Kevlar	1.9	2.12	25.1	50	1.4
10 layers of Kevlar	4.7	1.55	28.6	13	3.0
2ml STF impregnated in 4 layers of Kevlar	4.8	1.23	28.6	51	1.5

The reason for the STF being more effective when painted on Kevlar than alone, is believed to be partly due to it improving friction between the layers of Kevlar[35].

2.4   Chapter Summary

This section has reviewed existing literature in the areas of strain rate sensitive materials as well as the introduction of non-Newtonian materials and comparisons with shear thickening and shear thinning materials in the form of particulate suspensions. Dilatants and silicone based strain rate sensitive materials are introduced, and there mechanisms that give them there strange rheological behaviour explored.   Internal architecture of structures of foams, and re-entrant shapes have been discussed, and the internal geometries of auxetic systems reviewed. The applications and research of each of these topics has been reviewed in light of protecting the human body.

3 Impact Mechanics and Material Concepts.

3.1.1 *Introduction*

This section reviews the relationships which describe impact mechanics and how these apply to body worn devices. Also considered are resultant outputs that would actually happen to the person being protected during these types of impacts and how these equations might be used to predict the outcome of these impact events. Impact test outputs are reviewed and related to predicted levels of protection. These are compared to personal protective equipment (PPE) and sporting goods standard test methods, with a view to define what makes a body worn energy absorbing material desirable. Dilatant materials are introduced. Finally, the concept of an active material combined with an auxetic geometry is postulated as an energy absorbing system.

3.2 *Impact Mechanics*

"Impact mechanics is concerned with the reaction forces that develop during a collision and the dynamic response of structures to these reaction forces. The subject has a wide range of engineering applications, from designing sports equipment to improving the crashworthiness of automobiles" Stronge 2004 [36].

The following outlines the equations governing impacts, and there relevance to or for body worn protection. An important equation in physics is the mathematical form of Newton's second law;

Force equals mass times acceleration.

F=Ma.

3.2.1   Impulse.

Impact, generates a force as a result of a collision.

Types of impacts:

- o   Impact from one's own body
- o   Landing from a jump (vertical)
- o   Falling over (vertical / horizontal)
- o   Running into an object (horizontal)
- o   Impact from an external object
- o   Catching a ball
- o   Colliding with another player
- o   Being hit by a bullet.

Effects of impact: Primarily these are avoiding injury in terms of sport, but they could also relate to regaining balance and equilibrium.

- o   Avoiding injury
- o   Regaining equilibrium promptly

The other aspect to consider for impact isn Kinetic Energy.

Kinetic Energy changes as Velocity changes

$KE = 1/2\ mv^2$

Impact slows down the Object:

- o   Decreases its Velocity and Kinetic Energy In
- o   Requires that Work is done on the Object (W = Fd) or
- o   The Object does Work on the Body

$KE_{in} - KE_{out} = F(d)$ units (metric): $(kg*m^2)s^2$ [37].

Force and distance are, thus, directly related.

3.2.2 Momentum

Momentum also changes as Velocity Changes (M = mv) [38].

Impact again slows down the Object:

- o Decreasing its Velocity and Momentum
- o requiring that a Force is applied for a given period of time

Impulse = Force * time

Mo - Mf = F(t)

Impulse units (metric): N.s or kg.m/s

Force and time are intrinsically directly related.

Impulse I produced from time t1 to t2 is defined to be [39].

$$I = \int_{t_1}^{t_2} \mathbf{F}\, dt$$

Where **F** is the force applied from **t1** to **t2**.

From Newton's second law, force is related to momentum **p** by

$$\mathbf{F} = \frac{d\mathbf{p}}{dt}.$$

Therefore

$$\mathbf{I} = \int_{t_1}^{t_2} \frac{d\mathbf{p}}{dt}\, dt$$
$$= \int_{p_1}^{p_2} d\mathbf{p}$$
$$= \Delta\mathbf{p},$$

Where **Δp** is the change in linear momentum from time **t1** to **t2**. [40] This is often called the impulse-momentum theorem [41].

As a result, an impulse can be considered as the change in momentum of an object to which a force is applied. The impulse may be expressed in a simpler form when both the force and the mass are constant:

$$\mathbf{I} = \mathbf{F}\,\Delta t = m\,\Delta \mathbf{v} = \Delta\mathbf{p}$$

Impulse can be calculated using the following equation

$$\mathbf{F}\,\Delta t = \Delta p = m\mathbf{v}_1 - m\mathbf{v}_0$$

Where:

F is the *constant* total net force applied,

t is the time interval over which the force is applied,

m is the *constant* mass of the object,

$\mathbf{v}_1$ is the final velocity of the object at the end of the time interval, <u>and</u>

$\mathbf{v}_0$ is the initial velocity of the object when the time interval begins.

3.2.3   *Pressure*

Large Pressures, NOT large Forces, increase the likelihood of Injury [42].

Mathematically:

$$P = \frac{F}{A} \text{ or } P = \frac{dF_n}{dA}$$

Where:

P is the pressure,

F is the normal force,

A is the area.

Pressure is Force per unit of Area; Force and Area are thus inversely related.

Typically, high speed biofidelic testing today is performed with devices such as the crash test dummy [43]. In engineering terms, the usual methodology is to measure force and time. This has been the basis of mechanical testing in recent years. The force sensors are widely available at a range of speeds, as are speed sensors and accelerometers. Pressure can by calculated from force, but when working with the human body, most high speed devices measure force and acceleration.

Measuring force against time is the standard methodology in type testing CE certification in BSI, TUV, ISO and DIN, when body worn protection.

The graph in Figure 14 shows a typical impact event, measuring force and time. The graph shows transmitted force against time plot.
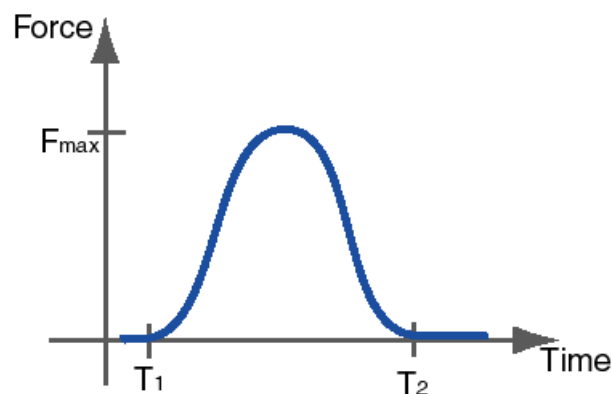
Figure 14 Force time trace of a typical impact

Where the impact time is T_1-T_2 and the peak force is F_{max}. A typical plot for standardised test would be a bell mouth type curve, as shown above. The characteristics of this curve can be classified in terms of the impact duration (T_1-T_2) and the peak force F_{max}. These systems can be tuned through the different use of materials, stiffness, thickness and geometry. A good energy absorbing material will have a low peak force, long duration and a flat bell-mouth shape. A material with lesser force attenuation properties will have a higher peak force and a narrower force plot, showing a reduced impact time.
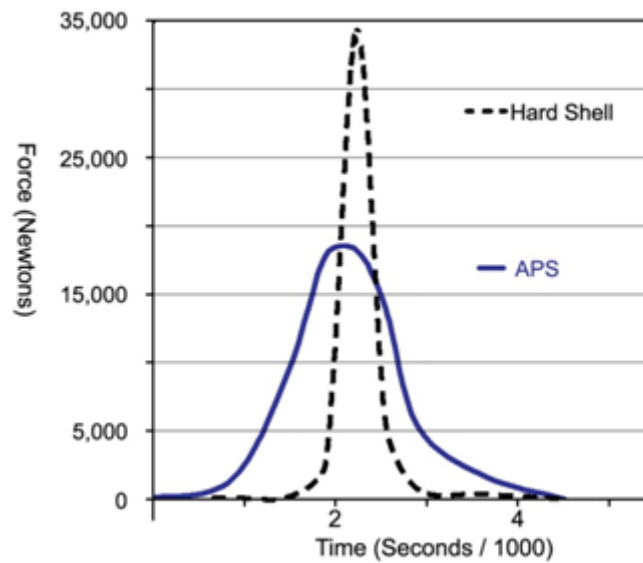
Figure 15 Force time plot of two types of protective systems

Of particular note in the example above, is the lower peak force and its duration, for the blue trace.

The plateau in the plot is typical of a tuned system and is practically desirable, as the energy of the force is dissipated over a longer time-frame than it is for an equivalent thickness hard armour system. The tuned system also provides more protection against the level of force that is capable of causing an injury, and it maintains the protection over a longer period than a hard armour system.

By contrast, the harder armour product shows a higher force response over a shorter time. For the wearer, this means the transmitted force is felt more and could lead to more soft tissue damage, if the pressure is high enough. It is important to keep the peak force as low as possible and to have the impact event last as long as possible.

A Heaviside function of force time captures the largest area under the curve for a known time and minimum peak force.
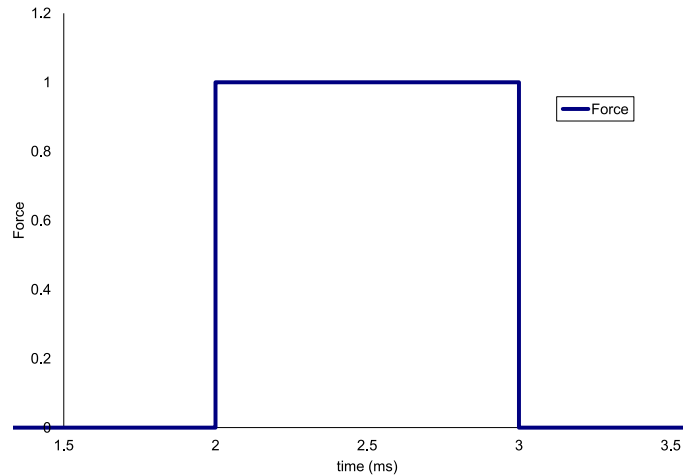
Figure 16 Heaviside function of force time

A sensitivity analysis on a simple impact can be used to find a peak force following a Heaviside function, for a given time or time delta. Figure 16 denotes such a force time trace. The y axis is arbitrary force and X axis is time in milliseconds. When considering a standard BSI motorcycle limb protector test, with a 5Kg mass falling at a velocity of 4.333m/s, impulse can be calculated from the impulse momentum theorem, assuming the final velocity is zero, or all of the energy has been absorbed by the protector.

$\Delta\mathbf{p} = \mathbf{mv_1} - \mathbf{mv_2}$

$\mathbf{mv_2} = 0,$

So $\Delta\mathbf{p} = \mathbf{mv_1}$

$\Delta\mathbf{p} = 5 \times 4.333$

$\Delta\mathbf{p} = 21.7$ kg.m/s

The lowest theoretical peak force for various theoretical impact times can be calculated. These are shown in Table 2.

Table 2 Lowest theoretical peak force

Mass (KG)	Velocity
5	4.333
FΔt	21.7
Δt	Lowest F (N)
0.001	21665
0.002	10833
0.003	7222
0.004	5416

By applying these concepts to materials and impacts, what we want is a force trace that rises to a peak, holds at that peak until the impact event is over, taking as long as possible. In reality, it is very difficult to get a Heaviside function for the force time trace; with active materials and auxetic tuned geometry it is possible to get an inverse 'W' force time trace. This gives us a longer rise time (time to peak force) with as long a time interval as possible, at or near peak force, providing a long duration, lower equivalent peak impact, as seen in Figure 17.
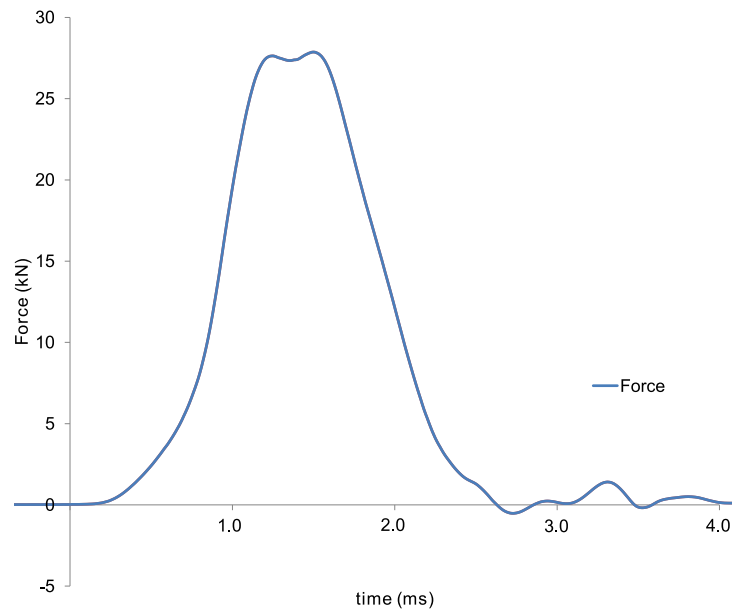
Figure 17 Inverted 'W' trace

Applying these concepts to falls and impacts:

In an ideal world, it would be beneficial to decrease velocity gradually. This is possible by:

- o   Increasing Distance through which Force is applied
- o   Increasing Time through which Force is applied
- o   Landing on "Giving" surfaces
- o   Controlled Flexion through Eccentric contractions. [44]

For an improved energy absorbing material, a force trace that rises to a peak, holds at that peak until the impact event is over taking as long as possible, would provide the lowest peak force.

3.3   Forces on Various Areas of The Body.

When considering protecting the human body, it is pertinent to consider the loadings or peak forces that the body can sustain in various different areas. Data from numerous sources and the research collected. This relates to the section of the body with the approximate maximum force that that part

37

of the body can take, for a 50th percentile 25 year old male in good shape. It is important to have an estimate of the peak forces that the body can ultimately take at different locations, when designing a protection system. These numbers are used as a guide only, as most test apparatuses use solid anvils and impactors with no soft surfaces and very little compliance, which is not typical of the human body. As can be seen, the loads on the body vary significantly from area to area. During the research in this field, these loads were taken from in excess of 80 papers to start to understand the forces that may be applied to the human body, at more that 100 load sites. The high level synopsis of these data, most relevant to this thesis, is shown in Table 3 below.

It will be seen that the fracture load of a femur from a 25 year old male in good shape, is above 6kN. These figures need to be related to the age and health of the person. Existing research shows that this number drops to about 1.9kN for an elderly female with osteoporosis [1]. However in general these figures can be used as a guide for sporting applications and military applications, which are activities typical of younger people.

Table 3 Highlights of data from cadavers, reconstructions and subjects.

Limb / Area	Load kN (Peak depending on test method)	Reference
Forearm radius + ulna	Male mean dynamic fracture force 2.4 kN	[45]
Femur – axial	Fractures at 6 – 17 kN	[46]
Knee to pelvis axis	Femur fracture at 6.4 kN	[47]
A-P breaking force of fresh human bones	Femur 8 kN	[48]
Knee to pelvis, axial	Femur fractures rarely below 10 kN	[49]
Knee	Fractures at 6.5 kN	[50]
(Impacts to fixed leg)	Cartilages damaged at 3.8 kN, simple fractures at 5 kN.	[50]
Knee, lateral impact	Fractures occur at 6 – 10 kN	[51]
Knee, lateral impact	Ligament strains below 2 kN	[51]

Thanks to Dr. Roderick Wood for help in gathering data for this table.

3.4   Previous developments.

In previous work by the author, an active material technology was based around a soft malleable and formable dilatant silicone, which is impregnated and combined into a carrier. For initial studies, a foam or 3d textile was used as the carrier. This work developed a 3D textile-based system that was coated in a commercially available grade of dilatant material. This worked well technically, but was expensive to manufacture. The extent of the impregnation / combination is controlled so that the system remains both fully breathable for maximum comfort and easily bendable to allow conformity to the body.

3.5   Dilatant composition

For the initial development reported in this thesis, the active silicone compound was sourced from Dow Corning Corporation, and was sold under the code of 3179 dilatant compound. This compound consists of polymers that show transient bonding to a cross-linking component.   Under normal conditions the polymers are bonded to the cross-linker in such a way that the bonds become open when subjected to a long period deformation force, which allows the material to flow. When this force is removed, the bonds reform again, returning the silicone to its original lightly cross-linked soft state. If the silicone is subjected to a sudden deformation force, the cross-linking bonds do not have time to open, the material resists the deformation force and takes the form of a solid. This dilatant nature of the material means that when it is being impacted, as a result of a collision, it instantly transforms from a soft flexible material to a solid, but only for the duration of the impacting force. After the force has been dissipated through the dilatant/fabric construction, the silicone is again soft and flexible[6].
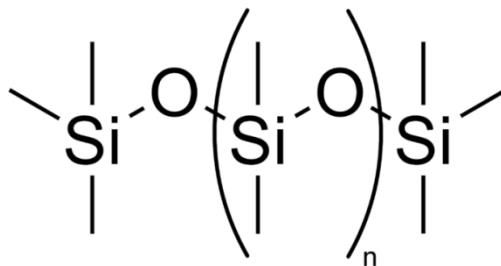
Figure 18 Polydimethylsiloxane (PDMS)

The backbone of the active material can be seen in Figure 18. This is the basic building block of Polydimethylsiloxane (PDMS). PDMS is reacted with Boron to give Polyborodimethylsiloxane (PBDMS). PBDMS forms numerous hydrogen bonds. These hydrogen bonds result from the dipole interaction between Boron atoms bond to the OH functional groups on the silicone backbone or polymer chain. The hydrogen bonds formed are not permanent covalent bonds, but are pliable or reformable bonds. These bonds can move slowly along the polymer chain while stresses are low. However, they cannot move along the polymer chain quickly and so give the polymer its obscure rheological properties [6]. This material can be described as a chemical dilatant in that the strain rate characteristics are created through chemical bonds within the polymer.

It is hypothesised that a chemical dilatant of this nature would exhibit these properties not only in compression, but also in shear and tension, but this needs validating.

Different types of active silicone dilatant have been provided or manufactured for the majority of this research and these are based around 3179.

3179 composed is comprised of 65% dimethyl siloxane (hydroxy-terminated polymers with boric acid), 17% silica (crystalline quartz), 9% Thixatrol ST (castor oil derivative), 4% polydimethylsiloxane, 1% decamethyl cyclopentasiloxane, 1% glycerine, and 1% titanium dioxide [52].
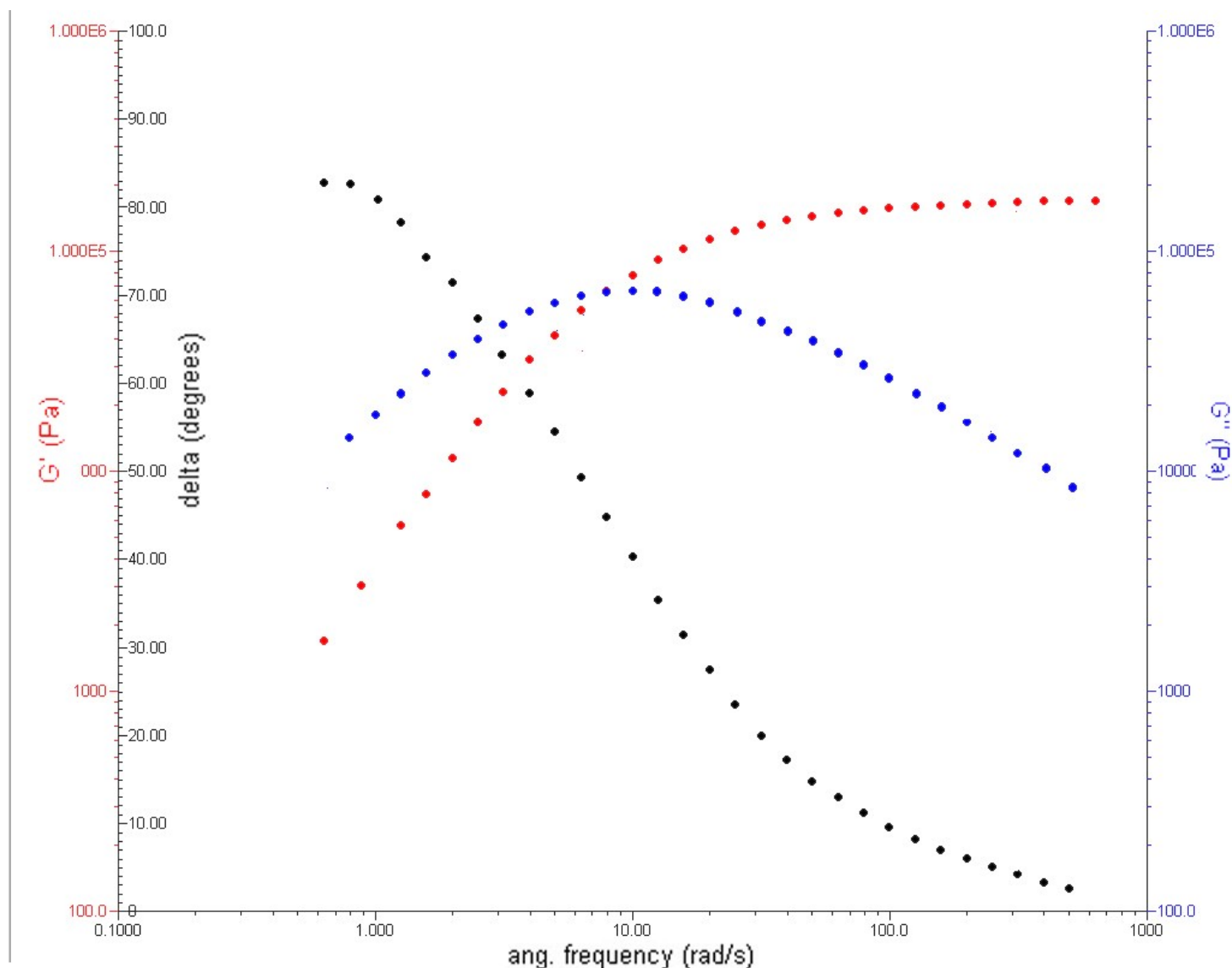
Figure 19 3179 tested on a shear rheometer.

3179 (PBDMS) has been tested on a shear rheometer. The characterising effect of this material can be seen from the large change in tan delta with increasing frequency in Figure 19. This effect is unusual in most other materials. Silicone rubbers would have no change in tan delta with change in frequency and silicone fluids, such as polydimethylsiloxane (PDMS), would have a linear response, reducing slightly over time.

The carrier also plays an important role in performance. The carrier initially chosen, has a diamond shaped surface configuration, made from multifilament polyester yarns, with the spacer yarns

formed from monofilament PP, to create a three dimensional structure, that is just 4.5mm thick. When this fabric is impregnated with the active silicone, it is particularly important to present the silicone in such a way that it can readily absorb the impacting force through the spacer yarns in the direction of the force. By careful design of the dimensions of the spacer textile, this orientation is assured, allowing the silicone to absorb maximum force, yet leaving the fabric completely breathable. This is shown diagrammatically in Figure 20.
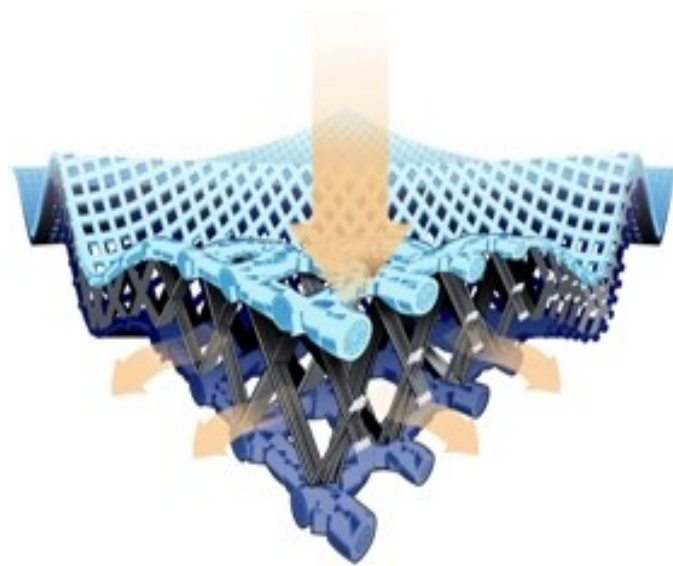
Figure 20 Illustration of 3D Spacer textile combined with Dilatant Material:
Active Protection System Spacer

When this fabric is impacted, the force is first received by the dilatant coating on the surface and spacer yarns, which are directly in the direction of impact. These become rigid and transmit load to adjacent spacer yarns, which also become rigid, thus increasing the impact area.

3.6 Concept of soft armour

This research aims to characterise and quantify the expected performance benefit with either a re-entrant geometry, or a tensile layer, preferably used with active materials. Known impact protection solutions currently available, tend to fall into two types, namely a rigid exterior shell, which can be

uncomfortable to wear (e.g. roller blade or skateboard knee or elbow pads) or foam, or foam laminate pads (e.g. inserts for ski clothing) which provide poor levels of protection.

There is, therefore, a need to provide an energy absorbing material, which is lightweight, flexible and comfortable to wear, whilst still being able to dissipate and absorb the shock loads applied to it, providing an effective protection.

When considering an energy absorbing material alone, often impact performance is related to the tensile strength of the parent material. This can be demonstrated in drop tower motorcycle protector CE type tests, namely EN1621-1[53] and EN1621-2 [10] where the anvils are typically curved or domed. The impact performance of flexible foam energy absorbing materials is limited as they often bottom out and fracture at the impact site. The material is forced away from the contact area (impact site), leaving less energy absorbing material, usually leading to a reduced energy absorption and higher peak transmitted impact forces. The fracturing and movement of material away from the impact site is common in many materials but is especially prevalent in flexible foam materials.

An energy absorbing material will initially compress under the force of an impact. For cellular products and foams, this is referred to as the plateau region on a stress strain graph [54]. Further compressions lead to local densification[54]. If total compression is limited to this, then this can be considered a recoverable energy absorbing system. Up to this point, the system is behaving in a repeatable manner and the materials are compressing elastically. Continued compression means eventually the material "bottoms out" and the transmitted force increases, resulting in the material starting to fail by fracture. Further compression (overload) will break the material apart (fracture) moving material away from the contact site, which means there is no material left to absorb energy at all. This overload regime is typical of foams and cellular systems with thin wall sections.

For an improved flexible energy absorbing material, it is worthwhile exploring methods to stop this final fracture of material and keep material in the contact high pressure area. It is the object of this research to show how the material's movement away from the contact site can be reduced, stopped, or even reversed, since in principle adding more material to the contact area would help. This research considers how the three methods listed below all improve impact performance and can be used individually. For a further, and sometimes unexpected performance improvement, any two, or all three, can be combined.

1) Add a tensile layer to the energy absorbing material.

2) Add re-entrant geometry to the system.

3) Add an active material to the energy absorbing system.

The intention of this research is therefore to design and provide a flexible energy absorbing material that provides improved energy management by controlling the movement of the material away from the contact site, either by local densification, or restraining the material with a tensile layer, when used in conjunction with energy absorbing materials. This research focuses on an active material which is a highly strain rate dependant material, in the form of a dilatant material. It was important for the development of this part of work that the technology platform should be easily manufactured in quantity and be reproducible. It had to be repeatable between separate samples and ideally a system will be created that can have impact resistance for multiple impact events. To this end, the development programs were always pushed towards scale-up, and the samples tested wherever possible would be produced using the final manufacturing process. Moving to scaleable manufacturing techniques, such as an injection moulding process, was the goal, in order to produce parts quickly and with an exact replication of parts.

A key aspect of this research is that the active, highly strain-rate sensitive material, polyborodimethylsiloxane (PBDMS), is polymer based, with the shear thickening effect created through chemical bonds between its polymer chains. Combining the energy absorbing capabilities of PBDMS with the combination of an auxetic structure, should lead to novel material properties, that are further researched in this thesis. Due to the fact that PDBMS exhibits stiffening properties, it is hypothesised that a soft armour containing PDBMS would also be more effective in preventing injuries.

3.7 Chapter Conclusions

This section has reviewed the equations that can be used to describe impact mechanics and how these apply to body worn devices. Various loadings on the body have been reviewed and discussed with a view to understanding what we might to protect various parts of the body, with considerations of how this might differ from person to patient.

Current methods for testing Personal Protective Equipment have been reviewed, and how these techniques can be utilised design and development of improved protection systems.

The ideal force time traces using these test techniques have been considered and a simple approach to reducing the peak transmitted forces has been applied to a best transmitted force trace for a theoretically ideal material.

Finally the concept of developing a novel protective system has been introduced, in the form of an active material combined with an auxetic geometry to give an improved energy absorbing system.

4 Development of Test Techniques and Drop Tower Design

4.1.1   Current Test Methods for PPE

Current armour is tested to EN1621-1[55] and En1621-2[10], which are the present standards for motorcyclists' protection clothing, and are used by numerous test houses and accreditation centres, as well as motorcycle protective equipment manufacturers. These test methods are well known to the writer who has recently been involved in developing these methods to include both temperature effects on testing and also including high humidity within the scope of the standard test. These changes are currently under review at BSI and the document is available for public comment. These standardised test methods use simple steel anvils in the form of primitive geometric shapes, to represent particular body or limb parts. The test specimens are subjected to the impact conditions in Table 4, with a pictorial representation opposite.

In these EN 1621 certification tests, a weight or falling mass is allowed to drop vertically onto the test piece.

Table 4 EN 1621 motorcyclist's PPE protection test requirements.

	EN 1621-1:1997	EN 1621-2:2003 Level 1
Impact energy, J	50	50
Striker mass, kg	5	5
Impact velocity, ms^{-1}	4.47	4.47
Striker dimensions, mm	80 x 40 radius 10	160 x 50 bar with 12.5 radius face
Anvil dome radius, mm	50	150
Requirement: Mean transmitted force:	Mean <35kN, no single impact >50kN	Mean <18kN, no single impact >24kN
Number of tests	8	5

EN 1621 Part 1
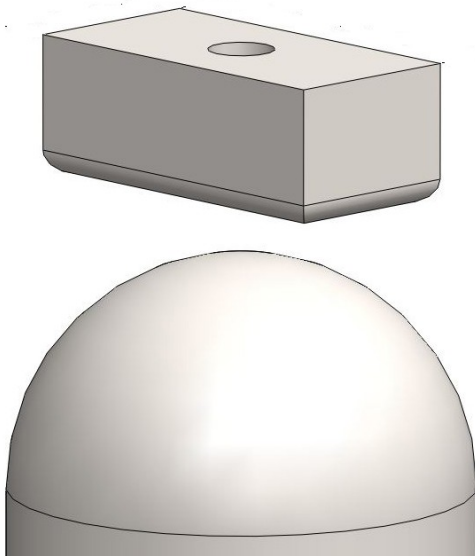
EN 1621 Part 2
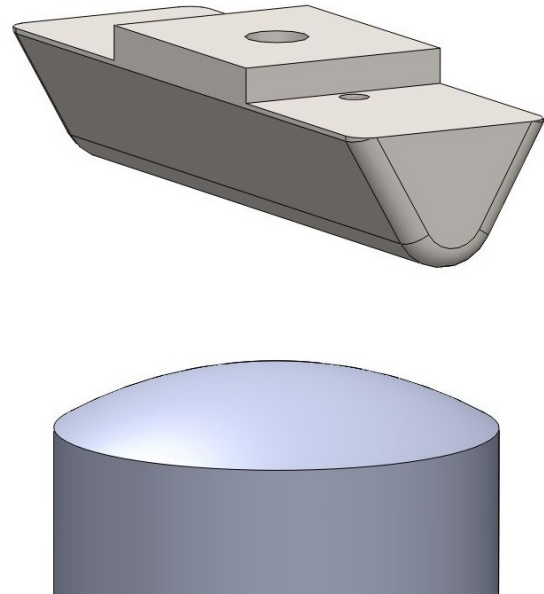
For the standard, transmitted force is measured with a piezoelectric load cell. However, it is possible to measure force, indentation, acceleration and peak pressure, as well as displacement with a high speed camera, on the same apparatus. This type of certification test method was used for developing general materials for the majority of this research, as it is simple and repeatable. When testing to these standards in this research the number of tests required by the standard was used unless otherwise stated. When the average has been used in this thesis, this is in accordance with the standard number of samples and then the arithmetic mean average taken.

The tests ordinarily consist of a mass of 5Kg free-falling from a height of just over 1m and impacting the sample, which is simply mounted on an anvil connected to a force sensor. The peak force is transmitted through the sample to the lower anvil and hence load is recorded and compared to the criteria for maximum acceptable values. EN 1621-1 utilises a hemispherical anvil and rectangular impactor (causing elliptical or spherical Hertzian contact) whilst EN 1621-2 involves a triangular prism with impact along a rounded edge, against a larger radius anvil (causing Hertzian line contact). These anvil and impactor combinations both exert subtly different loading regimes on the amour

being tested. In conjunction with parallel anvil work they give helpful insight during the development of a new armour system.

The BSI test method allows for a falling mass to be loosely guided on cables. However, this system is neither repeatable nor accurate enough for fundamental research. Primary research at UKAS approved test houses, as well as at key motorcycle apparel manufactures, showed a large average variation in results and also a large spread on the same apparatus. This spread is attributed to the poor design of the guide wires. With this type of guide wire design, it is not possible to test accurately and is also impractical to measure rebound and coefficient of restitution. The writer has taken part in two global "round robin" experiments on apparatuses provided by seven sites and studied the variation in the test towers. This information is confidential to the BSI working group and is also outside the scope of this section of the research, but does substantiate the need for a more reproducible testing regime.

For this research a highly accurate and repeatable drop tower has been designed, built and constructed to conduct the following tests more rigorously than existing certification equipment. A bespoke slider was designed to alleviate the problems caused by the guide wire designs. This has been possible through the design of a lightweight aluminium slider and guided drop weight on linear plain ball bearing (LPBR) bushes. This called for a guided slider to be below 1.6kg. The design is shown in Figure 21 .
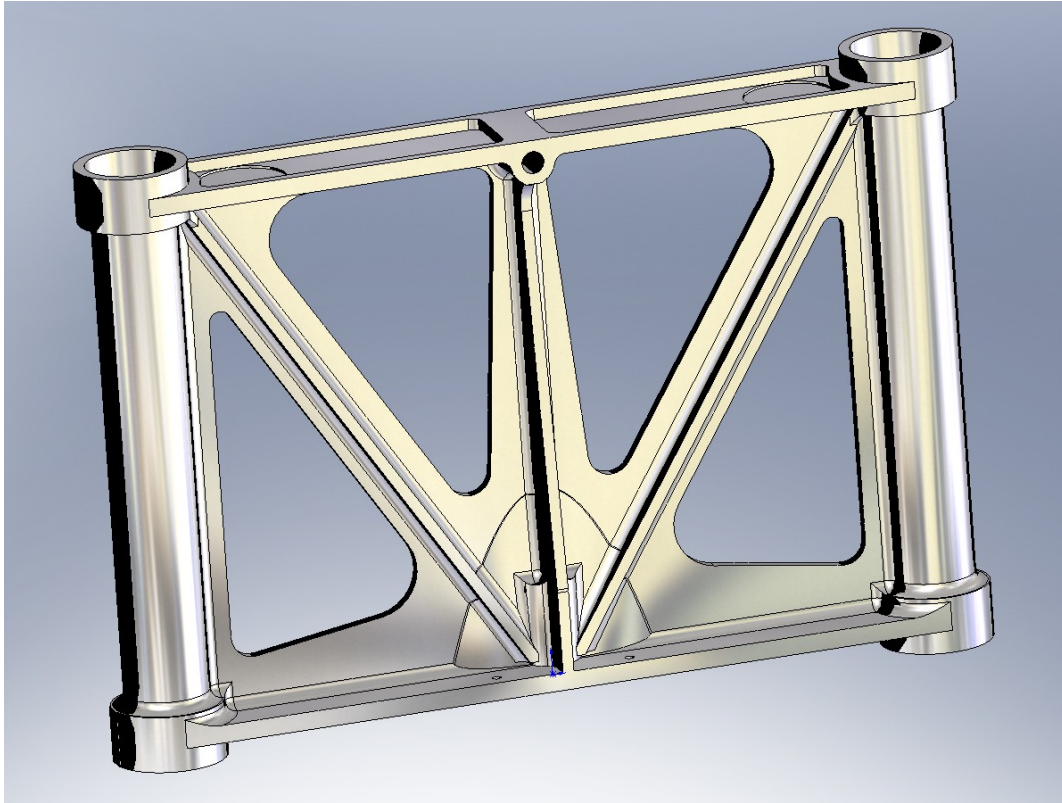
Figure 21 Slider image from CAD

The sides of the slider were machined as thin walled tubes. This is so that the part could be converted to include air bearings, if friction became a problem. This feature also stopped the bearings 'folding' inwards during impact and increasing friction over time. Air could be fed through small holes in the guide rails. The drop tower has performed over 14,000 impact tests to date and is still on the original set of bearings. Impact velocity is measured with a light gate in the final 25mm of travel. This has been checked and calibrated with a high speed camera. Impact velocity for this machine is highly repeatable, primarily due to the slider construction and design. This is important when developing new materials in order to have as few variables as possible. The impact velocity is repeatable to ±0.25%, in contrast the BSI CE standard which allows an error of 2%.

Figure 22 shows the finite element analysis (FEA) of the part during impact. As can be seen, flexure of the bearing is reduced to a minimum and the bearing's housings attempt to counter flexure in the slider at that point, so that the slider does not 'lock up' under heavy impact.
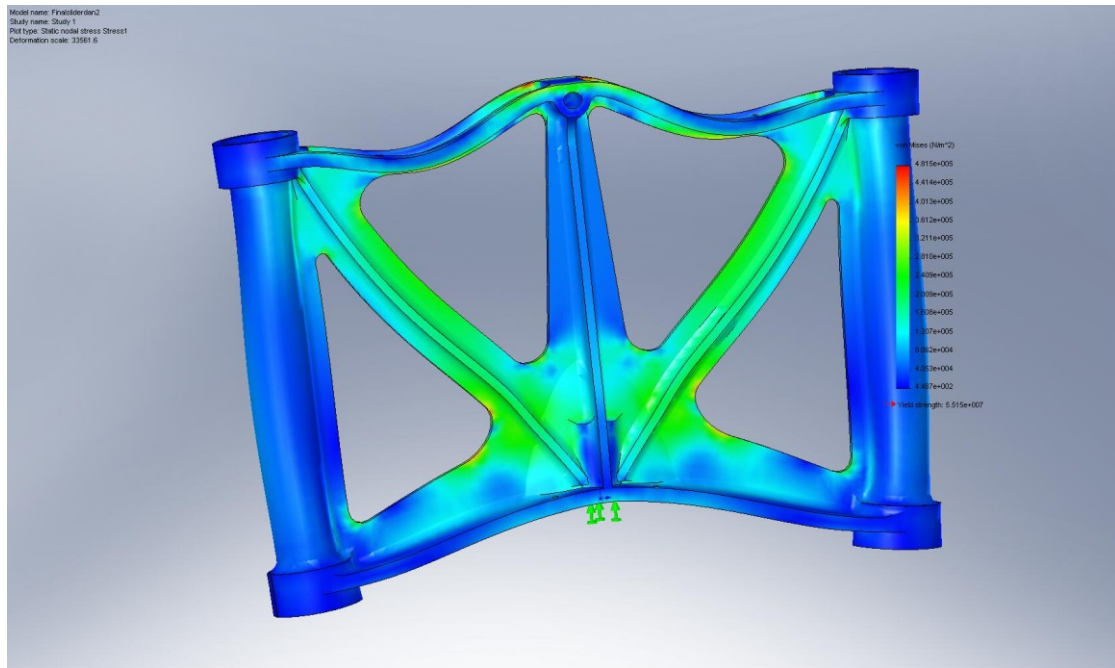
Figure 22 FEA of Slider

This Finite Element model was restrained only at the centre of impact as designated by the green arrows in Figure 22. The slider was evaluated using FEA and subjected to an acceleration of 500g. The design was optimised to reduce the peak stresses using this model, reviewed against mass and minimum wall thickness. The minimum wall thickness was set at 2.5mm and 3mm for the thin walled tubes, as there is difficulty in manufacture with thinner sections.

Figure 23 shows the manufactured slide, with an air release mechanism. These were made from billeted 6082 T6 Aluminium. During the development of this test machine, a magnesium slider has been cast and manufactured for a further weight saving, to give a super light-weight slider. This was needed in order to conduct research for the Home Office (HOSDB) on protective equipment for violent situations, where the falling mass needed to be lower at 1.2Kg. Magnesium with a lower density of 2,300 Kg/m^3 allowed for the reduced weight in the slider, without a redesign.

Figure 23 Slider and Release Mechanism

4.2 Description of Tower.

A drop tower is a simple device for impact testing of materials. This consists of a drop weight, various anvils and impactors, a load cell and recording equipment. The design is similar to that of the Dynatup™ 8200 range from Instron [56], but with an improved test area, and lighter slider. This drop tower has been designed to accommodate larger test specimens and had a lighter carriage than that of the Dynatup™ range. It meets the requirements to perform the following test standards:

Standards Primary
EN 13158-2000 Equestrian
EN 1621-1-1997 Motorcycle
EN 1621-2-2003 Motorcycle
HOSDB provisional

Secondary Standards are available.
EN 6183-3-2000 Cricket Various
EN 6183-4-2001 Cricket Gloves
EN 13277-1-2000 Field Hockey
EN 13277-1-2000 Martial Arts

52

4.2.1 Overview of the Design

The design of the drop tower is to some extent constrained by the scope of the standards or materials that are being tested but all contain the following major elements.

4.2.2 Dropping Apparatus

The apparatus shall be such that a mass (``falling weight'') may be released in order to drop along a guided vertical path onto the sample placed on a test anvil. The centre of the mass of the falling block shall lie over the centre of the anvil. The mass shall weigh (5000 ± 10)[10]. The masses on this research tower were all calibrated to within 1 gram with a high precision scale.

This impact tower, with a 1.3m drop height and 350mm wide working width and with a modular anvil and impactor system, will allow quick and easy switching between standards. By tuning the weights of the interchangeable impactors, the need for additional weights to be added to the slider can be negated. This allows for a significantly easier operation and leads to fewer errors during testing. To automate the system further, a pneumatic lift can be used to raise the slider, reducing the risk of user injury. Safety interlocks and release mechanisms are all pneumatic to improve reliability and safety in the event of power failures. With no air pressure, the device will not lift or release. Two release buttons ensure that the operator must use both hands to allow the mass to release. There are two air operated interlocks, one on the door and the other on the release mechanism, which will not allow the mass to be released unless the door is closed and the slider is in the release position. The tower is enclosed by an aluminium and polycarbonate protective cell, with two opening doors for loading. These doors are height adjustable for allowing large protective devices to be tested, in the space below the doors.

The tower in Figure 24 shows the evolution of the drop tower to HOSBD specification. This has multiple features including a dual load cell platform, lightweight magnesium slider, an air lift mechanism, and dual interlocking doors for safety. The slider cannot be dropped unless the doors are closed and the slider is at the top of its movement, against the stop. This allows for anvils and parts to be loaded safely as the release mechanism is not pneumatically engaged until the slider is lifted.

The tower also has a linear slide for the speed measurement, so that the height above different samples for the terminal velocity can be easily adjusted. The air valve at the top of

Figure 25 does not allow the release mechanism to fire until the slider is at the top of its travel against the height stop.
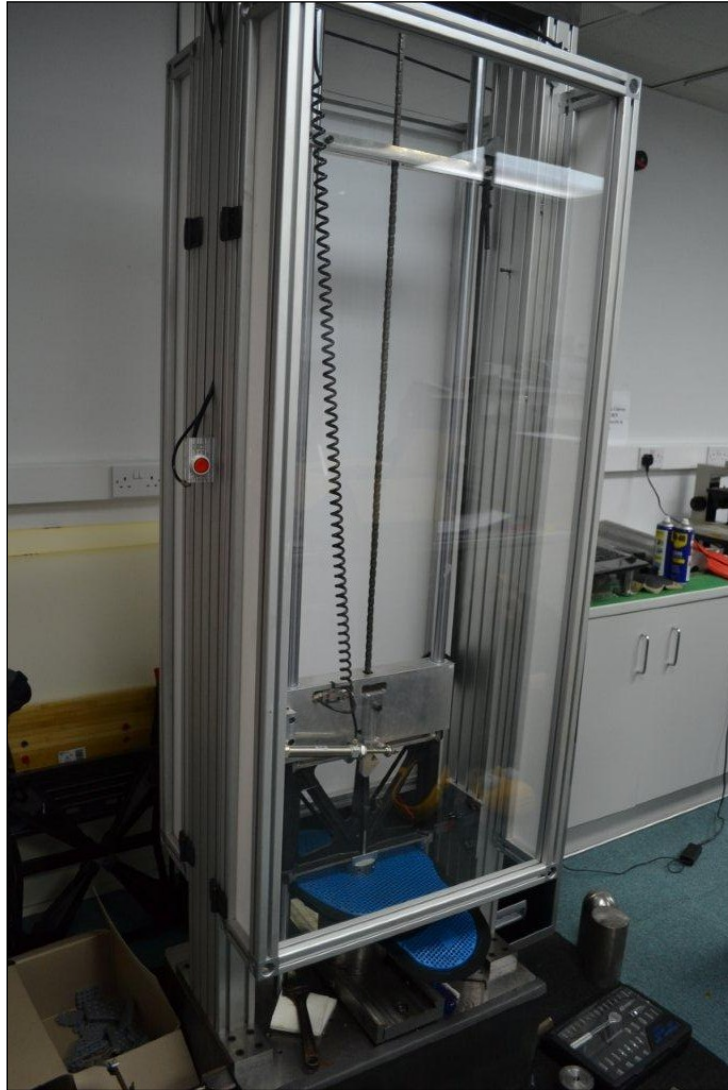
Figure 24 Drop tower evolution

4.2.3 Specification.

Size :   500mmx700mm foot print

Height: 2.55 meters

The Maximum drop weight is 5Kg

The Minimum drop weight is 1.6Kg

The Maximum drop height is 1.30 meters.

Figure 25 Detail of Release mechanism.

4.2.4   Modular Impactors and Anvils

The design and materials choice for the anvils and impactors is defined by the test standards. The overall design of these can be found in the standards, namely EN1621-1 and EN1621-2. However, a modular system of impactors and anvils has been designed to allow for very simple attachment to the drop tower. They have been constructed to be exactly the same height as well as the correct weight so that the tower can be quickly changed between one standard and the next, without the need to change the release mechanism height. The standard defines that they are made from polished steel but does not specify the grade. EN24T or EN8 steel (as appropriate) which was chosen for its ease of availability and good machining qualities. Typically the harder EN24T was used for the anvils or impactors that are more complex to machine, so that the softer EN8 would be semi sacrificial if metal to metal contact were to occur.

The vertical restraints, as specified in the test standard for the slider, release mechanism and stop are LPBR bushes and a 30mm diameter ground shaft, as supplied by SKF. These are held in the lower and upper supports made from plough ground steel. This base provides added mass for the tower of 1000 kg, as specified by the test standards. The base raises the test area off the floor by 300mm. This helps ease of use and also ease of loading.

A control system is mounted on the protective guards. This controls the release, lift and lowering of the release mechanism. In normal operation, the operator controls the system with a series of simple air actuated push buttons.

NOTE: There is an inbuilt safety system so that the slider will always slowly return to the bottom, via a small air bleed valve, this is so the test equipment cannot be accidentally left in a high energy state. The side of the main base houses the data logger and air pressure regulation systems. The

main guard is manufactured from extruded aluminium, and 5mm polycarbonate, to which the safety interlocks are mounted.

4.2.5   Control Panel

The machine has four buttons. These are clearly labelled on the sides of the machine.

The controls on the machine are as follows.

UP   Lifts the release slider up.

DOWN   Lowers the release slider

FIRE   Two buttons pressed together, allow the anvils to be released from the release slider.

4.2.6   Overview of the Data Logger Control System.

This is created in Labview software. The data is captured on a 9234 4 channel NI logger running at 50kHz.

The full raw trace is recorded, which is beyond the scope of what is required by the BSI standards. The peak force is also determined by the software. There is a software 4th order Butterworth filter that can be applied to the load cell trace, in accordance with CE BSI testing protocols, and again the peak force is determined and displayed by the software. The speed is measured by a fork light gate in the final 25mm of travel. A second channel measuring acceleration has also been implemented. The software was developed by employees of DJPdesign Ltd. under the guidance of the author.

4.2.7   Power failure

In the event of a power failure, the machine is still safe as the controls will still work, but the data logger will not function. In the event of an air failure or low pressure, the system will halt. The

release mechanism will not allow the slider and impactors to be released. If left for prolonged periods of time, the release mechanism will very slowly move to the bottom of the sliding rails.

In the event of an air failure, when the release mechanism, slider and anvil are ready to be fired, the system will NOT fire. The release mechanism, slider and anvil can be lowered by the operator without air pressure, giving an intrinsically safe system.

4.2.8   Component Specification.

Part Number	Company	Description
PCB Load cell 208Bx3	PCB.COM	Piezoelectric Load cell.
Signal conditioner	Four Channel 482CO5	PCB LTD
Four Channel Data Logger	National Instruments	NI 9215
		4-Channel ±5 V, 50 kS/s per Channel, 24-bit IEPE Analogue Input Module
779351-01	National Instruments	LabVIEW Application Builder for Win NT/98/95 is add-on package to create stand-alone executables.
LBBR30 - SKF	SKF.com	LINEAR-BEARING LBBR30 – SKF
LJMH30-ESSC4 2m SKF	SKF.com	LINEAR-SHAFTING
493-8319	RSwww.com	3N aluminium profile system,45x45mm
CP95SDB50-760	Pneu-Store (UK) Ltd	760mm stroke, 50mm diameter double acting cylinder
CQ2B50-20T	Pneu-Store (UK) Ltd	20mm stroke, 50mm diameter spring extended cylinder

4.2.9   Risk of Injury from Moving / Falling Slider and Anvil.

Injury within the enclosure is eliminated by secure interlocking of the cage door. This is further reduced by the addition of dual fire buttons. These are placed either side of the door and during normal operation so that a two handed operation is needed. These buttons are over 500mm apart. If the door was open and the door interlocks by-passed, it would be difficult to operate these buttons as the door would physically be in the way.

4.2.10 Risk of Injury from Slider Lift Chain Breaking.

There is a very low risk of the chain failing in the machine. This has been minimized by over specifying the chain and by examining the chain daily in the pre-checks.

It should be noted that:

The chain tensile strength is 8940N which is equivalent to 911Kg. Normal operating tension is <15KG. i.e. the Safety Factor against tensile overload is more than 50 times.

A chain that is out of line or old might be considered to have a tensile strength well below the manufacturers stated strength. To this end the chain will be changed periodically.

4.3   Chapter Conclusions

This section has reviewed, and analysed the current certification procedures for Personal Protective Equipment. It has highlighted two contact geometries (anvils and impactors) that can be used as basis to develop new techniques for developing energy absorbing protective systems. One is based around a point contact and the other is based around a Hertzian line contact. These geometries represent those used in current motorcycle PPE tests, namely En1621 part 1 and part 2. The geometries have been used to develop a set of tests that can be used to screen materials efficiently at a variety of impact speeds, strain rates and energies, as well as different environmental

conditions. These developed techniques are used to test the experimental materials in the next chapter.

To develop these techniques a bespoke highly accurate drop tower assembly was designed and manufactured, with an impact velocity is repeatable to ±0.25%, and a 50kHZ data acquisition system linked to a high accuracy piezo-electric load cell, with bespoke software. The testing techniques developed for this research have become the basis for some of the recent changed to these standardised tests within Europe. The machine design has become the basis of a newly developed Home Office standard.

5 Homogeneous Polymer Development.

Introduction

Chapter 3 examines impact characterisation of different energy absorbing systems and what characteristics would be advantageous in an efficient system. Dilatant materials on their own are good at absorbing energy and conforming to the body, but a dilatant compound will not remain conformed to a known shape, or return to a known shape, and is essentially a fluid at low strain rates. It is very difficult to test dilatant fluids on their own, and moreover it is not possible to produce a self-supporting material from pure dilatant.

As hypothesised in Chapter 4, it was necessary to produce a blended polymer that could be used for future experiments, which could also be used to produce an injection mouldable material with highly strain rate sensitive properties.

This chapter reviews the initial study conducted during this research, that looked at creating different polymer blends to characterise the effect of changing the dilatant volume fraction with different polymers in monolithic form.

To this end, self-supporting polymer samples were moulded into standardised test plagues on an injection moulding machine. An initial TPE grade was selected by reviewing the processing temperatures and glass transition temperature (TG) and determining what would be compatible with a silicone. A thermo plastic elastomer (TPE) was selected, as it is commonly used in conjunction with silicones. The chosen initial polymer was Hybrar™ which has a (TG) well below test temperatures and so should not affect the results. This has been achieved or attempted by utilising homogeneous co-polymers with silicones in the past, but co-polymers with silicone dilatants have

not been tried previously. Samples were developed on a twin screw extruder, the extrudate was pelletised and then injection moulded into plaques 2mm and 6mm thickness, 150mm square, with an edge knife gate. Samples were prepared externally and provided by the sponsor, as shown in Figure 26.

Figure 26 Picture of 6mm Plaques. Hybrar left, 90/10 middle, 70/30 right.

5.1.1 *Impact testing of Thermoplastic Elastomer (TPE) and dilatant blends, single blend screen.*

The tests carried out during this investigation are analogous to those described by EN 1621-1 and EN 1621-2; common tests for certifying the performance and safety of motorcycle protective wear. By increasing the drop height or changing the falling mass in a series of tests, it is possible to carry out tests at different impact energies, above and below that of the standard at 50J specified in the standard test. Each test was carried out three times for each sample, allowing an average peak transmitted force to be calculated and used in comparison. In addition, measurements were made of thickness and mass of each sample.

The following tests were carried out on standardised plaques of Hybrar-dilatant blends, with varying degrees of dilatant content, 0%, 10%, 30%, 50%, 70% and 90% by mass.

The data sampling rate was set to 50Khz, faster than needed for the standard, and the filter necessitated for the standard was implemented in the software. Both the raw traces and the filtered traces were recorded. The standard tests of 50J were completed and then the drop height raised to increase the energy in 10J steps to a maximum of 80J. This was done to gain knowledge of the failure mechanisms and to see at what point the samples started to fail with different degrees of TPE content, as well as to start to understand the failure mechanisms.

The initial tests were also completed at low and high temperatures; -25°C and +40°C, which are lower and higher than those specified in most certification standards, including military specification, but these represent the limits of what is practically possible on an open drop tower, and gave a wide spread for the initial screening tests. The samples were removed from the chamber where they had been conditioned for 24 hours and tests were completed as soon as possible, which in practice was limited to a maximum of 60 seconds.

The samples were also immersed in water at 22°C for 24 hours, to see if the samples were hydrophobic, this was reviewed by physical inspection and any deviation from expected impact performance, when compared to the air conditioned experiments.

Repeat impacts were also conducted, in order to explore relaxation effects, as well as damage tolerance. These were conducted at 15 second intervals.

Unless specified, the laboratory temperature was 22°C and 50% relative humidity. The peak transmitted force value was taken from the force time trace as an electronic value in the software.

Figure 27 shows a typical screen capture from a test in the software; the software stores the raw and filtered data in the same file. This screen capture shows the peak raw transmitted force, which was used in preference to the filtered peak force, as required by the standard test method. Figure 28 shows an equivalent force time plot for the 12mm plaque (2x6mm) tested to EN1621-2. Again the peak of the raw data was used. The screen capture images were saved for quick reference and the complete data was captured in a text file. It should be noted that the accelerometer was not plugged in for these tests. Other than the filter, and the impact speed, which was changed for different test energies, tests were always run in accordance with CE EN1621 specifications.
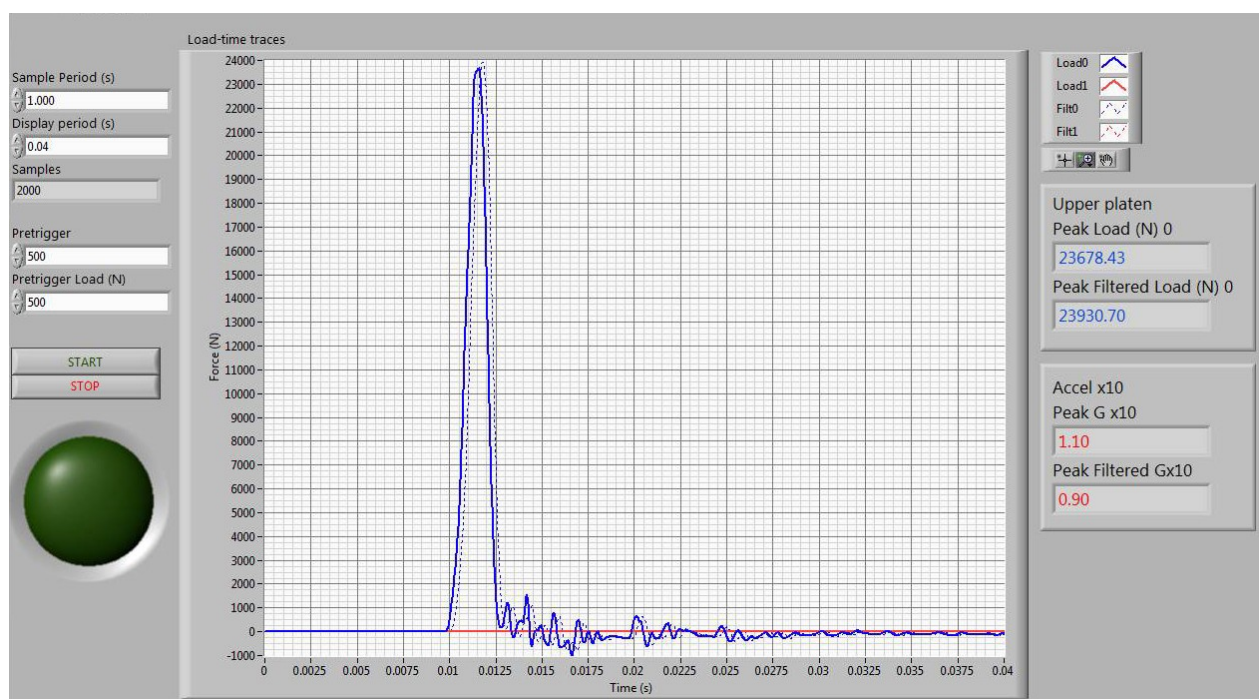
Figure 27 Screen capture of software for EN1621-1 Force time trace for 50/50 Hybrar dilatant blend 6mm
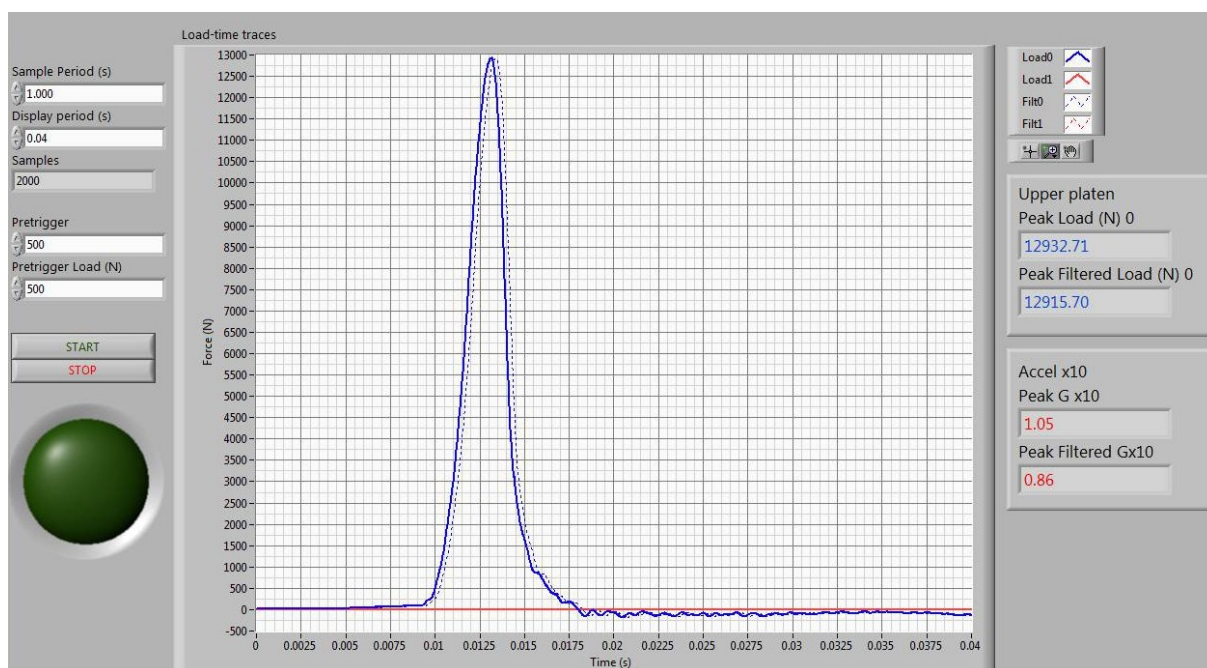
Figure 28 Screen Capture of Software for EN1621-2 Force time trace for 50/50 Hybrar dilatant blend 12mm

The objective of the work described in this chapter was to look for trends and optimisations. A full set of test results of this initial screening of materials, are shown in Figure 31, along with the testing notes. Tests were repeated, and in general had a variance of less than 1. Where variance was higher, it was often the case that there was significant damage to the plaque, as shown in the notes. Continued testing was not conducted on these samples to reduce variance, but the poor variance was used as an indicator to examine the samples further.

Lower transmitted forces measured in samples coincided with less damage and less variance. The data had the greatest variation of results at 30% dilatant volume fractions; these samples were not as well made and were not as homogenous as the others. There was visible "skinning" on the surface of the samples. All tests on the 2mm plaques were halted, due to excessive loads on the load cell. Tests on batches 20-25, namely, 50J on 6mm samples according to EN1621-1, were halted due high loading and samples splitting as shown in Figure 29.

Figure 29 Samples splitting

Some samples have some flow orientations from the Injection moulding process. The plaques were moulded in a standard test plaque tool with a knife gate at the end of the tool, it was felt at the time that this would produce more useable samples rather than injecting into the middle of the tool, which could produce uneven flow around the centre of the plaque. The knife gate at the edge of the tool did however leave some undesirable flow characteristics at one end of the plaques, as can be seen below. Tests wherever possible were conducted on the more homogeneous end of the plaque. Flow lines can be seen on the pure Hybrar sample in Figure 30.

Figure 30 Hybrar standard sample showing flow lines from gate.

Figure 31 First Screen Test Results.

Constants: Mass (kg) = 5 · g (ms⁻²) = 9.81

Material	Dilatant %	Blend	Number	Thickness mm	Total mm	Height m	Speed m/s	Energy J	PF 1	PF 2	PF 3	Ave	SD	VAR	Notes
Hybrar	0		1	6	6	1.000	4.43	49.05	31.01	31.99	32.85	31.95	0.92	0.85	Basic EN1621-1
	10	9010	1	6	6	1.000	4.43	49.05	25.93	27.58	26.57	26.69	0.83	0.69	
	30	7030	1	6	6	1.000	4.43	49.05	27.66	27.79	22.84	26.09	2.82	7.94	
	50	5050	1	6	6	1.000	4.43	49.05	22.63	23.42	22.24	22.76	0.60	0.36	
	70	3070	1	6	6	1.000	4.43	49.05	23.33	21.76	22.51	22.63	0.79	0.62	
	90	1090	1	6	6	1.000	4.43	49.05	22.77	22.35	22.64	22.59	0.22	0.05	
Hybrar	0		2	6	12	1.000	4.43	49.05	18.93	18.47	18.30	18.57	0.33	0.11	Basic EN1621-1, 2 layers
	10	9010	2	6	12	1.000	4.43	49.05	16.95	17.47	16.33	16.92	0.67	0.33	
	30	7030	2	6	12	1.000	4.43	49.05	16.42	16.78	14.94	16.05	0.98	0.95	
	50	5050	2	6	12	1.000	4.43	49.05	14.98	15.68	15.02	15.23	0.39	0.15	
	70	3070	2	6	12	1.000	4.43	49.05	16.34	16.31	16.14	16.26	0.11	0.01	
	90	1090	2	6	12	1.000	4.43	49.05	17.03	17.72	17.30	17.35	0.35	0.12	Test 2 split bottom layer
Hybrar	0		2	2	4	1.000	4.43	49.05	34.63	37.58	39.26	37.16	2.34	5.49	Basic EN1621-1, 2 layers of 2mm
	10	9010	2	2	4	1.000	4.43	49.05	32.07	30.49	30.24	30.93	0.99	0.98	Dual convex layers
	30	7030	2	2	4	1.000	4.43	49.05	26.66	26.96	25.83	26.48	0.59	0.34	Dual convex layers
	50	5050	2	2	4	1.000	4.43	49.05	25.22	25.84	25.92	25.66	0.38	0.15	Dual convex layers
	70	3070	2	2	4	1.000	4.43	49.05	32.92	32.31	34.51	33.25	1.14	1.29	1 and 2 cracked, 3rd significant damage
	90	1090	2	2	4	1.000	4.43	49.05	31.25	32.31	31.62	31.73	0.54	0.29	Test 2 failed catastrophically
Hybrar	0		1	2	2	1.000	4.43	49.05	56.30			56.30			Damage through
	10	9010	1	2	2	1.000	4.43	49.05	62.08			62.08			Damage through
	30	7030	1	2	2	1.000	4.43	49.05	85.05			85.05			Damage through
	50	5050	1	2	2	1.000	4.43	49.05							Tests halted due to excessively high forces
	70	3070	1	2	2	1.000	4.43	49.05							
	90	1090	1	2	2	1.000	4.43	49.05							
Hybrar	0		1	6	6	1.226	4.90	60.14	38.16	39.19	40.14	39.16	0.99	0.98	
	10	9010	1	6	6	1.226	4.90	60.14	24.54	26.43	28.75	26.57	2.11	4.45	
	30	7030	1	6	6	1.226	4.90	60.14	30.86	30.09	24.97	28.64	3.20	10.25	
	50	5050	1	6	6	1.226	4.90	60.14	24.79	24.89	24.31	24.66	0.31	0.10	
	70	3070	1	6	6	1.226	4.90	60.14	27.04	27.15	28.45	27.55	0.78	0.62	First two tests through
	90	1090	1	6	6	1.226	4.90	60.14	27.83	29.23	28.92	28.66	0.74	0.54	Firs two tests through
Hybrar	0		1	6	6	1.427	5.29	69.99	37.51	39.35	39.28	38.71	1.04	1.09	
	10	9010	1	6	6	1.427	5.29	69.99	29.60	31.18	32.03	30.94	1.23	1.52	
	30	7030	1	6	6	1.427	5.29	69.99	32.69	32.80	27.55	31.01	3.00	9.00	
	50	5050	1	6	6	1.427	5.29	69.99	26.56	25.77	27.18	26.50	0.71	0.50	
	70	3070	1	6	6	1.427	5.29	69.99	29.68	29.61	29.38	29.56	0.16	0.02	All through
	90	1090	1	6	6	1.427	5.29	69.99	30.69	28.65	29.09	29.48	1.07	1.15	All through
Hybrar	0		1	6	6	1.628	5.65	79.85	39.17	39.42	41.56	40.05	1.31	1.73	
	10	9010	1	6	6	1.628	5.65	79.85	27.61	30.07	28.59	28.76	1.24	1.53	
	30	7030	1	6	6	1.628	5.65	79.85	30.18	33.07	34.55	32.60	2.22	4.94	Dome shapes again
	50	5050	1	6	6	1.628	5.65	79.85	29.96	31.39	30.90	30.75	0.73	0.53	All through
	70	3070	1	8	6	1.628	5.65	79.85	31.23	30.84	38.49	32.85	3.16	9.96	All through
	90	1090	1	6	6	1.628	5.65	79.85	41.28			41.28			Shattered catastrophically, tests stopped
Hybrar	0		2	4.5	9	1.000	4.43	49.05	30.85	32.82	30.93	30.93	1.12	1.24	1 x 2mm plaque + 1 x 7mm APS
	10	9010	2	4.5	9	1.000	4.43	49.05	25.41	25.79	25.30	25.50	0.26	0.07	
	30	7030	2	4.5	9	1.000	4.43	49.05	26.31	24.10	23.83	24.75	1.36	1.85	Dome shapes again
	50	5050	2	4.5	9	1.000	4.43	49.05	21.19	22.96	22.72	22.29	0.96	0.92	All through
	70	3070	2	4.5	9	1.000	4.43	49.05	22.06	23.30	23.37	22.91	0.74	0.54	All through
	90	1090	2	4.5	9	1.000	4.43	49.05	24.21	22.03	24.53	23.59	1.36	1.85	All through

69

5.2 Graphical Data and Trends.

The test results have been tabulated and graphed in accordance to test type, energy, thickness, and environmental conditions. Average peak values were used and trend lines applied in order to help review the trends. These are now reviewed in test order.

5.2.1 Thickness

EN 1621-1 tests at 22°C were carried out on plaques in the following formations – two layers of 2mm plaques (4mm total), one layer of 6mm plaques, and two layers of 6mm plaques (12mm total).
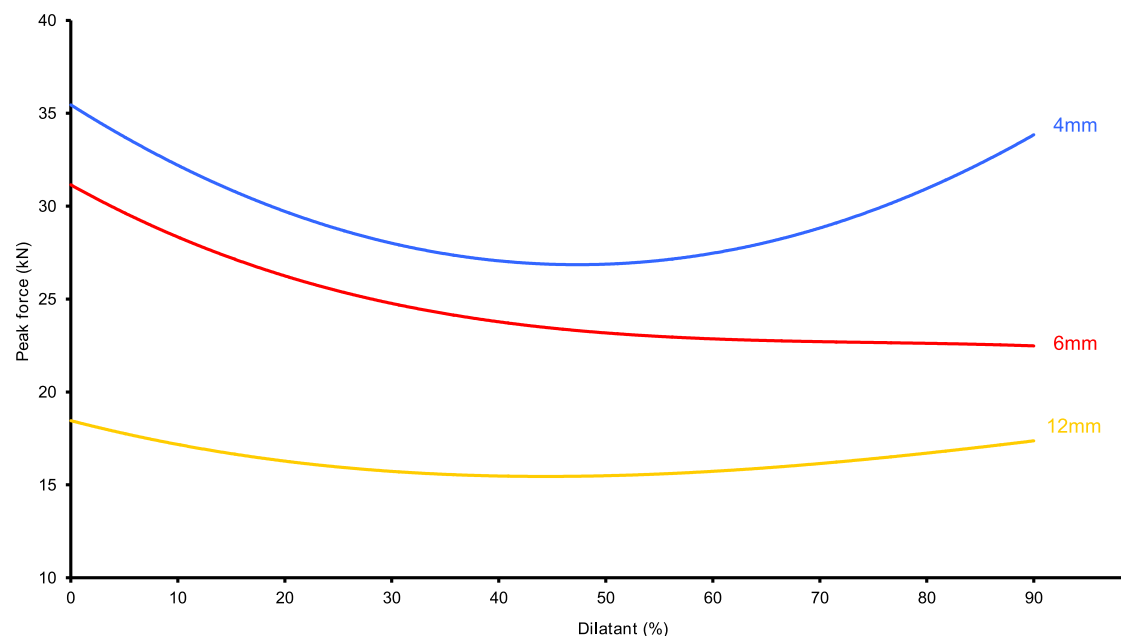
Figure 32 Peak transmitted force versus dilatant content for different thicknesses (EN1621-1, 50J)

As seen in Figure 32, two clear trends become apparent. Firstly, the transmitted force appears to reach a minimum for the 50/50 blend of Hybrar and dilatant. Secondly, as is to be expected, thicker layers of material provide better force attenuation.

5.2.2   Impact energy

Tests were carried out using the EN1621-1 apparatus for energies of 50J (standard), 60J, 70J and 80J, by increasing the drop height keeping the mass the same.
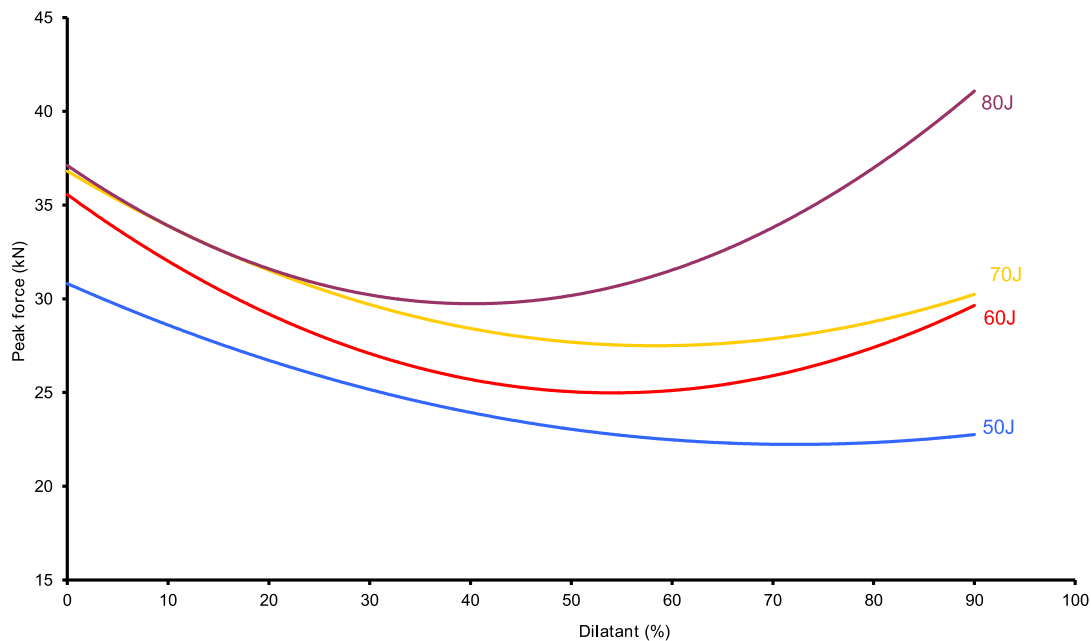
Figure 33 Peak transmitted force versus dilatant content for different energies (6mm)

Again, a curve with a minimum transmitted force of between 40% and 70% plaque was obtained for each series of tests (Figure 33). This trend appeared to be true for tests at higher energies. Interestingly, most of the blends saw little increases in peak transmitted force, despite the higher energies. This is probably due to the fact that not only is the impact energy being increased, but so is the rate at which the impact occurs – hence the dilatant has a greater contribution.

5.2.3 Environmental effects

Tests were carried out at room temperature (+22°C), +40°C, -25°C, and after 24 hours soaking.
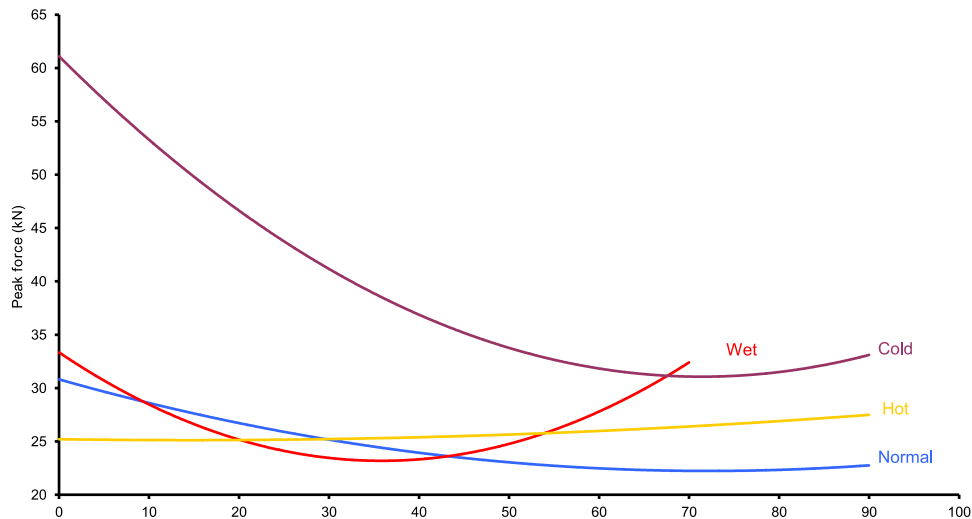
Figure 34 Peak transmitted force versus dilatant content for different environmental conditions

Peak transmitted forces trended towards a lower value for a certain percentage dilatant, depending on the environmental variables. As seen in Figure 34, certain percentage blends appear to be more susceptible to temperature effects than others. The 90% dilatant blend also gave poor performance after 24 hours immersion in water, shattering upon impact and giving a measurement that saturated the load cell at over 115kN. This has not been plotted in Figure 34.

5.2.4 Repeat impacts

Figure 35 shows different compositions tested under repeat impact in the same location for 6mm parts. It appears that each of the materials behaves in a similar way under repeated impact. In general, the transmitted force increases towards a threshold. One notable exception is the 30% dilatant blend, which was observed to exhibit a decreasing peak force after the initial increase, possibly due to Hybrar breaking down and becoming more compliant. This requires further investigation.
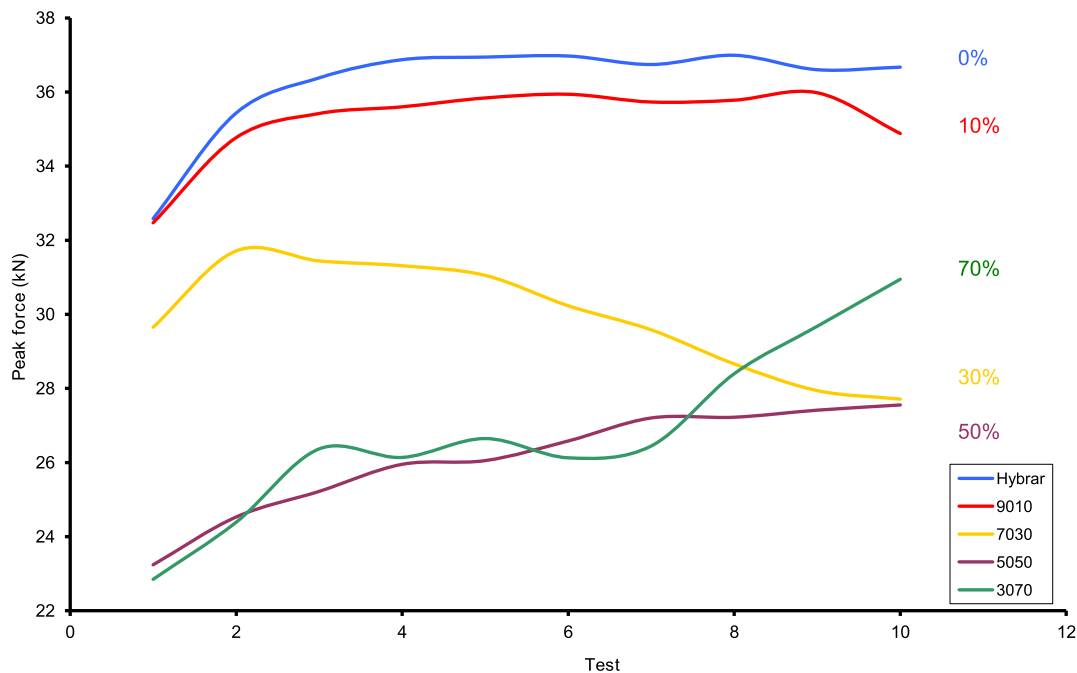
Figure 35 Peak force for different concentrations of dilatant over repeat tests (15s 50J)

5.3   Initial feasablity discussion First Screen

The initial co-polymer blends show a potential benefit of adding dilatant mass to the TPE to make an energy absorbing co-polymer. The findings from this initial screen demonstrate that the performance improvement is shown throughout the tests over the raw TPE. A good compromise was obtained at a 50% co-polymer blend of Hybrar and dilatant. When examined under a microscope, the Hybrar material did not form a homogeneous compound with the dilatant, as shown in Figure 36. The flow characteristics of dilatant compounds in a co-polymer are not well understood and there is no existing data in any publications. For the second round of studies, different TPE materials were trialled with lower melt viscosities and different TG temperature, it was felt that this could alleviate the skinning effect of the Hybrar samples and give a more homogeneous co-polymer.

Figure 36 90% Dilatant 10% Hybrar showing skinning.

5.4   Impact testing of TPE and dilatant blends, Second Screen.

5.4.1   Overview

A second round of materials was developed, learning from the results of the first round of studies.

Different polymers were tested, along with simple composites, and finally tested together with some

primitive geometry. The composites were fabricated by adding a textile to the back of the TPE and

dilatant blends in a heat press. These have been described as tensile layers in the concept Chapter 3.

The simple geometry in this case consisted of drilling multiple holes in the samples to reduce the

weight and improve breathability.

5.4.2   Testing Description

Various blends of thermoplastic elastomer (TPE) and dilatant were subjected to a series of impact

tests at various impact energies. The average peak transmitted forces for each blend were

compared, and data traces reviewed. These formed a base line setting for the materials. The tensile

concept was then added to the materials and a series of TPE/dilatant blends were moulded in a heat

press, in an array of configurations, with and without being over moulded onto a variety of fabrics of

differing tensile properties. These samples were impact tested on the drop tower and the average

peak transmitted forces compared. Finally, a series of TPE/dilatant blends were drilled through and

tested, with the average peak transmitted forces compared to see what the effect of adding simple

geometry to the parent materials would be. This experiment was designed to investigate the

optimum volume fraction of dilatant in combination with parent material (TPE), as well as studying

these materials with an additional tensile layer (making a primitive composite), and the effect of

adding a simple geometry to these moulded parts. The following summarises the findings of

mechanical testing of the thermoplastic elastomer and dilatant blends, and the effect of various

techniques to introduce geometry, weight reduction and increased performance.

5.5 Materials Selection

Because of the surface skinning evident in some plagues when using high volume fractions of dilatant, as shown in Figure 36, four different TPE polymers were selected for further trials. Volume fractions were confined to 70%, 50% and 30%, to limit the amount of testing and samples needed.

Table 5 lists a series of blends of thermoplastic elastomer (TPE) and dilatant, as supplied by the sponsor. Again each blend was supplied as a series of injection moulded plaques of thicknesses 2mm and 6mm. The final column lists the code by which each blend is known

Table 5 Second samples of co-continuous blends

TPE(s)	Proportions			Code
Septon 2063	70% / 30%	50% / 50%	30% / 70%	S2063
Septon 4033	70% / 30%	50% / 50%	30% / 70%	S4033
Infuse D9507.10	70% / 30%	50% / 50%	30% / 70%	D9507
Sibstar 103T	70% / 30%	50% / 50%	30% / 70%	S103T
Hybrar 7125		50% / 50%		H7125
Hybrar 7125 / Arkon P140		40% / 10% / 50%		H7125 P140

Table 6 shows the tests carried out during this investigation in terms of test geometries, test energies and materials used. The textiles used ranged from simple textiles, including abrasion resistant fabrics, to ballistic fibres.

Table 6 Tests for second screen

Test geometry	Energy (J)	Materials used
EN 1621-1	5, 10, 15, 20, 30, 40	6mm H7125
EN 1621-1	5, 10, 15, 20	2mm H7125
EN 1621-1	10, 30, 50, 70	6mm all blends
EN 1621-1	50	Moulded H7125 5050 with various fabrics
EN 1621-2	50	Moulded H7125 5050 with various fabrics
EN 1621-1	50	Drilled H7125
EN 1621-1	50	Moulded blends

5.6 Results

This section shows the peak transmitted force from results of further testing of blends of dilatant with different TPEs, at various impact energies, and using the EN 1621-1 test geometry.
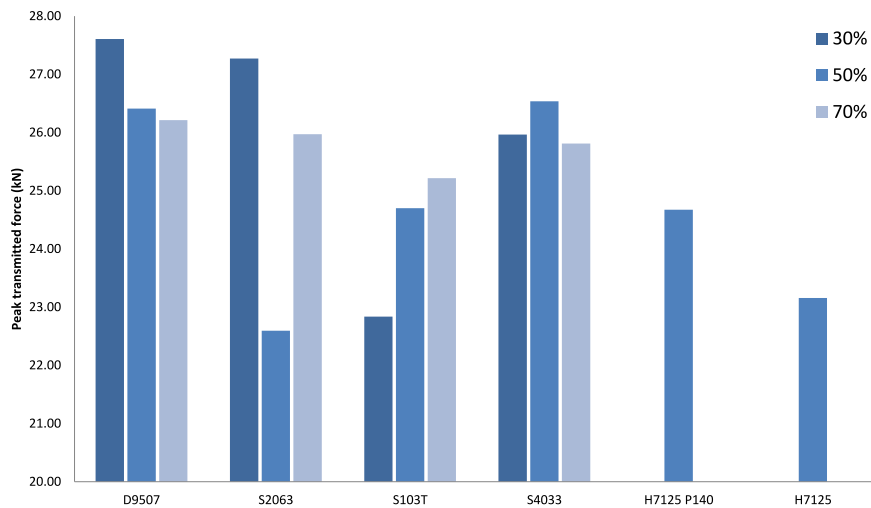
Figure 37 Comparison of peak transmitted force for six blends of TPE and dilatant (EN 1621-1, 50J, 6mm)
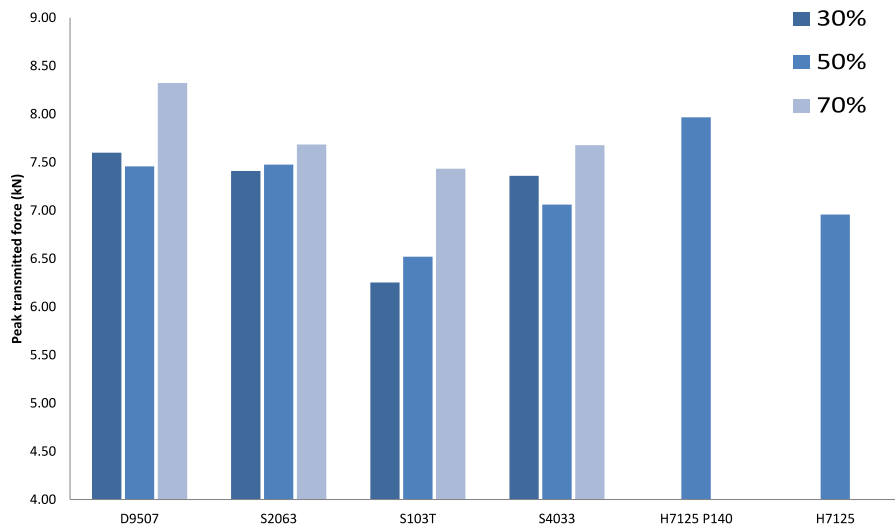
Figure 38 Comparison of peak transmitted force for six blends of TPE and dilatant (EN 1621-1, 10J, 6mm)

Figure 37 and Figure 38 show the peak transmitted force from the second round of plaque tests. Figure 38 specifically shows the same blends when subjected to 10J impact energy (low energy tests); this confirms the previously seen trend of optimum performance from equal blends of TPE and dilatant composition. Both graphs, when considered together, indicate that several of the newer blends outperform the original H7125 50% / 50 % plaque (the control chosen from the initial screen). Each of these series of tests was carried out on a single 6mm plaque of each blend. The results for Infuse D9507 and Septon 2063 appear to show similar trends to those found for Hybrar 7125 in previous investigations, i.e. an equal blend of TPE and dilatant generally performs best. Less clear is the relationship between dilatant content and performance for Sibstar 103T and Septon 4033. Comparison of each of the TPE blends with the original Hybrar 7125 suggests that at higher energies, H7125 performs best, whilst at lower energies the softer Sibstar 103T outperforms most other blends. At 10J, there appears to very little difference between the different blends of Sibstar, Septon and Hybrar.

5.6.1   Impact testing of moulded TPE and various fabric samples – EN 1621-1

A dozen moulds were manufactured from aluminium plates, one shown in Figure 39, allowing geometry control and weight reduction to be imposed on TPE blends through the use of a heated hydraulic press. These were maufactured on the authers CNC mill. Typically a tapered ball end mill was used in a triagualr tool path. The tool path height offset was vaired to give different mould depths ranging from 4mm to 8mm.
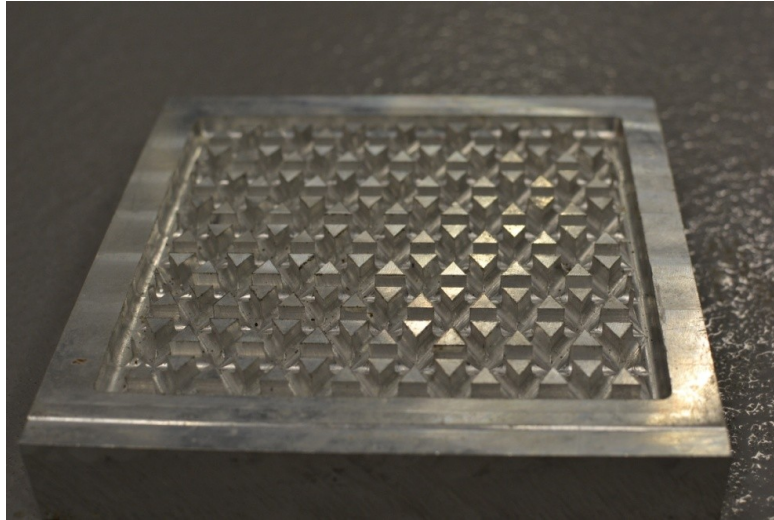
Figure 39 Aluminium hot press tool.

The mould surfaces were sprayed with a PTFE release agent, a TPE plaque was laid on to the contoured surface, a swatch of fabric was included, and lastly the flat top platen added. The assembly was then heated and compressed to achieve a moulded sample with a fabric backing. Using this tool 6mm 50% H7125, 50% dilatant plaques were moulded. Eight different types of textile were used as the 'tensile layer'; one of the samples is shown in Figure 40.
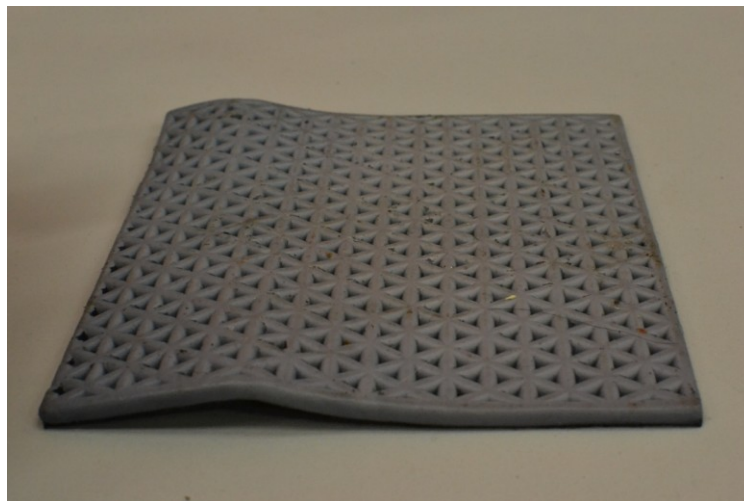
Figure 40 Sample of simple moulding textile face down.
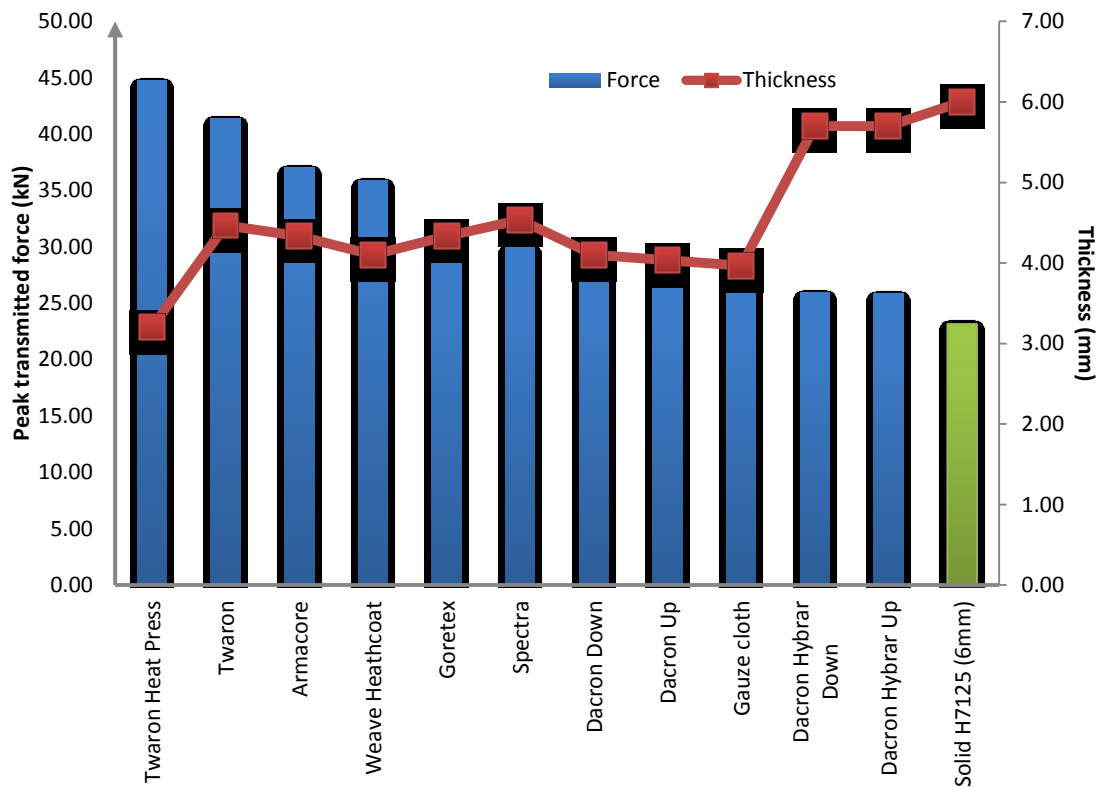
Figure 41 Comparison of peak transmitted force and thickness of various moulded TPE and fabric parts (EN 1621-1)

Figure 41 shows transmitted forces and thickness for each sample tested against EN 1621-1. For these tests thicker samples have a lower transmitted force, which intuitively appears correct. However, comparison of the results between the moulds with Dacron and Gauze, and the H7125 6mm plaque, reveals that a thinner and lighter heat press moulded part with a fabric backing can still provide more than adequate performance. For comparison purposes, the performance of a solid 6mm plaque of H7125 50% / 50% blend is included and highlighted in green.

5.6.2   Impact testing of moulded TPE and fabric samples – EN 1621-2

Figure 42 shows the performance and thickness of various configurations of TPE and fabrics when subjected to EN 1621-2 testing. Due to the added severity of the test, as discussed in Chapter 4, the

materials used in the previous testing were cut in two and assembled in double layers. Again, the performance of 8mm of H7125 50% / 50% blend was included and is highlighted in green. It was shown that thicker samples generally tended to perform better; however a combination of two layers of TPE and two layers of Dacron can again be compared to the slightly thicker H7125 plaque, showing that a thinner and lighter moulded part can outperform the raw plaque.

Most interestingly, the order of performance of fabric backed moulded parts is different from that in Figure 41.
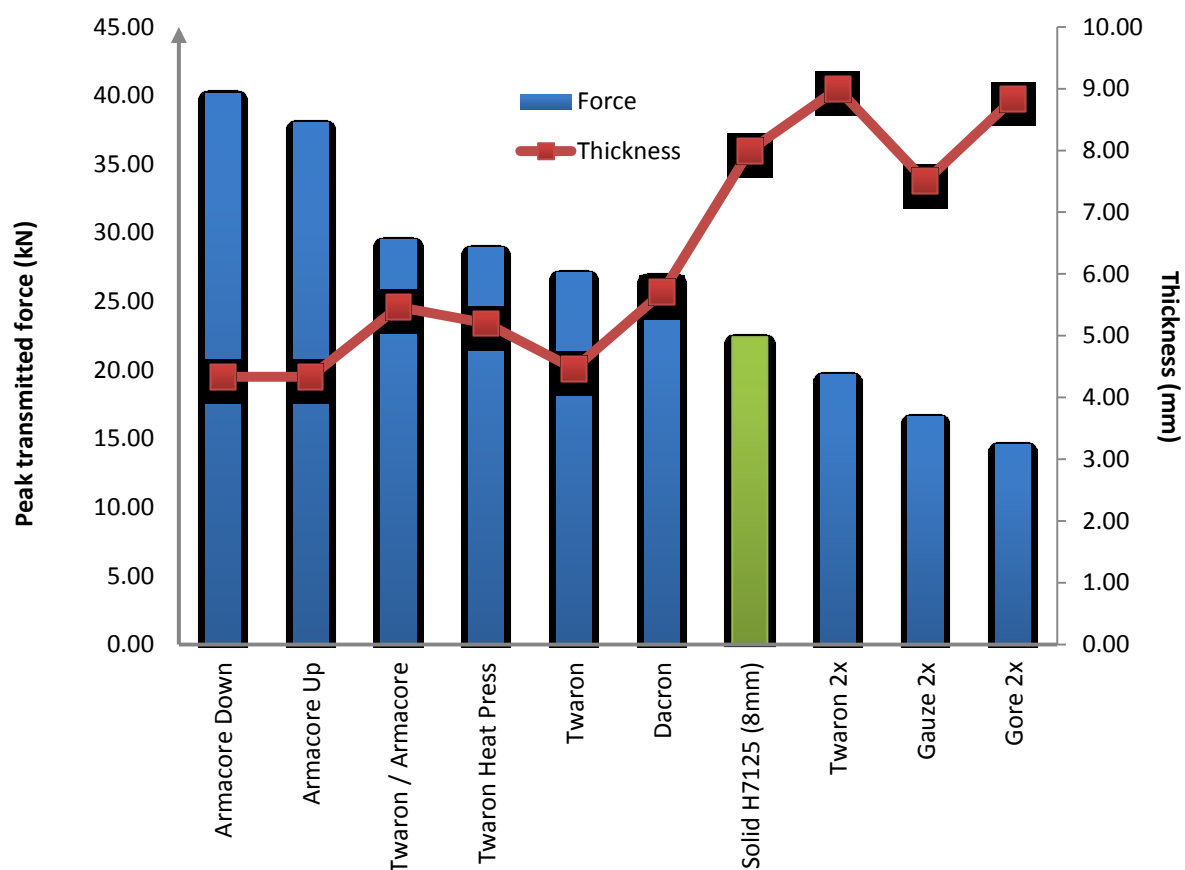
Figure 42 Comparison of peak transmitted force and thickness of various moulded TPE and fabric parts (EN 1621-2).

5.6.3 Comparison of performance between drilled and moulded TPE plaques

Sample plaques were drilled with an array of holes, on a CNC machine with a custom fixture. Holes were 8mm in diameter and a hexagon spacing of 20mm to achieve a 33% reduction in mass, thereby creating a crude breathable part.

Figure 43 shows a comparison between the impact performance of 6mm plaques of H7125 compared with different blends of TPEs with a 50% dilatant ratio at comparable thicknesses. The most interesting aspect is the comparison between a drilled H7125 50/50 plaque and that of its solid

parent plaque. The undrilled plaque achieves the best performance, whilst the drilled plaque is only slightly worse but has 1/3rd less material.
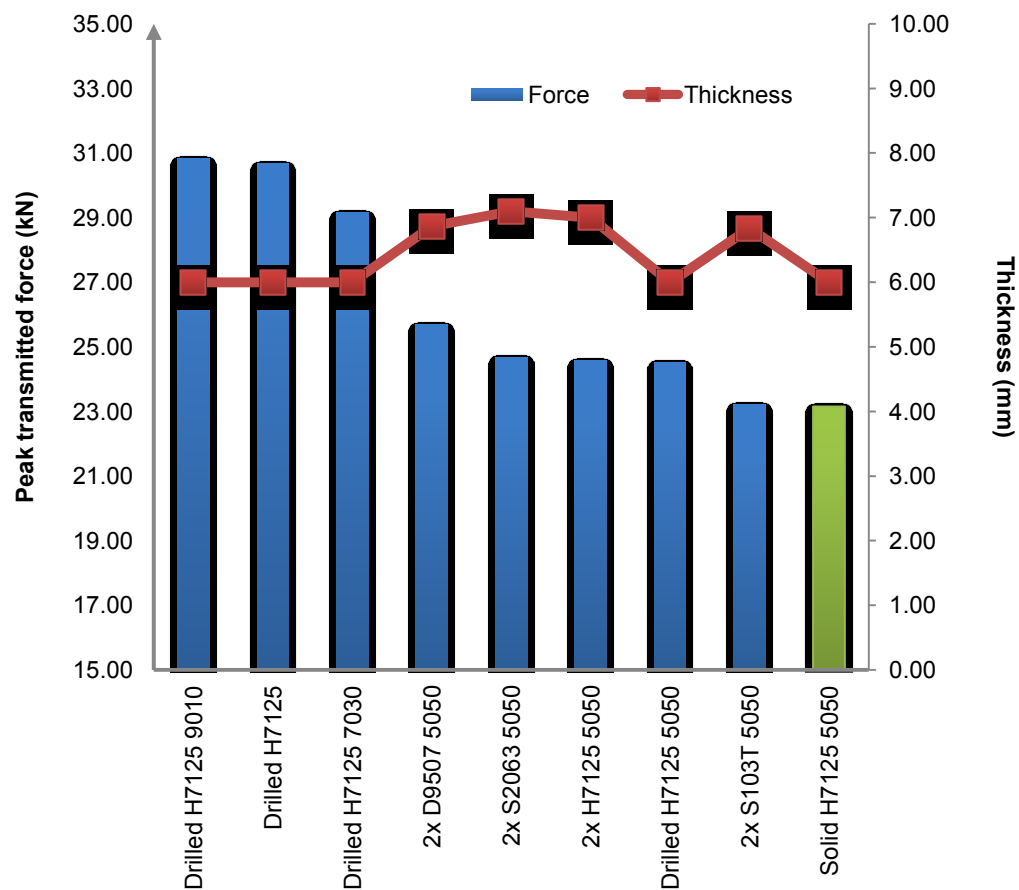
Figure 43 Comparison of peak transmitted force and thickness of various moulded TPE blends (EN 1621-1).

5.6.4   Low energy performance of H7125

Further tests carried out on the original blends of H7125 suggest that the trend of best performance for an equal blend of TPE and dilatant continues even at lower energies. However, this trend is less significant as energy is decreased. The mass of the slider was the same, so impact velocity was also decreasing, along with initial strain rate.

5.7   Discussion of Second Screen

5.7.1   Performance of second round of co-continuous blends of TPE and dilatant

It can be seen from the results that H7125 still outperforms the newer blends at higher impact energies (Figure 37). However, when the impact energy is reduced to below that of 50J, a softer blend begins to give a lower transmitted force. It is assumed that this is due to the softness of the newer blends, resulting in a longer stroke length (i.e. the material deforms over a longer distance, absorbing more energy) or potentially by allowing more dilatant to be involved in the energy absorbing process.

For low energy impacts, a softer TPE should be used in the blend – in this instance, Sibstar 103T or Septon 4033 would be favoured, as demonstrated in Figure 41.

5.7.2   Performance of moulded and drilled TPE samples

Whilst the initial results are promising, it remains clear that more testing needs to be carried out to identify the optimum mould geometry and processing characteristics to produce an energy absorbing or force attenuating device. In the meantime, the results from Figure 38 suggest that most of the blends tested would be suitable for moulding into such a device. The most promising aspect of the testing, shown in Figure 42, is that the drilled H7125 50% / 50% plaque achieves a very

respectable transmitted force when compared to its solid parent, despite the fact that it has had almost 33% of its volume removed. A single controlled geometry moulded plaque can result in approximately 50% of volume reduction, although it must be doubled over before it can surpass the performance of a drilled plaque. A refinement of mould geometry to allow more than 33% of material reduction whilst remaining at 6mm (or possibly a thickness somewhere between 6mm and that of a current moulded part) could potentially achieve even greater performance.

5.7.3 Performance of TPE blends moulded onto fabrics.

Figure 41 and Figure 42 show the effect of various fabric backings on the performance of moulded TPE blends during EN 1621-1 and EN 1621-2 testing. Interestingly, fabrics that perform well in one test generally failed in the other. It is hypothesised that this can be explained by the test geometry and the fabric tensile properties, although further research needs to be undertaken.

EN 1621-1 produces an elliptical or circular contact area and the fabrics that performed best were those that were able to accommodate the deformation of the TPE whilst preventing the whole part from splitting, allowing material to remain between the anvil and impactor. Hence those materials with a high elongation to failure, performed well (e.g. Dacron), whilst those with poorer elongation to failure did not perform as well (e.g. Twaron, Armacore).

EN 1621-2 produces a line or rectangular contact area, and the fabrics that performed best were those that have high strength and were able to withstand fracture from what is essentially a blunt knife. These higher tensile strength textiles accommodated the highly localised deformation of the polymer whilst preventing the whole part from splitting, again allowing material to remain between the anvil and impactor. As a result, high strength fabrics were able to withstand the tests without

failing at such low TPE thicknesses. The more elastic materials failed permanently and were unable to be tested without being doubled up, at which point they performed with merit.

When comparing the controlled geometry moulded parts with their monolithic counterparts tested in the first screen, initial simple conclusions can be drawn. The results of the first screen showed that 4mm of solid TPE and dilatant could achieve as little as 26 kN, by which these modifications can be reviewed. A 4mm controlled geometry moulded plaque of 50% / 50% blend could only achieve 54 kN, which is not desirable, however, with the addition of a layer of fabric moulded onto the same controlled geometry part, it could achieve 28 kN, which is approaching the performance of the solid plaques. This research shows that there is merit in exploring composite structures used in conjunction with a TPE and dilatant blend.

Whilst the moulded parts needed to be doubled in thickness to pass (<18kN) EN 1621-2, the fact that a 7.5mm thick moulded part with gauze either side achieved roughly the same transmitted force as 12mm of solid TPE and dilatant plaque, is worthy of note, suggesting that with further refinements a thinner, lighter, breathable, better performing protective device could be constructed with the aid of improved mould design and, significantly, the addition of layers of fabric.

NOTE : These tests were conducted using samples supplied by Multibase SA, and tested under contract by DJPdesign Ltd. (sponsor). Tests were completed by DJPdesign Ltd. These results are replicated with the permission of DJPdesign Ltd.

5.8 Chapter Conclusions

This chapter follows the development of thermoplastic elastomer (TPE) and dilatant co-polymer blends. This research is an iterative approach spanning three rounds of experiments. Experimentation and analysis of each stage were completed before moving onto the next iteration.

In the first iteration TPE and dilatant samples were blended at different ratios from 100, 70,50, to 30% TPE by mass. The initial screen was a wide sweep, initially to see if it was possible to co-polymerise over this range of blends. This also gave 100% TPE samples that could be used as a control. All of the screened ratios produced samples that could be moulded in plaque form and subsequently tested.

 The secondary aim of this work was to determine if a stable co-continuous blend could be made that would be suited to the injection moulding process; allowing repetitive preproduction of samples. This aim has been completed; prior to this it was uncertain that this would be possible using production equipment. The testing techniques and equipment in chapter 4 could now be used to screen these samples. The techniques could be used to test the impact performance of these newly developed co-continuous co-polymers. This section outlines the merit of certain blends and answers the initial aim of the thesis, to a small extent.

The performing blends with the optimal overall characteristics were in the region of 40-60% dilatant composition. There were some processing issues which have been reviewed. The second iterative round of samples was produced, this time with a narrower dilatant ratio focused between 30 and 70 percent.

The final section of this chapter has explored the use of simple heat press and drilling operations to assess if simple architecture could benefit these polymer blends with these 'primitive' weight saving techniques and a tensile layer.

These experiments showed that up to a third of the mass could be removed from the samples, with very little reduction in impact performance, generating a lighter more flexible part.

The aim of using internal architecture through simple changes in geometry and addition of a simple tensile layer to make a primitive composite has been fulfilled.

6 Re-entrant Geometry -Auxetics

6.1.1 Preface

Chapter 6 reveals that a co-continuous blend of dilatant and TPE, in essence an active Injection Mouldable Dilatant Silicone Material (IMDS) could benefit from a weight reducing geometry. As already mentioned, it is important for body worn protective materials to be breathable, flexible and as light as possible[1]. Improved impact performance has already been seen in a foam which has a negative Poisson's ratio or re-entrant geometry [54]. As stated previously, a material that densifies can give an impact performance improvement over one that does not. The merits of negative Poisson's ratio fibres have already been seen on recent blast protection curtains, and these materials are now known as 'Auxetic' materials, as they were developed as double helix yarns by Evans and Hook [57].

6.1.2 Concept of Auxetic IMDS

A method of moulding and combining active materials with a re-entrant geometry has been discussed by the author below in patent application EP2361023 (A2). This description is included in its entirety, as this IP has now been reviewed and granted. The writer does not wish to publish this information in a form different from the form of the granted IP.

Geometry.

"An additional method of improving the performance of an energy absorbing material is to add re-entrant geometry. This type of geometry gives an unexpected benefit for energy absorption. Impact attenuation, vibration and comfort, performance is improved, as the geometry does not allow for the rarefaction of material at the impact site and can allow more energy absorbing material into the impact site; thus giving an improvement in performance. In a similar way that a tensile layer holds the energy absorbing material in the impact zone, the re-entrant geometry acts to locally densify material at the impact site, to give a substantial performance improvement.

First consider, by way of example, an extrusion of energy absorbing material, as can be seen in Figure 1. Figure 1 shows a front three quarter view showing a re-entrant section of a flexible energy absorbing material. In this example, re-entrant means that if the material is cut through in vertical sections (H) the material must have parts, or columns, or features that are non-vertical. The geometry must be re-entering or pointing inwards, the geometry will thus have a re-entrant angle. This example will have a different Poisons ratio in different directions. When stretched, the sample with gain thickness has a negative Poisons ratio, as the columns move from their re-entrant angle to a vertical angle. When compressed, the energy absorbing material will collapse inwards, giving the equivalent of three thicknesses of material (t) in the impact zone. The geometry locally densifies when subjected to a downwards force (F). The re-entrant geometry will not open up giving only one thickness of material.

Samples have been tested with the same geometry as above where the total height (H) is 12mm, with a section thickness (t) of 3mm. When compared to a the same energy absorbing material, in this case a 50/50 TPE dilatant blend material, of similar mass, or same density but without re-entrant geometry the impact performance is improved by between 30% and 50%, with a further improvement in flexibility.

There are many other types of re-entrant geometry that can be used for the energy absorbing material. For ease of description, these are now described as a repeat unit. First let us consider a simple cylinder protruding in the direction of impact, in this case vertically. If however the cylinder were to taper outwards it would be re-entrant. It is the inclusion of a re-entrant angle that is the distinguishing feature of this geometry. A further embodiment, when considering a single unit, would be to consider the same cylinder, tapering out, but also shelled out from the top, as shown on the left in Figure 2. When manufactured, it would be moulded this way and not subsequently shelled out. If repeated, this would give an energy absorbing material with re-entrant geometry, which if sectioned at an angle crossing the mid axis would give a re-entrant geometry. Thus we have a 3D repeated unit re-entrant geometry.

Similarly, basic geometries can be tessellated to give a re-entrant geometry. Instead of the circle to give the tapered cylinder, we can use a square. This is shown in the central diagram in Figure 2. The visual representation is shown to be shelled out from below. Again when sectioned vertically though the centre, this gives a re-entrant geometry. A hexagon is shown as the unit on the right of Figure 2. These units can be repeated in any regular base pattern. Triangles, squares, hexagons or any other suitable repeat can be used. They can also vary in height and thickness for changing impact needs. They can also be flipped do give a double re-entrant geometry; this can include different materials on each side of the axis, or different geometries, to attenuate energy at different "tuned" levels.

Manufacture.

The hexagon on the right of figure 2 is shown without a base. It may have a base, like the other two, from parent energy absorbing material or from a different material. In one embodiment this can be a tensile layer. In this case a sheet material, preferably a textile based material can be used. If repeated, we can now have a re-entrant geometry, moulded onto a tensile layer. The benefits of both systems can be combined. In this case our energy absorbing material is moulded onto a textile layer, Ideally this would be a injection mouldable material containing a dilatant, preferably a TPE dilatant blend, with the tensile layer being a textile.

Re-entrant geometries can be difficult to manufacture, especially in an open shut type tool. Geometries with a slight draft angle for better mould release or vertical geometry is possible with a two part tool. The amount of re-entrant geometry effect can be related to a re-entrant draft angle. Flexible, energy absorbing materials, especially the active ones disclosed in this patent, can be manufactured with a re-entrant geometry which will allow a certain amount of elastic behaviour allowing them to be removed from the tool i.e. repeat units can be "peeled" from an open/shut type tool.

An energy absorbing re-entrant geometry, 45 degrees to the normal, can be "peeled" from a mould tool when moulded onto a tensile layer, preferably textile. Here the aforementioned benefit of the tensile layer also doubles as an aid for removing parts from tools with high re-entrant geometry. In this manner is it possible to manufacture energy absorbing materials that have re-entrant geometry, or come from a tool with negative draft angle, preferably a draft angle of over 15 degrees.

A more simple 2D geometry, like that shown in Figure 1, can be extruded by any means necessary, and again may be backed by a tensile layer.

A further embodiment can be manufactured by means of an open/shut tool with no overlap or negative draft angle. Here the moulded geometry would be similar to that of castellations. Alternatively this can be extruded. This however does not have any re-entrant angle. The part can be compressed across the castellations and adhered to a textile backing. This then leaves a re-entrant geometry, similar to Figure 1. This can be done in several ways but the outcome is to have re-entrant geometry with a re-entrant angle.

Alternatively a stretch textile can be used, pre-stretched, then attached to the castellations, and once released this would fold the castellation inwards to give a re-entrant geometry. Two layers of

castellations can be joined while compressed at different angles, to give re-entrant geometry. If any of these were to be sectioned they would show a material with a re-entrant geometry with its characteristic re-entrant angle." [58]

F

H

t
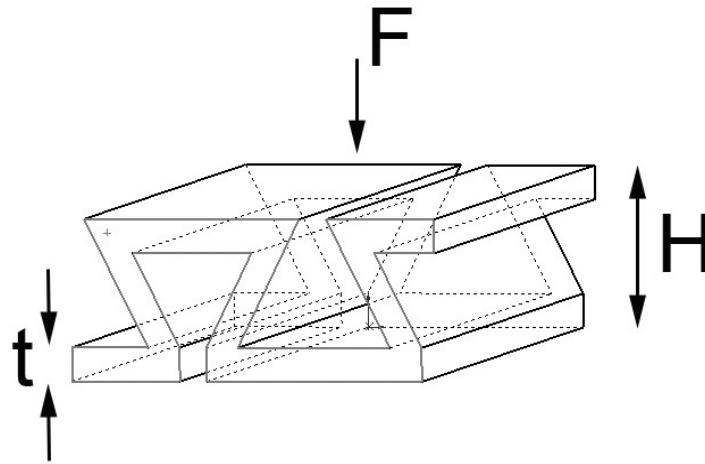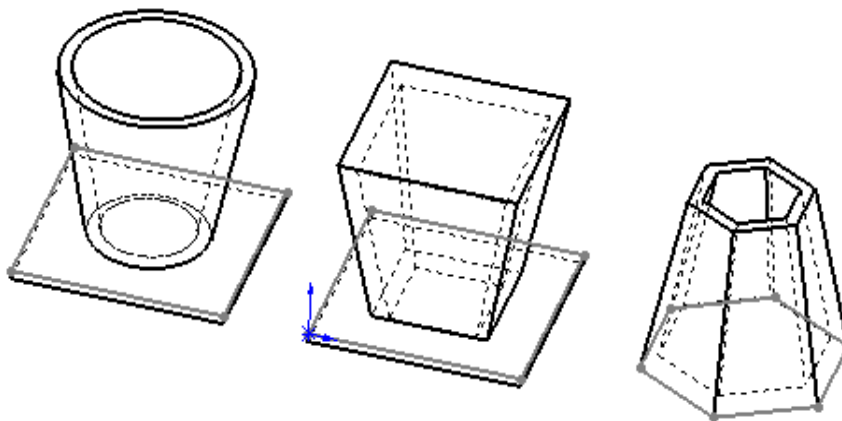
Figure 1(p)

Figure 2(p)

6.2 Initial Geomery.

The geometry in Figure 1p from the patent [58] was produced as a first test piece,as it is expensive and time consuming to cut a complicated 3D injection moulded tool, and there were concerns about the parts being extracted from a complex tool with such high negative draft angles.   This simple extrusion was made to gain

confidence in the structures before moving to a complicated 3D auxetic, as pictorially described in Figure 2p, from the patent.

A simple tool was adapted from a large press, with a water-jet-cut die grafted onto the side to make a primitive extrusion tool. Plaques from Chapter 5 of this document were ground up, and the whole tool put in a hot press. Primitive extrusions were produced as shown in Figure 44.
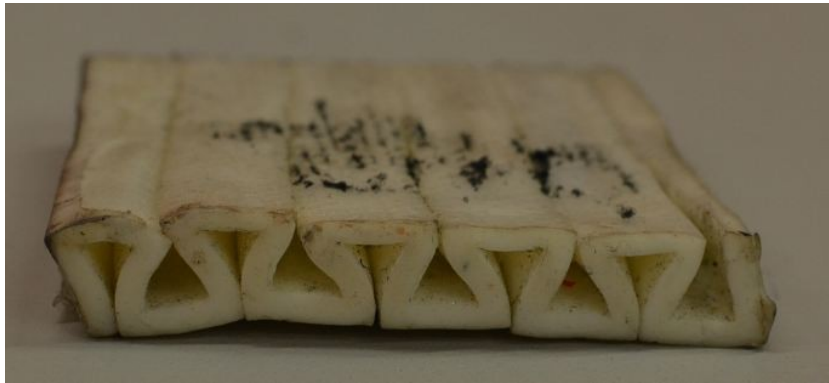
Figure 44 Picture of original extrude sample

6.2.1   Preliminary Results.

The primitive parts, were not perfect, but could be tested and attained an average of 18.83kN transmitted force when tested in accordance with En1621-1. This is similar to the performance of the 12mm plaques which attained 17.73kN. These extruded parts were 11mm thick as there was some shrinkage from the tooling, but were 43% lighter, making them nearly the same area density as the 6mm plaques. The 6mm plaques when tested gave results of 22.76 kN. For the same mass, there was a 20.8% performance improvement in impact performance when considering transmitted force. It would not be appropriate to compare these results to the wider data as these were non-injected primitive samples.

The primitive extrusion gave an impact performance improvement over the same mass of monolithic material in plaque form and was also qualitatively more flexible than the solid homogeneous polymer plaques. This

primitive experiment allowed for the progression to a small injection mould of the shape shown in Figure 1(p) from the patent.

6.2.2 Auxetic design for injection moulding.

When moving from 2D to 3D, the design of the parts becomes more complex. There are multiple ways to tessellate the repeat auxetic cells. In addition, this leads to considerably more difficult mould tool design and also to some abnormal moulding techniques. Particular attention to tool design and negative draft angle were considered.

Figure 45 below, shows one development logbook page by way of example, It shows some of the consequences when moving from 2d sections to 3d parts, when considering the multiple development sketches used to make the auxetic shapes, leading to moulding and tool design.

The original designs often featured hexagon shapes, but they were more difficult to manufacture. The final design was based upon a plurality of circular cells with undercuts. These would have to be made in the thousands for production. The first were CNC turned, but in production these were made with a form tool on a Swiss style machine.
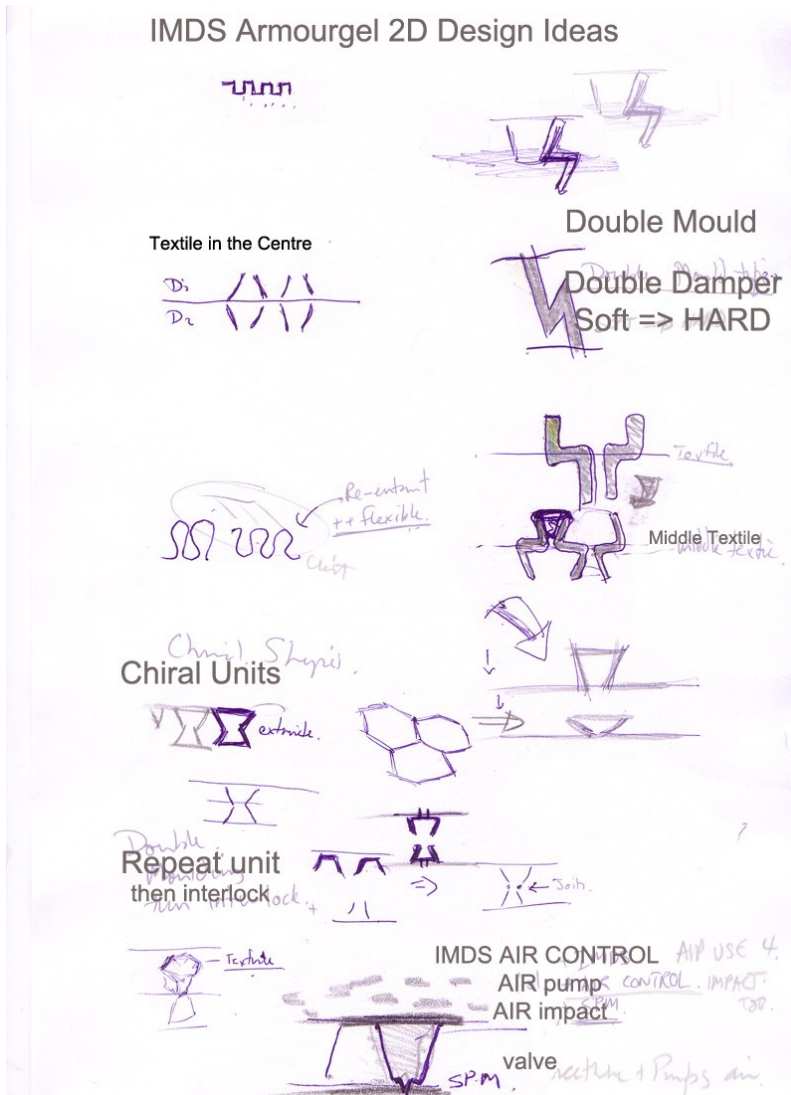
Figure 45 Design Ideas 2D

Figure 46 Single Auxetic Cell core, tooling pin.

The cell 'core' repeat unit is shown in Figure 46. This was originally made in 10mm height for 10mm thick parts.

A re-entrant geometry that allows for improved breathability, flexibility and comfort was designed. Figure 47 shows the final drawing of the part in 10m section (S2), the single cell cores here are set out in a chess board polarity. The section B-B shows the cells as they flip from one way up to the other, leading to the test name S2.

This would be the same section in the perpendicular direction.

The section A-A is a view at 45 degrees to the cross section. This also shows the cells and the cross cut extra sectional holes to add further undercuts, more breathability and save a little more weight. The tool was manufactured and the parts were injection moulded in 50% Dilatant 50% Hybrar co-polymer from Chapter 5.

VIEW TOP

SECTION A—A

SECTION B—B

100.10

10.50
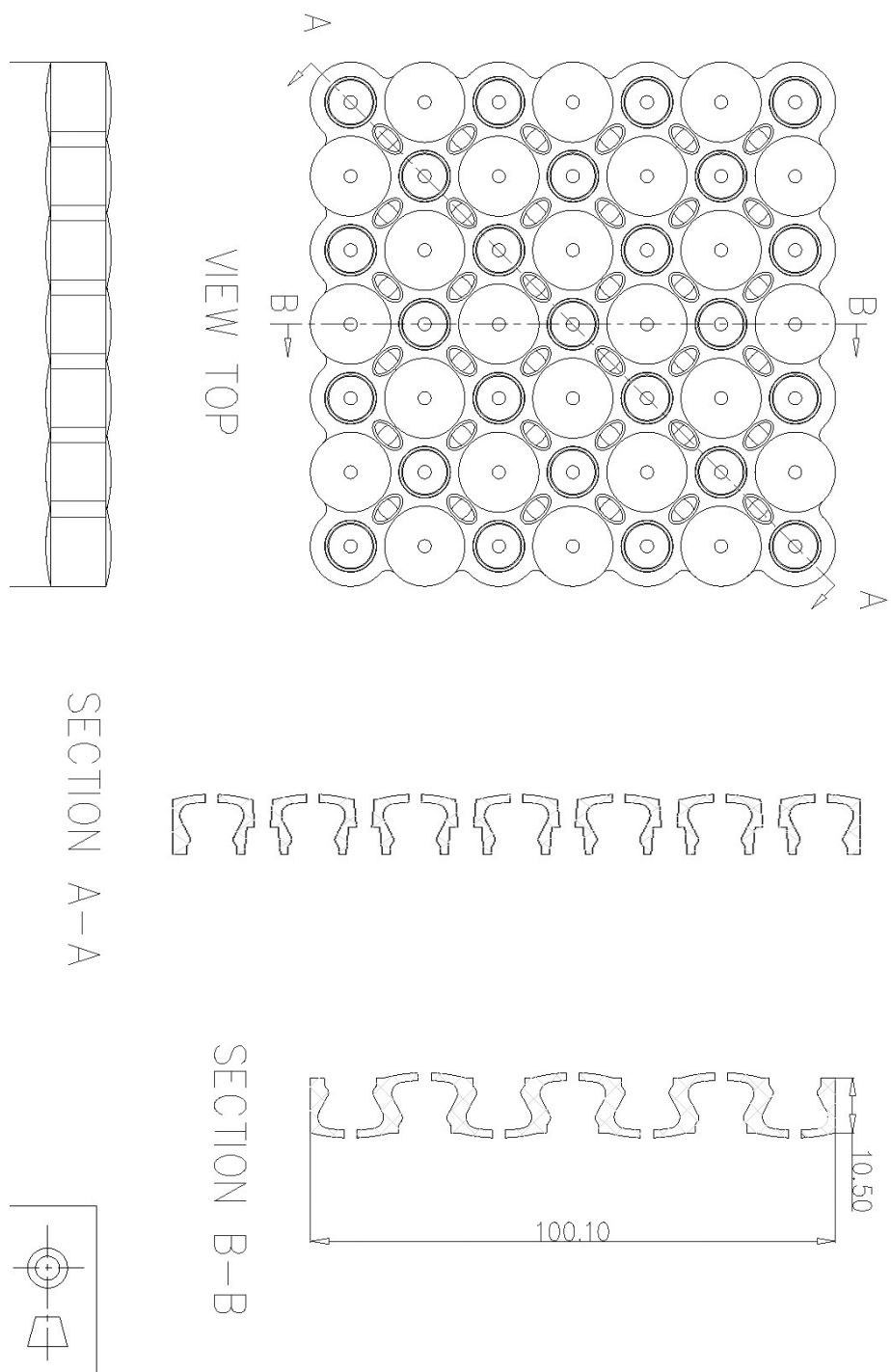
Figure 47 Drawing of S2 Auxetic Geometry.

98
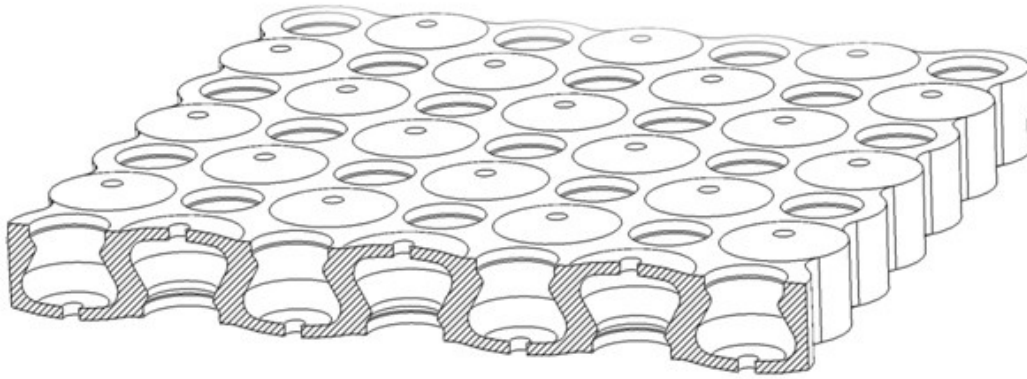
Figure 48 Re-entrant shape. S2 IMDS

6.3 Testing of Auxetic IMDS.

32mm diameter samples were tested on a 250kN Instron frame, with flat platterns.

The tests were conducted on new samples at three different frame speeds, 500, 50, 5 mm per minute. This gave three different strain rates for the sample, approximately 8.3, 0.83, and 0.083 s^{-1}. Compared to the impact speeds and strain rates that happen in the CE type approval tests of Chapter 6, which are over $140s^{-1}$, these are considerably lower. However, due to the thickness of the sample being tested, at only 10mm, the velocity of the machine is changed to give two magnitudes change in strain rate, however this is at the lower end of strain rate that is typical for these devices. The traces have been plotted in Figure 49, load against compression. It is possible to see an effect from the three different test frame speeds, and from the relative increase in compressive force that accompanies these increasing rates.
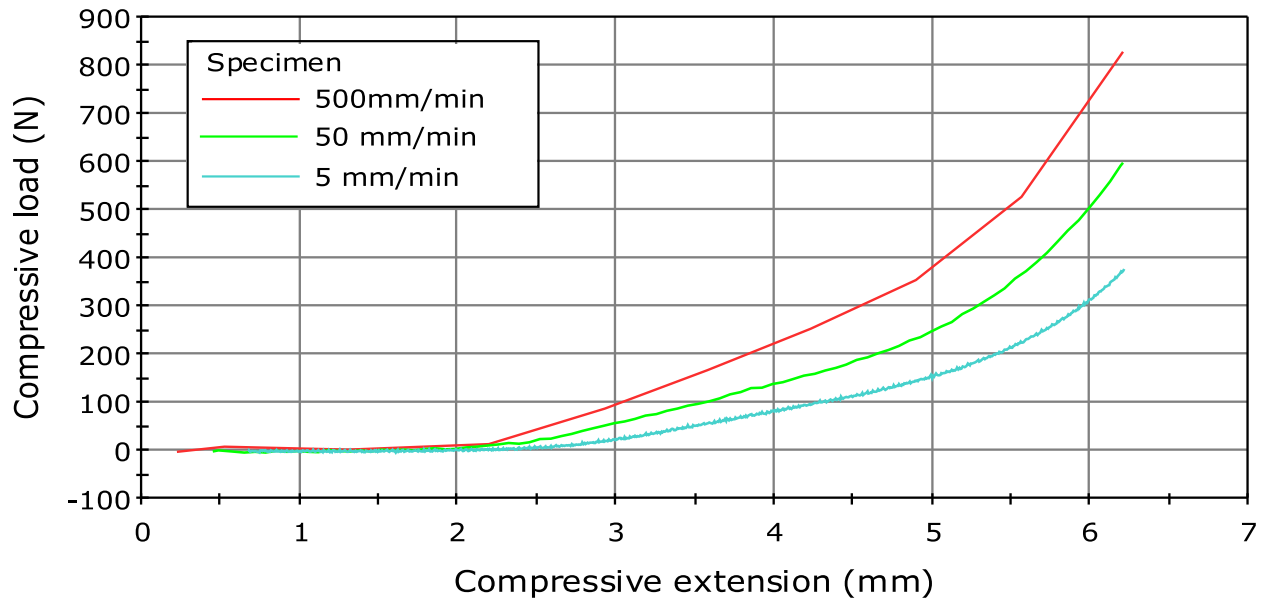
Figure 49 Load Compression curves at 3 rates

For comparison, these parts were tested against a hard EVA 40C memory foam of the same density on an

Instron, using flat patterns, at a rate of 100mm/minute, as shown in Figure 50.
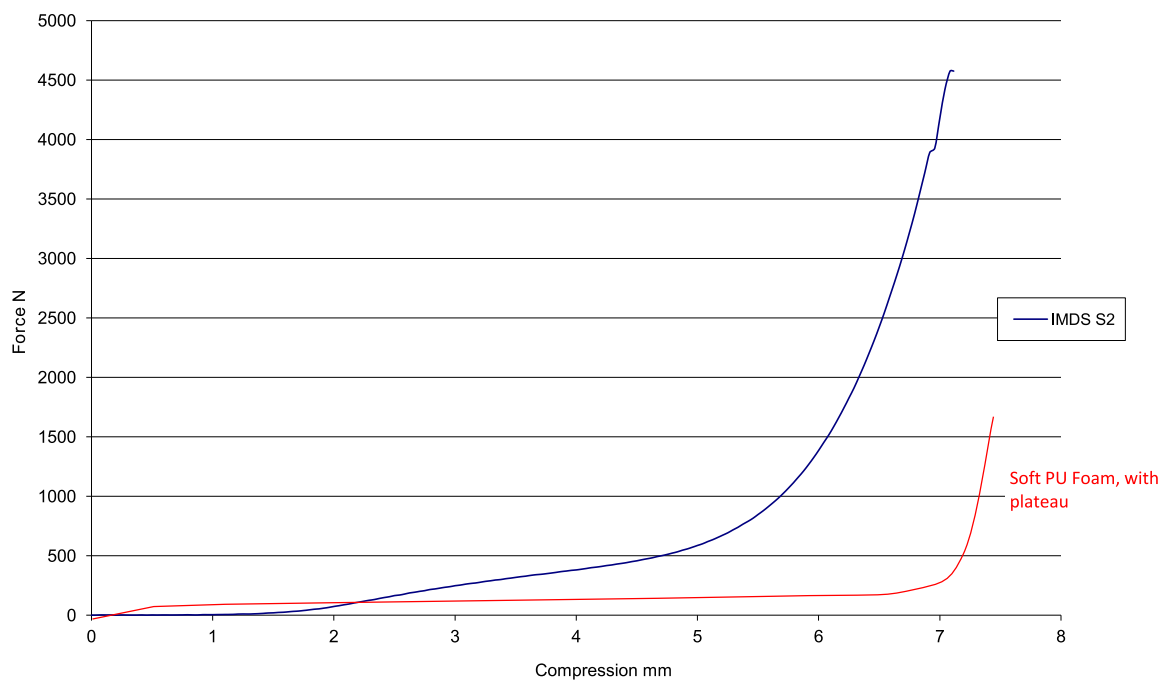
Figure 50 Low speed compression of IMDS S2 and a memory foam of the same density.

100

The S2 parts are softer to the touch than the harder foam, but load up faster than a foam system of similar density. The foam has a flat plateaux region, as is typical, and then quickly densifies after about 7.3mm of plattern compression.

The test was repeated with the samples cut through section B-B in Figure 47. A camera was used to take stills with every 0.2mm of compression. Four frames are shown In Figure 51, depicting the behaviour of the cells during compression. It should be noted that this is a representation of what is happening as the sample was cut in half and will have "edge" effects. With reference to Figure 50 and Figure 51, stage 1 comes from the design of the small domes above the cells, stage 2 is the elastic compression of the part, and at stage 3 there is a sharp rise in compressive force. In stage 4, the 'S' of the 'S2' shapes have almost been compressed completely, to touch the top and bottom surfaces. It should be noted that the through holes are now smaller in the 6.5mm compression photograph, as the material has been displaced. Two reverence lines are shown.
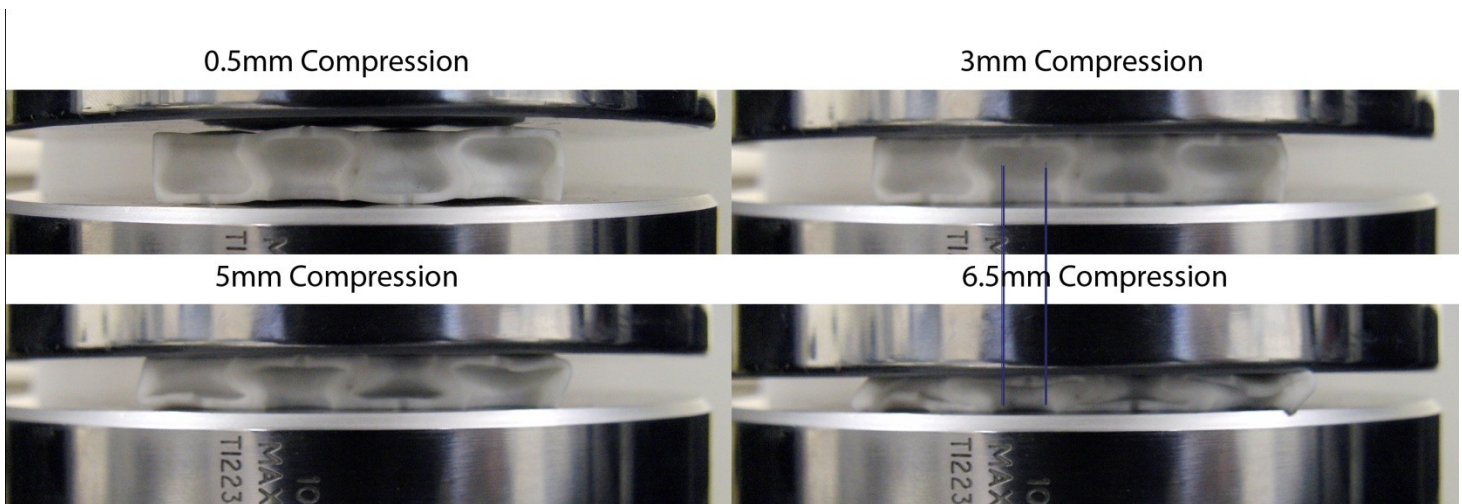
Figure 51 Still images from sectioned compression sample.

6.3.1   Impact Testing

To look at the combined effect of the geometry and the active materials, three parts have been moulded from different materials. The first is a strain rate sensitive material in solid form called Injection Moulded Dilatant Silicone (IMDS), as tested in Chapter 5. The second has the re-entrant geometry moulded in a Thermo Plastic Elastomer (S2 TPE), and the third has the re-entrant geometry together with the strain rate sensitive material denoted (IMDS S2). These have been tested on an impact test rig in accordance to EN1621-1, and the results are shown in Figure 52. The graphs show that the longest recorded trace, with the lowest peak force, is attained when combining the S2 auxetic geometry with the IMDS. This gives a lower transmitted force over a longer time than homogeneous IMDS monolithic plaques. This confirms the potential benefit in using the auxetic shapes.

When looking to compare the impact performance of the geometry, only S2 IMDS and an S2 TPE moulded with the same 'shore D' hardness, can be compared. There is a performance improvement using the active material combined with the auxetic geometry, not only in terms of peak transmitted force but also longer rise time and longer impact duration, as compared to the TPE in the same shape.
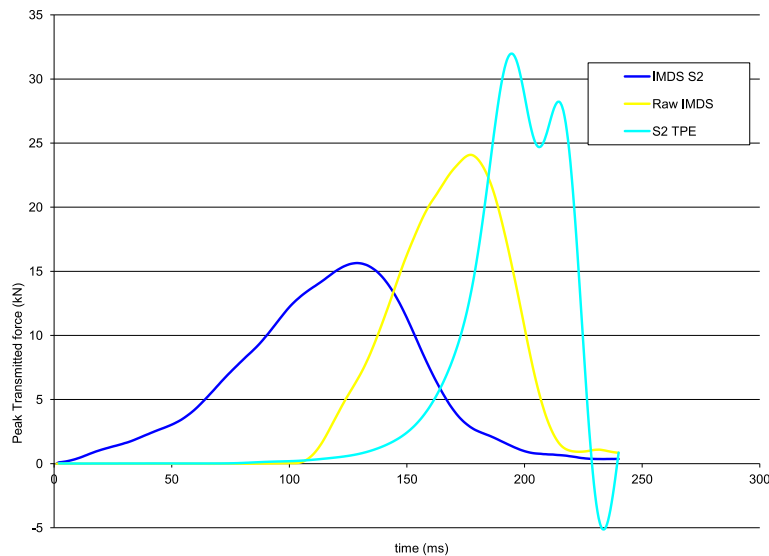
Figure 52 Geometry effects tested to EN1621-1, Raw IMDS, S2 IMDS and S2 TPE

102

The initial findings of these results show the additional benefit of combining a re-entrant geometry with a stain rate sensitive material.

6.4 Scaling the Geometry.

A sample mould was manufactured for injecting IMDS S2 Armourgel re-entrant shapes, as shown in Figure 48. The original CAD was drawn in a 10mm thickness. These re-entrant shapes were scaled up to 14 and 18mm thick, and down to 8, 6, and 4mm. Some initial moulding considerations for flow were considered on the thinner pieces and it was felt that the channels between the pins were just not large enough to ensure that the injection mould tools would fill, especially as the material stiffened at high strain rates during the injection process. The spacing on the 4mm and 6mm parts were adjusted, to allow bigger channels through the parts, to aid moulding as shown above.
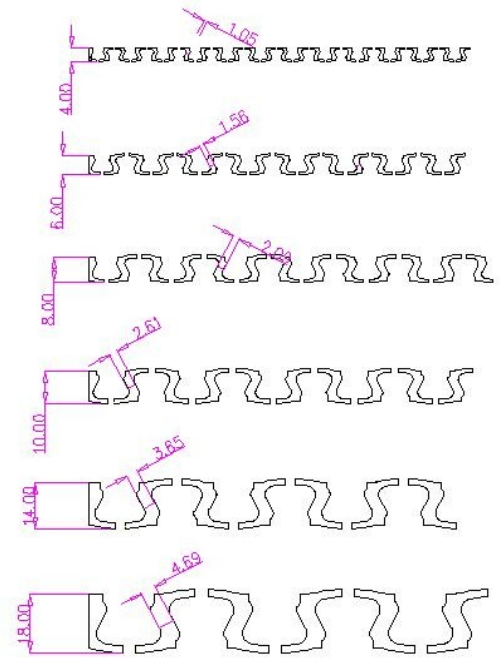
Figure 53 S2 Section Scale

These parts were tested in accordance to EN1621-1. Tests were repeated 5 times in accordance with EN1621-1 and the average values were used in this graph.

There is an optimum point on the graph in Figure 54 for the 10mm, which is unsurprising as the geometry was developed at this point, and scaled from here. The density of the parts actually increased for the 4 and 6mm parts, when compared to the other samples. This could be why the line in the graph deviates slightly from the expected decay graph in Figure 54.

103
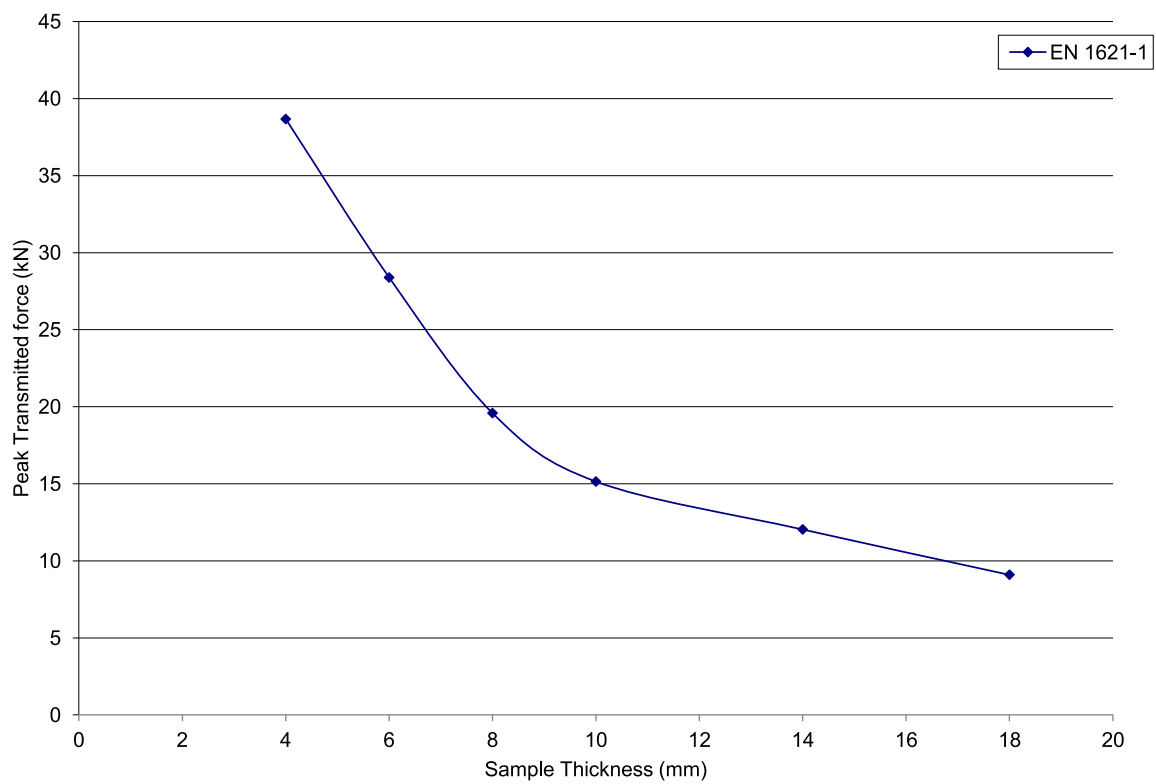
Figure 54 EN1621-1 Thickness VS Transmitted impact force kN.

104

6.4.1 Foam comparison

The mass of the parts was also mapped out against the same IMDS material in its foam form. Figure 55 shows similar thickness parts, at different densities tested to EN1621-1. The green line is the foamed range of IMDS, plotted alongside the S2 IMDS. In accordance to EN1621-1, again 5 repeat tests were performed on new samples. The benefit of the geometry, as opposed to simple traditional weight saving approaches such as foaming, is shown. This equates to a 12% reduction in peak transmitted force for the same mass, or a reduction in mass of a 25%.
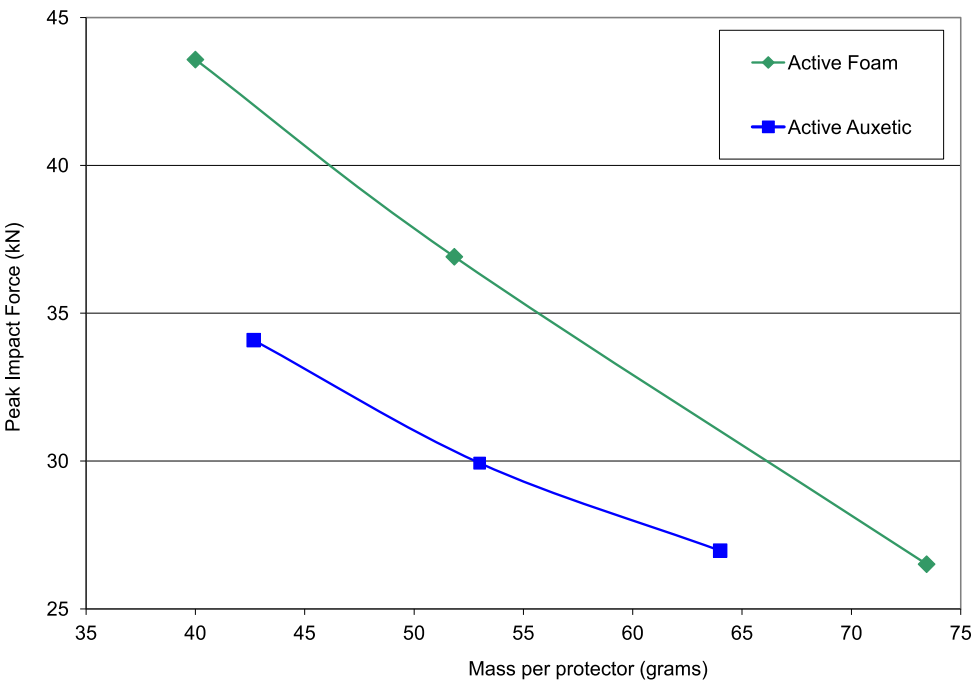
Figure 55 Re-entrant geometry and foam parts of the same IMDS material, referenced against part mass.

6.4.2   Layering development.

The base materials have been developed and screened in Chapter 5. To understand the best way to use these materials, they were tested in stacked multiple layers, the hypothesis behind this was twofold. Multiple layers should be more damage tolerant than a single layer and secondly two layers should be much more flexible than a single thick layer. A set of experiments was designed to understand this effect and see what benefits the design could incorporate from this information.

The systems have been compared and ranked for both EN1621-2 and EN1621-1. All-in-all nearly 1000 tests were performed on the structures and the lay-outs of the systems. Figure 56 below shows some of the highlights of these tests. There is additional benefit from staking and layering the samples, i.e. a single layer of 8mm S2 Armourgel performs to 19.2kN for EN1621-1, and conversely two layers of 4mm S2 IMDS perform to 17.3kN. So there is an impact performance benefit to layering the systems. There is also certainly no loss in impact performance when the parts are layers.   There is a secondary benefit of layering; in that the relative stiffness of the parts in bending are one quarter as stiff.
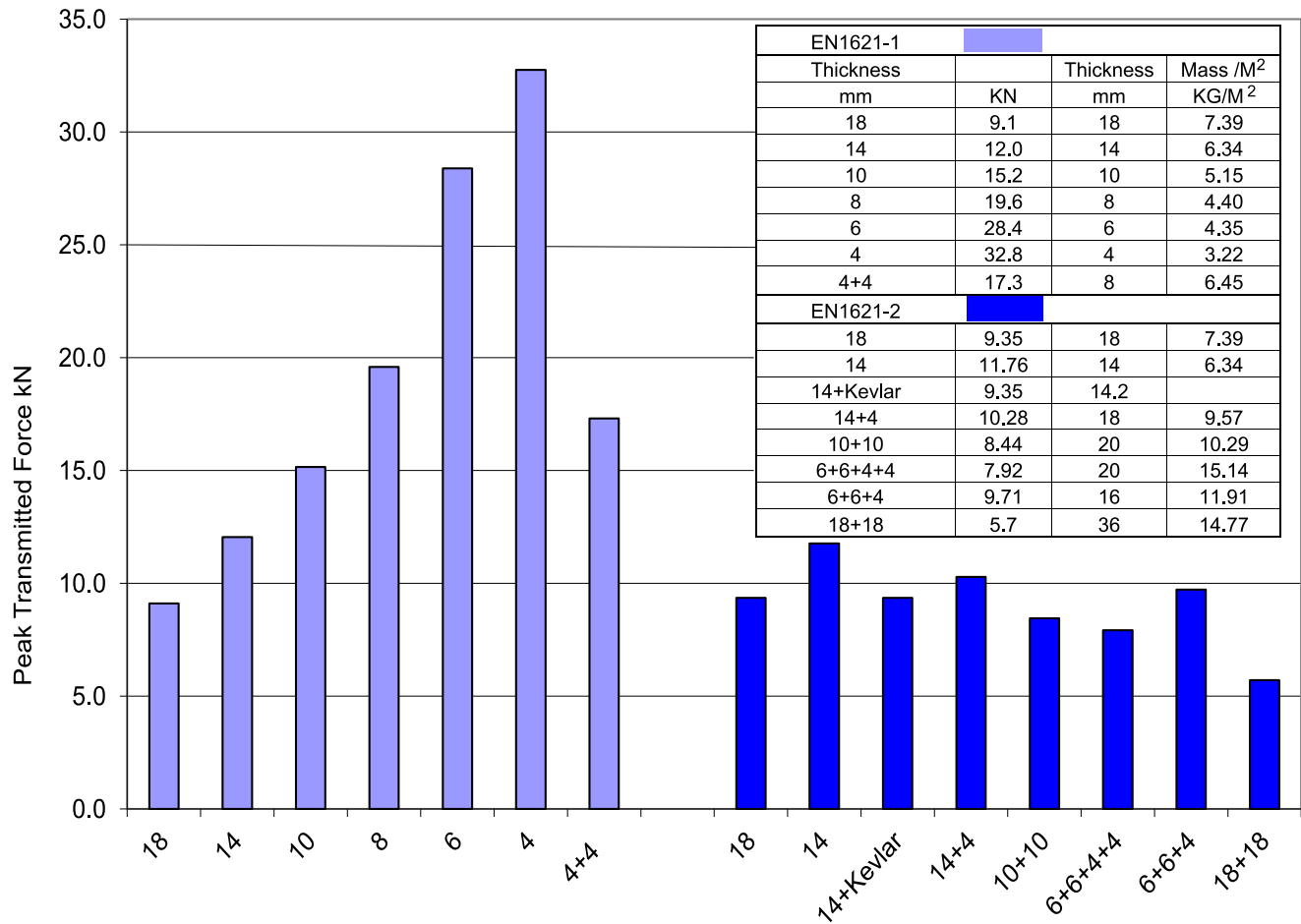
Figure 56 Layering effects of IMDS S2 structures. Peak transmitted force for samples tested under EN1621-1 and 2.

EN1621-1		Thickness	Mass /M^2
Thickness			
mm	KN	mm	KG/M^2
18	9.1	18	7.39
14	12.0	14	6.34
10	15.2	10	5.15
8	19.6	8	4.40
6	28.4	6	4.35
4	32.8	4	3.22
4+4	17.3	8	6.45
EN1621-2			
18	9.35	18	7.39
14	11.76	14	6.34
14+Kevlar	9.35	14.2	
14+4	10.28	18	9.57
10+10	8.44	20	10.29
6+6+4+4	7.92	20	15.14
6+6+4	9.71	16	11.91
18+18	5.7	36	14.77

6.4.3   Textile Layer

The research effort was further refined by attempting to combine the auxetic material moulded in the IMDS with a textile, as discussed in section 6.1.2 . Figure 57 shows samples that were injection moulded, with the textile being added to the tool, before the injection moulding process began. The textile was die-cut accordingly. The process was carried out as per a production environment.

Figure 57 IMDS S2 with textile in mould.

6.4.4 Comparative Performance.

It is possible to directly compare the relative performance of this development for 10mm samples. It is also possible to see the comparison between the mass change and the performance change when compared to the monolithic plaques. Three parts have been tested and performance changed when compared to monolithic IMDS in Figure 58 below. Monolithic plaques can be directly compared against those with auxetic geometry and also with the addition of a textile layer.   Relative merit is shown as an improvement for impact performance against the monolithic IMDS part, shown as a reduction in transmitted force (blue), and mass change from the monolithic plaque, shown in red.
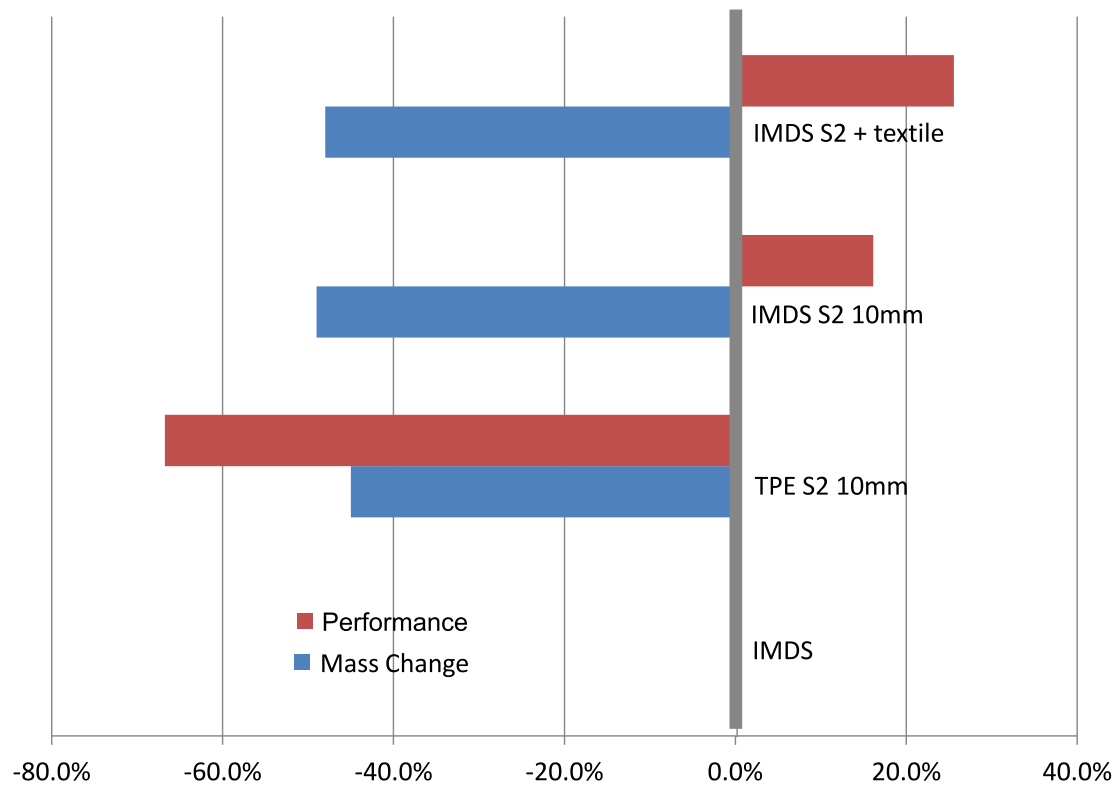
Figure 58 Relative Performance of 10mm thick samples

Figure 58 shows the performance of the samples, mass change expressed as a negative number, shows parts that are lighter that the monolithic IMDS part. Performance change is the EN1621-1 peak transmitted force change in kN as a percentage of the monolithic IMDS part. The TPE part moulded in an auxetic geometry, (no active IMDS) is lighter than the IMDS by over 45.0%, but its performance is worse by some 66.7%, so here the geometry on its own fairs worse than is potential mass saving. The IMDS part mould in an auxetic S2 geometry is nearly half the weight (49%), and has a 16.1% performance improvement, over the monolithic plaque in protection terms. When combining the auxetic geometry and a textile layer (top), the IMDS S2 textile part shows the largest performance gain. It's only a fraction heavier than its counterpart, but shows a further improvement of 25% over the monolithic IMDS part, whilst being nearly half the density (48.0%).

6.5 Auxetic Development Concluison.

The design of the internal architecture which provide weight savings has been reviewed. Geometry has been designed on CAD with auxetic internal geometry. Samples were produced in the newly developed injection mouldable dilatant silicone (IMDS) with this internal architecture. Injection moulding production tooling was designed and manufactured and samples made and tested. These samples have met the aim of producing repeatable parts using the injection moulding process and adding the tensile layer during that process with an auxetic geometry.

The benefit of designing and utilising an auxetic geometry combined with a strain rate sensitive material has also been shown, and compare directly with standard TPE materials in the same geometry and also the simple plaques of chapter 5. This is of particular interest as the new auxetic parts are half the area density of the homogeneous plaques, with improved performance.

The auxetic system has been scaled in thickness and also cell size and shows that this system can function well at a variety of different thicknesses and strain rates. These parts have also been compared to typical weight saving techniques such as foaming and have shown further improvement in impact performance. Quasi-static tests also show how the auxetic system has a softer initial stiffness than the foamed parts, which should benefit body-worn products. Strain rate sensitivity has been measured at low strain rates on an Instron.

Additional benefits can be observed in that auxetic parts are breathable as they contain through thickness holes. The samples are considerably more flexible than their monolithic homogenous counterparts made from the same material. The auxetic shapes will also bend more easily in two planes and form a saddle, as described in Chapter 3 and shown in Figure 13. Tactile properties are improved; they are more flexible than foamed or monolithic parts, and have a softer initial touch.

These samples have achieved the aim of producing repeatable parts using the injection moulding process. These parts have shown the performance improvement over traditional weight saving techniques.

7 Optimisation for Specific Developments.

7.1.1 Industry and Market Characterisations

The following section provides both a qualitative and quantitative analysis of the industries, markets, and market segments that were researched in these phases of the project. These have been reviewed in order to help facilitate the selection of the chosen projects. These three selections formed the basis of the focused development, moving from the test samples to product prototypes. Details of specific markets and corresponding test methods will be included in subsequent sections in Chapter 8.1 to 8.3.

This section firstly reviews the market as a whole, and then looks to set out three development areas. These three areas are chosen to be at very different strain rates and magnitudes of impact. The sections then review each of the chosen markets, with analysis on market size, existing technology and barriers to entry. The total market review was significantly more detailed than this, but this information should give a good overview of the market development and strategic direction for the work development in this thesis.

7.1.2 Total Industry & Replacement Market Sizes

Figure 59 provides a quick synopsis, in dollars, of the total size in annual revenue terms, of the particular Industries that were investigated.
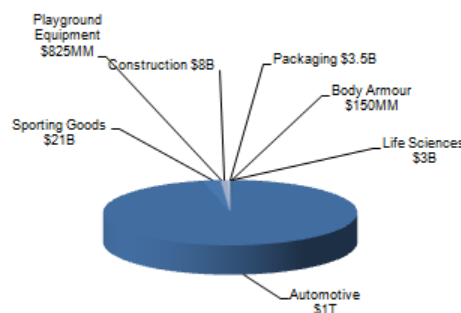
Figure 59 Total Industry Size Based on Revenue.

112

As can be seen, the automotive industry is clearly the largest. On an annual basis, the automotive industry returns about $1 trillion in revenue. The second largest industry is sporting goods, at around $21 billion annually, and the third largest was the security construction industry at approximately $8 billion per annum.

Figure 60 summarises the profitability and expected growth of the end-device markets targeted during this phase of the research into the compilation of a short list of market areas.
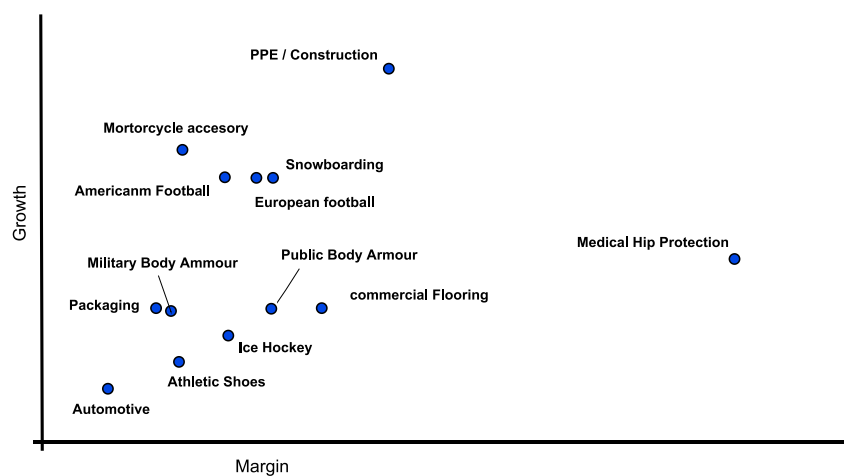
Figure 60 Growth versus Margin for development sectors

Overall, the markets are concentrated in the lower left quadrant of the figure. Market exceptions appear to be those of the medical protection market, the safety construction market, and a few of the sports dynamics markets, such as the motorcycle accessory and football markets.

7.1.3   Unmet Need

This aspect of the market research completed was the most important. Following the market segmentation process, understanding the needs of the customer was the fundamental piece of information focused on in order to screen the potential opportunities further. More specifically, given that a large number of markets and market segments were to be researched as part of this process, it was critical to determine if a compelling unmet

need existed within each market segment. If an unmet need could not be found, all else being equal, that particular market segment probably would not be very attractive from a business investment perspective.

It was important to understand if the technology could be optimised at different strain rates for three very different applications.

- o   For the high strain rate development, soft ballistic amour was chosen.

- o   For the medium strain rate development, motorcycle PPE was chosen.

- o   For the low strain rate development, medical hip protection was chosen.

Within each market segment, the value of the materials procured that could be replaced by an active technology as a product, was determined. Figure 61 focuses in more detail on some of the selected areas and summarises the total annual value of this raw material replacement market within each industry researched.
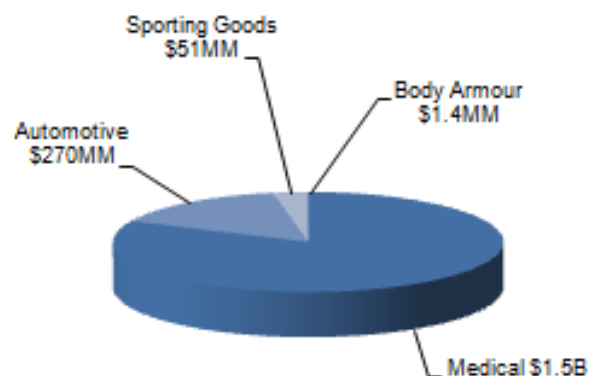
Figure 61 Industry Value

The next section reviews these choices from a market perspective, examining each of the three chosen markets in more detail.

7.1.4   Medical Hip Protectors Market

It is known that on any one day up to 20% of orthopaedic hospital beds in Northern Europe are occupied by sufferers of a hip fracture. 'Osteoporosis is a systemic skeletal disease characterised by low bone mass and deterioration of bone tissue, with a consequent increase in bone fragility and susceptibility to fracture'.

- o   The clinical significance of osteoporosis lies in the fractures that arise.

- o   In the UK, osteoporosis results in over 200,000 fractures each year, causing severe pain and disability to individual sufferers at an annual cost to the NHS of 1.73 bn.

- o   Approximately 50% of patients suffering a hip fracture can no longer live independently.

- o   20% die within 12 months of the fracture.

- o   10% of the world's population are over 60 years old, by 2050 this is estimated to double.

7.1.5   Trends Supporting the Unmet Customer Need

There is an unsatisfied demand for either a regime that minimises the likelihood of injury, or a device that reduces the chance of fracture in the elderly, following a fall. Analysis of the leading brands of hip protectors shows that they lack comfort. It appears that the technical efficacy of the products is sound; however, the compliance associated with their use is extremely low, especially over time, making these products less effective than they would otherwise be.

7.1.6 Motorcycle Accessory Market

The motorcycle accessories market includes the helmet, clothing, and luggage segments. In 2001, it is estimated that the size of the combined helmet and clothing segments, excluding the Americas, was $6 billion. The estimated size of the protective padding procured as a component for the production of helmets and clothing within this market was roughly $15 million.

7.1.7 Trends Supporting the Unmet Customer Need

Global trends for this market, and specifically for the motorcycle clothing and helmet segments, include the following:

- o Increasing levels of safety and protection in order to satisfy customer needs.

- o Increasing motorcycle usage globally, but especially in Europe and Japan where space is limited and emission limits are more stringent.

- o Increasing interest in motorcycles from the female perspective.

- o Enacting of directives by governments, which mandate clothing claiming protective qualities meets certain safety standards.

- o Decreasing need of "hard" armour and increasing need for "flexible" armour.

7.1.8 Ballistics Market

The global body armour and personal protection market is estimated at a value of US$1.5 bn in 2012 and to increase at a Compound Annual Growth Rate (CAGR) of 4.89% during the forecast period (2012-2022), to reach its peak of US$2.4 bn by 2022[59].

The US military is developing new body armour for female troops to provide them with increased protection on the battlefield. The new outfit is tailored specifically for the female form and consists of more curves in the chest and hips, shorter torsos, and narrower shoulders.

Reducing the weight of soldier equipment without compromising protection and combat performance is a key challenge for the body armour and personal protection industry.

7.1.9 Trends Supporting the Unmet Customer Need

The advancement in ballistic armour is ongoing, and in recent years has led to various innovations which are helping to address the current demands for improved comfort, lower weight, greater flexibility and most importantly better protection.

7.2   Low Strain Rate Testing : Medical Hip Protectors.

A frustratingly common injury amongst the elderly is fracture of the hip occasioned by a fall. More than ninety percent of hip fractures are due to falls, and external "hip protectors" (wearable pads or shields typically embedded in an undergarment) represent an attractive strategy for reducing femoral impact force and preventing hip fractures in high-risk elderly individuals [1].

Previous reviews in Chapter 3.6 have identified a need for a flexible, comfortable, unobtrusive protector for this market. The main challenge in the development of hip protectors has been to create a device that is user-friendly, which is comfortable yet discreet, whilst providing adequate protection.

It is important that the protector be as effective as possible whilst being as thin as possible [1]. There is a perceived need for a slender profile in such a device and this is considered to be the primary driver [1], to this end several investigators have even suggested an air bag type of inflatable device [60].

This medical application is one of the most demanding for an energy absorbing technology, as the "device" needs to be worn on a daily basis, for significant time periods. Many of the systems available today are passive systems and may not provide the user with adequate system performance. In this case, performance means protection, comfort, breathability and flexibility; users demand the highest impact protection with a performance exceeding that of any currently available commercial product, packaged in a very thin product [1].

Analysis of the leading brands of hip protectors indicates that the greatest barrier to adoption is a lack of comfort. It appears that the medical efficacy of the products is sound; however, the compliance associated with their use is low, especially over time, which makes these products ineffective [1].

7.2.1 Existing Hip Protector Technology

Hip Protectors are devices worn over the hip to protect the femur from the impact of a fall.

Currently available devices have been shown to work in mechanical studies and clinical trials, but are rarely worn in routine clinical practice. Their effectiveness is limited by poor patient compliance [61]. Those based on a rigid exterior shells are too inflexible and uncomfortable, and those employing some form of foam laminate are too bulky and thick, too warm and too obtrusive to be acceptable [62]. Recent studies have shown a trend towards soft shell protectors, which may provide better comfort and compliance[63].

Thus there is a strong argument for the use of a device to help protect a vulnerable hip joint from any knock or abrasion, whilst making the device as comfortable and unobtrusive as possible, so that it is worn more often. Improved compliance will lead to better protection over longer periods of time, with concomitant reductions in National Healthcare costs. Today there is a clear *unmet need*, which has been characterised and defined.

Hip protectors represent a promising strategy for preventing fall-related hip fractures. However, clinical trials have yielded conflicting results, due in part to lack of agreement on techniques for measuring and optimising the biomechanical performance of hip protectors as a prerequisite to clinical trials [1].

7.2.2 Impact

There is a stark contrast between most PPE & hip protectors for the medical market.

Osteoporosis causes reduced bone density which means the bones are more easily damaged than strong healthy femurs.

The impact loading regime for frail patients is significantly different from "sporting accidents" and damage typically occurs at slow speed. There are documented cases of particularly frail patients suffering hip fractures whilst getting out of bed [64].

It is estimated that a force of 2000 Newton's or less (1900N ±300N) is all that would be needed to break the neck of the greater trochanter in an osteoporosis patient [1]. This force could be up to three times as much to cause a fracture in a normal healthy human. In fact is very unlikely that the greater trochanter would even break at this location on a healthy young person and it is only because of the weakened bone that they fracture in this position.

7.2.3 International Research Group.

The International Hip Protector Research Group (IHPRG) has been working to develop recommendations for (a) standard techniques for measuring the biomechanical performance of hip protectors, and (b) the design of future clinical trials of hip protectors.

The recommendation of the IHPRG, of which the author is a member, has recently been published. This chapter will not look to mimic that work, but show the latest unpublished development. This work outlines the development of an improved biomechanical test method that has run in parallel with the IHPRG and completed various round robins tests.

7.2.4 Biomechanical testing.

The current output from the IHPRG has issued guidelines for manufacturing a test device to mimic a fall in a biofidelic way, including pelvic stiffness and soft tissue.

The current guide has been developed within these guidelines and forms the basis of a draft standard for BSI 8575.

There have been many test machines developed to date and this is an approach to standardise the machine and provide a single simplified test method.

The drop tower in Chapter 4.2 has been modified to the following specification:

It consists of a test rig frame that allows a mass to be dropped vertically (+/-0.5°) onto a hip protector mounted on an anatomical hip form. The anatomical base is supported on a flat, rigid concrete, or equivalent substrate of sufficient mass, density and thickness that its deformation during the test makes no significant contribution to the test result.

A drop weight assembly comprising a mass guided by appropriate bearings, with a spring of stiffness 40 +/-1 kN/m which can compress by at least 50mm attached to its lower surface. An impact plate is attached to the lower end of the spring. The mass of the spring shall be no greater than 1.6 Kg and the total mass of the impact plate and any other components attached to the lower end of the spring shall be no more than 0.5 Kg. The total mass of the assembly shall be 28 +/- 0.01 Kg. The spring may be made of any appropriate material; a suitable design consists of 13 turns of Ti-6Al-4V bar of diameter 12.7 mm, with an outside diameter of 74 mm and a free length of 315 mm. The impact plate shall be large enough to completely cover the hip protector. Lateral movement of the impact plate shall be restricted by appropriate guides or by the stiffness of the spring. The machine built to develop and meet this standard is shown in Figure 62.
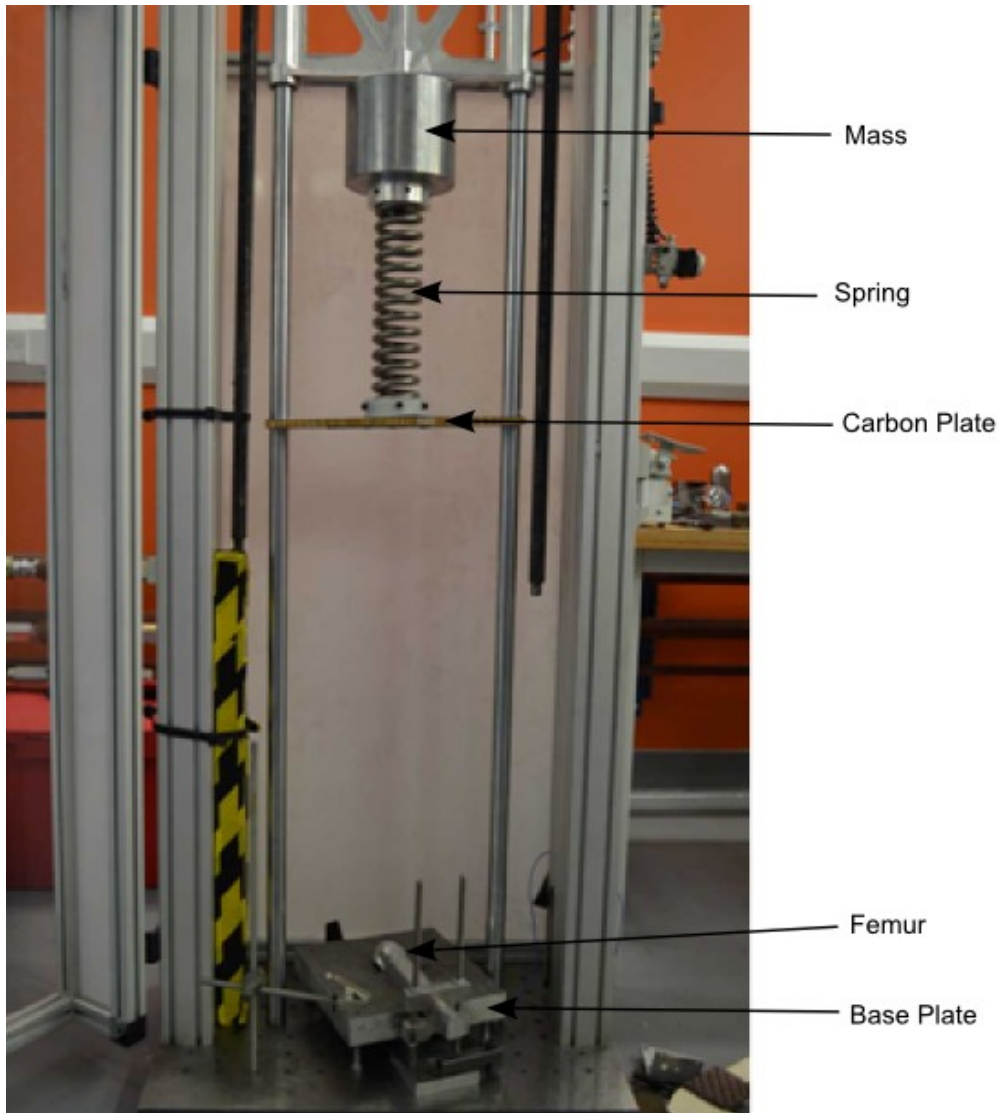
Figure 62 Drop Tower, top to bottom: Slider, Mass, Titanium Spring, Carbon plate, Femur. (soft tissue removed).

A standard femur has been developed relating to the standardised femur geometry [65].

A duplicate of this femur was machined from solid and also a simplified version of this femur for type testing. These are simply supported on a substantial base, with a load cell directly below the greater trochanter (GT) as shown in Figure 63, which shows the anatomical femur and the simplified femur.
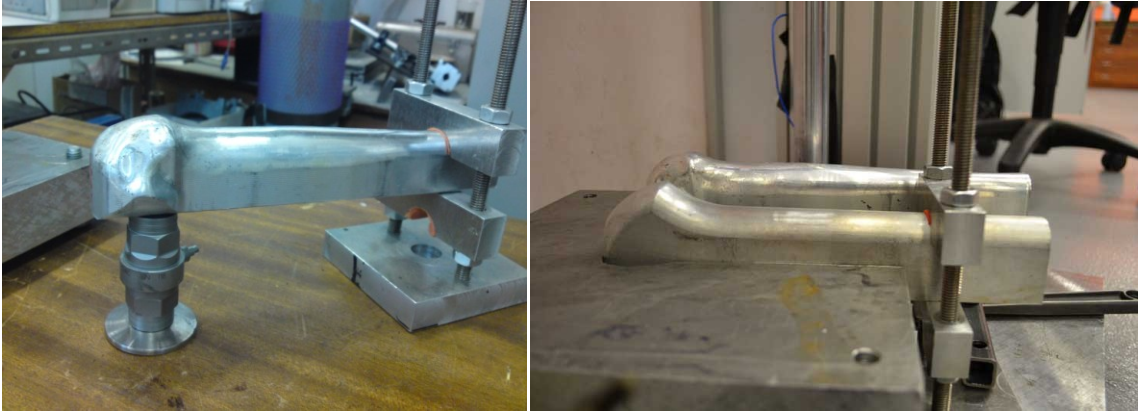
Figure 63 Aluminium femur and piezoelectric load cell and support (left), femur and simplified femur (right).
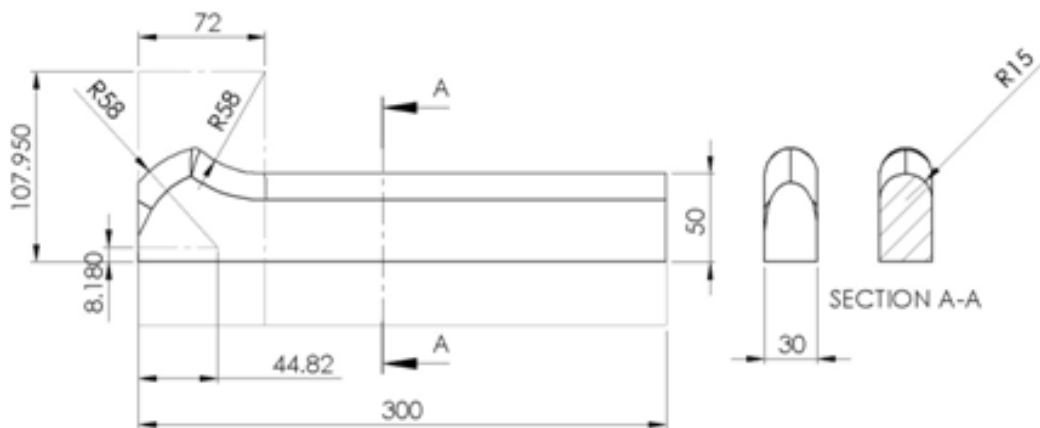
Figure 64 Drawing of Simplified Femur.

These femur geometries shown in Figure 64 were developed with the IHPRG testing group and the simplified femur was manufactured by Prof Sam Evan at Cardiff University, where a research group conducted the task of gathering data and measurements around the greater trochanter. Recent work has shown that the area nearest the GT has the highest force and particular attention to the anatomical shape in this region and the surrounding 20mm radius is important [66].
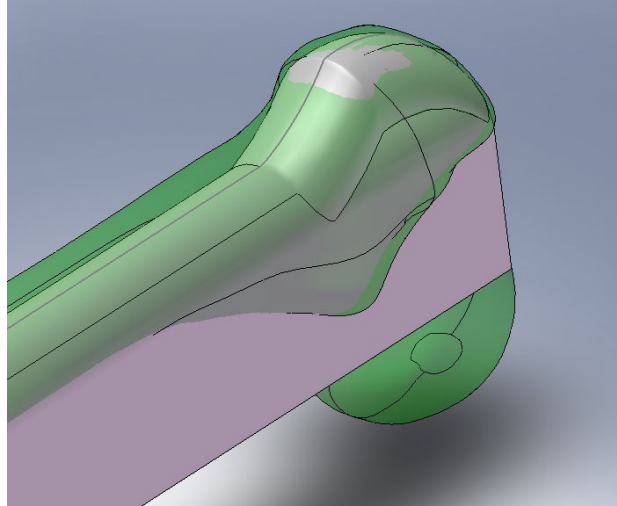
Figure 65 CAD comparison of femur and simplified femur

In Figure 65 the CAD of the two femurs is visually compared. It is best to visualise this in 3D on a computer, but these parts are within 1.2mm of each other, near the GT. There would be more natural variation between individuals' bones. The screen shot in Figure 65 above was taken to illustrate where the largest differences could be found between the models.

Femurs have been represented in a similar fashion on an alternative test apparatus as shown in

Figure 66. The design of this femur is more similar to the simplified femur than the anatomical one [67].
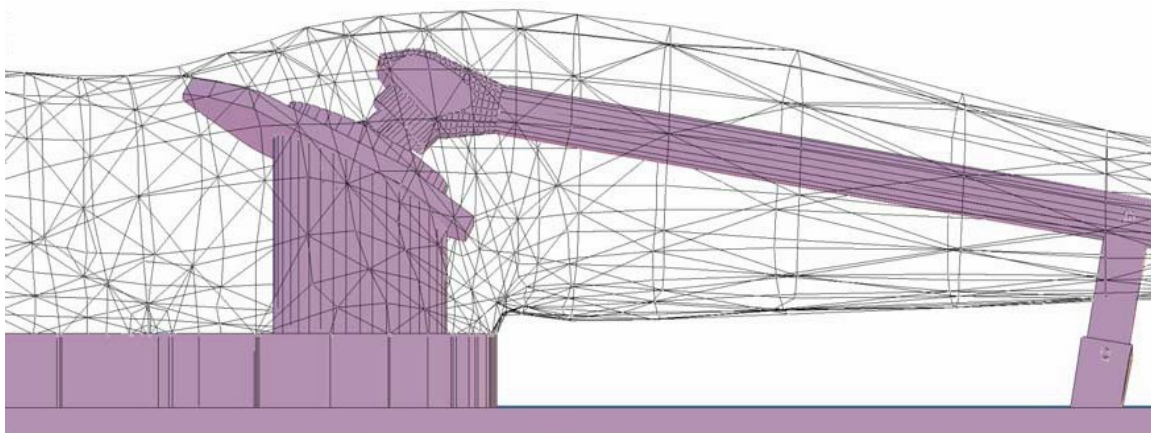
Figure 66 alternative femur design [67]**.**

124

A key difference is the angle of the femoral shaft to the horizontal. The angle of the femoral shaft perpendicular to the impact has been set to either zero simulating impact to the knee, simultaneous with the hip, or set to 12 degrees as shown in

Figure 66.

When set to zero, the knee would just be about to impact the floor which could change results, although more research needs to be done in this area, especially on machines that mimic pelvic stiffness.

7.2.5   Soft tissue Geometry

In 2006, Andrew Laing and Stephen Robinovitch created a three dimensional map of average hip surface geometry from the data of fifteen volunteers of ages between 66 and 91 years. The height range was 1.51 to 1.75m, body mass between 48.4 and 72.6kg and body mass index range of 21.2 to 28.9kg/m^2 as tabulated in Figure 67.

		anterior-posterior angle (degrees) (+ represents anterior)								
		+40	+30	+20	+10	0 (GT)	-10	-20	-30	-40	-50
	+4	108,91	125,72	140,51	151,27	156,0	156,-27	149,-54	135,-78	115,-97	92,-110
	+3	112,94	130,75	146,53	160,28	167,0	167,-30	160,-58	145,-84	124,-104	99,-118
	+2	114,96	134,77	152,55	167,29	175,0	175,-31	166,-61	130,-109	130,-109	104,-124
	+1	113,95	134,78	156,57	172,30	179,0	178,-31	168,-61	132,-111	132,-111	107,-128
vertical level of horizontal plane (+ represents superior)	0 (GT)	109,91	132,76	156,57	175,31	181,0	177,-31	165,-60	130,-109	130,-109	106,-127
	-1	105,88	132,76	158,57	177,31	184,0	178,-31	165,-60	128,-107	128,-107	104,-124
	-2	103,86	133,77	159,58	177,31	184,0	180,-32	166,-60	123,-103	123,-103	98,-117
	-3	102,86	134,77	158,58	175,31	183,0	180,-32	166,-60	116,-97	116,-97	87,-104
	-4	102,86	133,77	156,57	172,30	179,0	177,-31	163,-59	109,-91	109,-91	78,-93
	-5	100,84	129,74	151,55	165,29	172,0	171,-30	156,-57	102,-85	102,-85	68,-81

* z coordinates are 128, 96, 64, 32, 0, -32, -64, -96, -128, and -160 for vertical levels of +4, +3, +2, +1, 0 (GT), -1, -2, -3, -4, -5, respectively.

Figure 67 Map of average hip surface geometry as measured by Laing & Robinovitch[68]**.**

A simplified geometry was developed to work with the simplified femur. The drivers for this work were two fold. The first was to be able to test either the left or right protector on the same machine. The second was to reduce complexity and cost of such testing so that it could be more easily tested at accredited test houses and form the basis of a CE standard. The work of Laing and Robinovitch has been modelled on a computer and compared against a simplified geometry.

3D screen shots of anatomically correct skin modelled from the Lang and Robinovitch data and simplified shape are shown in Figure 68.
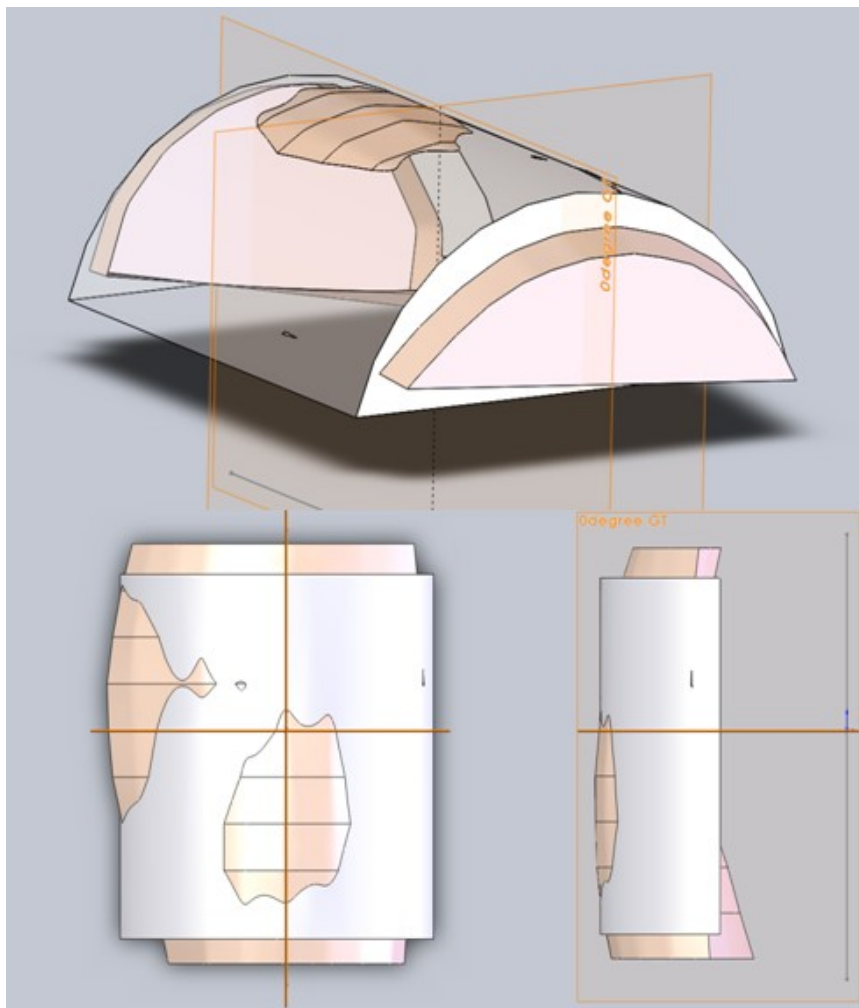
Figure 68 Anatomical skin surface and simplified surface.

This can be represented as a single simple part as shown in the diagram below (Figure 69).

FULL RAD ALONG TOP EDGE

FULL RAD (R15)

R115

100

200

88.7

103.7

118.7

SECTION A-A
SCALE 1 : 3
SEE ATTACHED DRAWING FOR DIMENSIONS

250

300
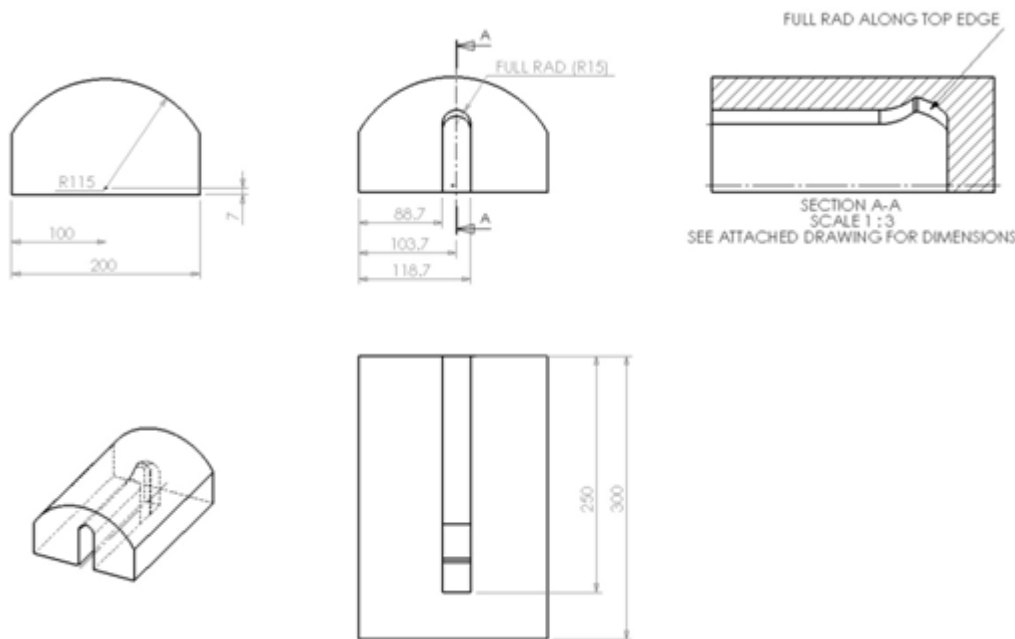
Figure 69 Drawing of soft tissue

7.2.6   Soft tissue Stifness

As well as hip geometry, Laing & Robinovitch measured the surface stiffness of nine regions of the hip, taking data from the same fifteen volunteers. In addition to the medial-medial region, directly overlying the greater trochanter, stiffness measurements were taken at points in a 3x3 grid of 6cm intervals. Force-deflection properties were measured using a 38mm diameter cylindrical head indenter combined with a load cell and LVDT. The secant stiffness was calculated for each measurement and their results can be seen in Figure 70. There was a wide variation in stiffness between subjects and the standard deviation for each region appeared large in proportion to the stiffness measured. There was a definite overall trend of threefold greater stiffness in the areas overlying the proximal femur compared to the softest region, and nearly twice that of the stiffest region above the femur. The medial-medial region was on average the highest in stiffness and the posterior-medial the lowest.

subject	AS	AM	AI	MS	MM (GT)	MI	PS	PM	PI
1	25689	18780	20207	26610	20318	35250	14322	12380	11384
2	7673	7695	11981	53147	27621	20592	23888	9805	2622
3	18514	13338	26539	15698	47549	24668	21211	11134	3499
4	20076	6042	6921	16827	18005	29934	12993	6698	3242
5	21726	17258	17655	17815	47419	35500	25399	10981	3882
6	17854	8441	9799	17688	40348	19712	13026	18571	4284
7	43114	14836	10471	16073	44222	26198	13294	18531	15003
8	12019	7734	5402	10755	71036	5402	16111	10137	2800
9	14924	22358	17197	18586	40191	16323	13247	34783	28535
10	7646	9914	16365	8654	18883	37139	9046	7773	4503
11	11755	26584	26117	17120	36245	67521	14504	9665	1925
12	NA*	12538	8123	20125	14360	26293	17418	15550	1077
13	24128	17310	28999	30251	23027	70245	19649	13574	2189
14	16823	16906	18850	18991	32482	50090	12126	9861	2390
15	15454	57209	25216	11623	NA**	NA**	14322	12380	11384
Average	18385	17130	16656	19998	34407	33204	16819	14091	18819
SD	8986	12520	7714	10681	15546	18478	5244	7167	11573
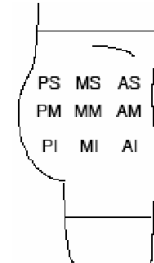
* AS location was medial to anterior inferior iliac spine and very soft. Data was not collected so as to avoid damage to underlying soft tissues / organs.
** Insufficient deflection to calculate valid stiffness value

Figure 70 Hip soft tissue stiffness data for the 15 subjects [68]**.**

The data used as a basis may raise some questions as to true representation of the average. The range of body mass index indicates that whilst there were some in the overweight demographic measured for hip geometry and surface stiffness, no underweight subjects were measured. (BMI<18.5). This data may be an appropriate representation for a Western demographic, and as such, research based on this data may be assumed to have such a focus. Some hip protector development has also been conducted with anthropometric focus on Chinese older women, this research suggests that currently available hip protectors are designed for Caucasians and may not be suitable for the Chinese population [69],[70].

Numerous soft tissue simulants have been developed to mimic the soft tissue and skin in the region surrounding the femur [67],[1], ranging from foam, silicone and neoprene.

Multiple simulants look to represent the soft tissue. These have been designed to take into account stiffness, both dynamic and static, as well as anatomical shape.

These have been completed in a number of different methods; several compositions were made to replicate the stiffness of skin as tested in Figure 70, as well as to verify the soft tissue findings on human subjects.

This program focused on the variation of stiffness of soft tissue surrounding the hip, in ways that could be measured externally by indentation. The focus was on developing an easily manufactured, reusable soft tissue model that mimicked these characteristics and also to consider how such a model could be improved in subsequent iterations.

7.2.7 Creation of an anatomically correct skin simulant.

The information presented by the IHPRC and its contributors, has been replicated at Imperial College on the hip drop tower, by the writer.

Soft tissue measurements were duplicated on 15 volunteers, by a Mechanical Engineering third year student, supervised by the writer. The average BMI and age of the volunteers was lower for the Imperial College data set, than the Laing and Robinovitch set. However the graphs show good correlation, especially at the MM site as shown in Figure 71.
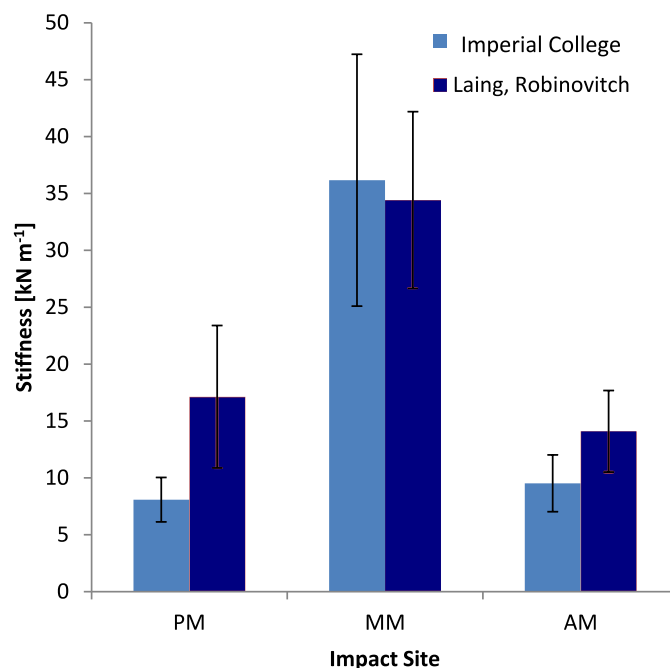
Figure 71 Graph showing peak dynamic human stiffness as collected by Imperial College as well as Laing & Robinovitch data for comparison

From these data, skin simulants were developed to biomechanically represent these stiffness levels on the biomechanical test machine. All of the materials below have been tested and developed over the last few years in an iterative program looking to develop a standardised test method that could be used for development and certification.

7.2.8   Simulant Materials

Different materials were trialled on the drop test rig as well as in samples on an Instron. These ranged from Silicone RTV (Imperial 2008), RA12 foam Recticel (Imperial 2010), RS55H (Minns /Evans/ Plant), and castable silicone (Imperial 2011). These are shown in Table 7.

Table 7 Different Skin Simulant

	Material	Graphic	Advantages	Disadvantages
1	Silicone This comes in many different grades.		With the addition of silicone oil there is direct control over its viscosity, and can be thickened for the curing process using a thixotropic fluid that will not affect the final stiffness, non toxic, pourable into moulds.	Very messy to cast. Expensive
2	Polyethylene foams e.g. RA12, LD60		Foams can be easily varied by using bubble agent, are easy to shape and cheap.	Poor damage tolerance
3	Bovine Gelatine Good results when fibres were added		Is similar to subcutaneous tissue when made up and is easy to pour into moulds	Goes off within days, cannot be used repeatedly.
4	Non homogenous foam. Density changed for different stiffness		Simple construction.	Requires a great deal of testing to empirically find the best performing result. Not very damage tolerant.

Target results were found for RA12 foam and silicones. These were the most damage tolerant parts when measuring the dynamic hip fall, other options above could only be used a few times as they were found to become damaged at femur loads above 3kN in the dynamic setup.

The most promising were calibrated in accordance with nine sites surrounding the GT [68].

Presented in Figure 72 are the stiffness data for skin and the various materials tested in relation to historical data at Imperial College. The green line is the human data, and the blue line is the RA12 data from 100mm/min tests (low Speed) on an Instron. The red line is the same RA 12 foam measured dynamically with the same equipment used to measure human skin stiffness.
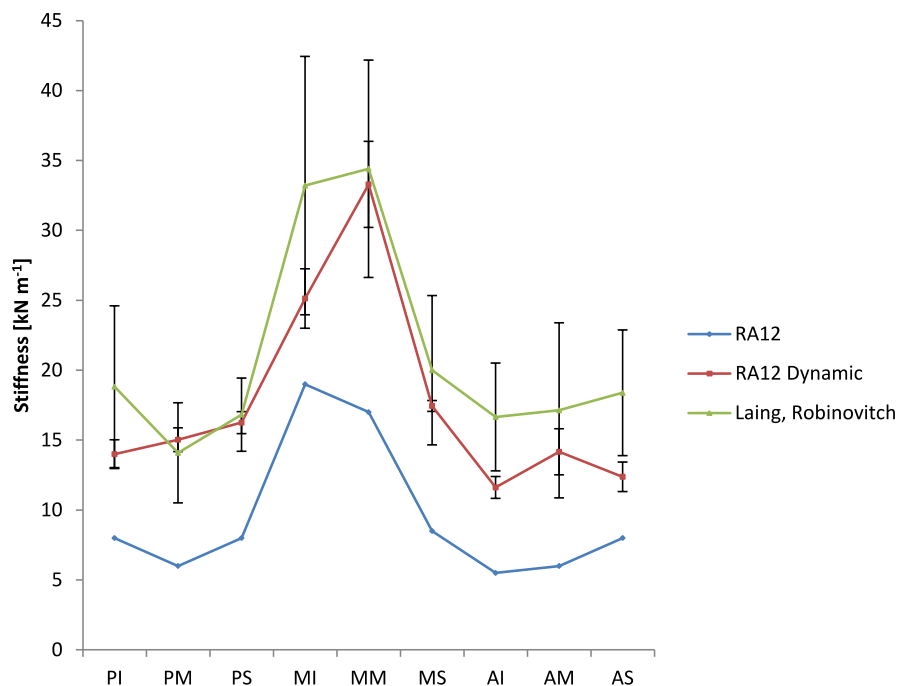
Figure 72 Graph showing peak dynamic human skin stiffness data by Laing & Robinovitch and dynamic tested RA12 with quasi-static testing on RA12.

The data points denote the average peak secant stiffness; the error bars denote the range of one standard deviation around the average (0.5σ to either side). It can be seen from these data that the RA12 foam in dynamic conditions actually approaches the stiffness obtained by Laing & Robinovitch for human skin. Clearly RA12 dynamic performance is different from its static performance.

Figure 73 Damage from impact tests on the surface of a RA12 hip

Figure 73 show a damaged region of the RA12 simulant above the GT after only a dozen or so impact tests, showing that either this region or the whole part would need to be changed after every high loading event.

7.2.9   Silcone skin simulant.

RTV-C204 silicone is a two part curing silicone system available from Jacob's chemicals with possible ratios of mixing between 1:0 to 4:1. These parts can be modified with silicone oil to reduce the cured stiffness of a sample. After mixing, 5% of the mixture weight of catalyst (81B) must be added to begin the curing process. Pour time lasts approximately 30 minutes after adding the catalyst and thoroughly mixing. After this the moulds should be left to cure for approximately 24 hours.

A great deal of time was invested in developing the most anatomically correct skin simulant, which would give similar values to the Laing and Robinovitch data set and also be able to withstand multiple impact events and have little degradation with time.

Samples of differing simulant were prepared at different ratios and tested for secant stiffness to try and replicate the stiffness of skin as tested by Laing and Robinovitch. These are shown in Figure 74.
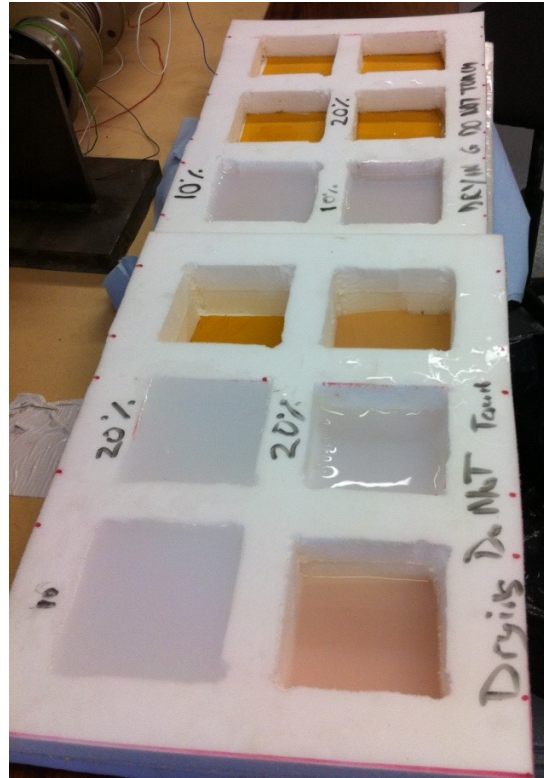
Figure 74 Sample silicone compositions.

To replicate the increasing stiffness over the greater trochanter a two part mould was used, moulding a different grade of silicone around the femoral head which was held 12 mm above the surface during moulding, over an area prescribed to be an 80mm diameter circle.

The final piece was manufactured using a composition by mass of 10% silicone oil to RTV C204 in the core and 20% silicone oil to RTV C204 in the outer layer, catalysed with 5% by mass of catalyst 81B.

Testing the simulant across the 9 points tested by Laing and Robinovitch, revealed a good correlation in stiffness.
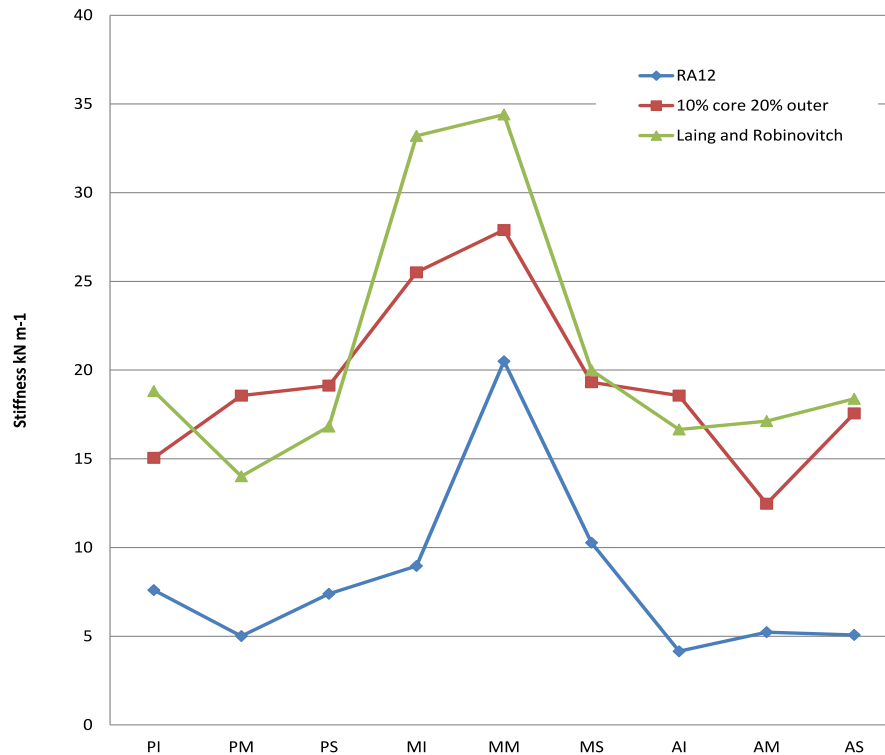
Figure 75 Stiffness at 9 points measured and compared.

Figure 75 shows a strong correlation between test data and the new simulant, with a significant performance improvement over the existing RA 12 simulant. The core could be made stiffer by reducing the amount of silicone oil in the core from 10% to 5%. These tests were performed with the anatomically correct femur. This silicone has since been tested dynamically and gives repeatable performance even after in excess of 300 tests.

7.2.10 Dynamic testing Results.

The previously developed skin simulants have been tested in the drop tower and calibrated with no hip protector to give an 'unprotected' load of 3.3kN measured on the femur load cell. This dynamic testing will focus on the RA 12 and silicone simulants. Calibration consists of tuning the drop mass or the height in order to get the un-protected dynamic calibration to 3.3kN. There are guide lines in the standard as to the limits of what is an acceptable dynamic calibration.

135
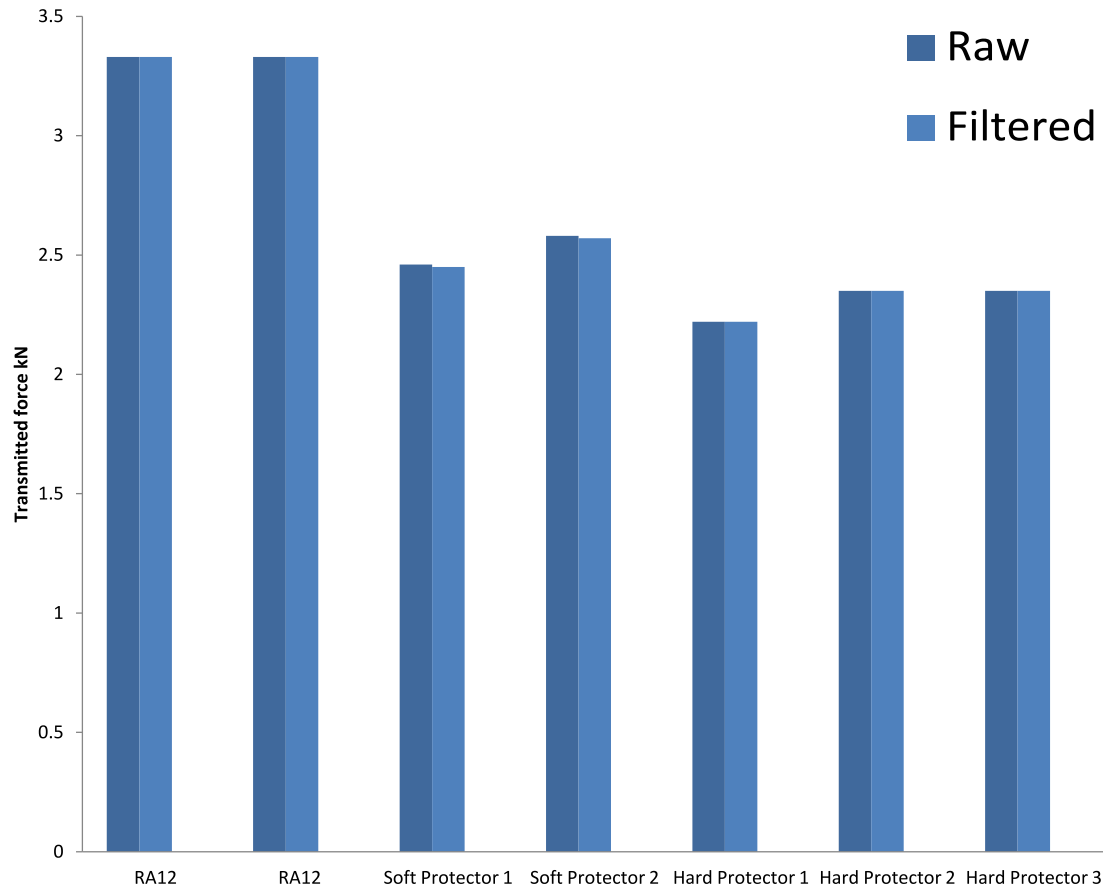
Figure 76 RA12 Simulant. 500mm drop. Simplified femur, simplified anatomy.

A range of screening tests were carried out on the RA12 simulant. These were conducted with the simplified femur, and the simple anatomical shape of the skin simulant. Figure 76 shows a number of these tests. These were conducted with a falling mass of 27 Kg, from a height of 500 mm. For these tests a 2mm neoprene skin cover was used. This setup gave good correlation to the non protected impact, having a repeatable reading of 3.33kN with no hip protector. The setup was repeatable and gave multiple (unprotected) readings of very similar magnitude. A known hard protector and a soft protector were dynamically tested using the RA12 base with the simplified femur. The successive tests show repeat impact performance of the protectors. The known protectors have been the subject of many studies, both on test machines and also in clinical trials. A good protector should attain below 1900N in this dynamic test [1]. During these dynamic tests on existing hip protectors a higher than expected transmitted force was attained, which suggests that this setup with the RA12 simulant is too soft [71].

Similar tests were performed on the dynamic drop test apparatus using silicone simulants covering the femur. These tests were completed with 28Kg, the drop height raised from 500mm until they gave the required dynamic calibration of 3.3kN in accordance with the consortium paper and draft BSI standard. In this particular setup the free fall drop height was set at 560mm. This setup was tested with the simplified femur shape, in all over 300 tests have been completed for various tests and developments with this setup. The skin simulant has held up well and is still in dynamic calibration.

The graph in Figure 77 shows some of the periodical tests completed on the dynamic setup with no hip protectors in place. The average of these tests is 3.28 kN with an SD of 0.0152.

The name number denoted the sequential test number, three were done at the beginning, one is shown from the middle, and three from the last tests in that batch of tests.

	Calibration 1	Calibration 2	Calibration 3	Calibration 73	Calibration 182	Calibration 183	Calibration 184
	3.29	3.26	3.28	3.3	3.29	3.26	3.28
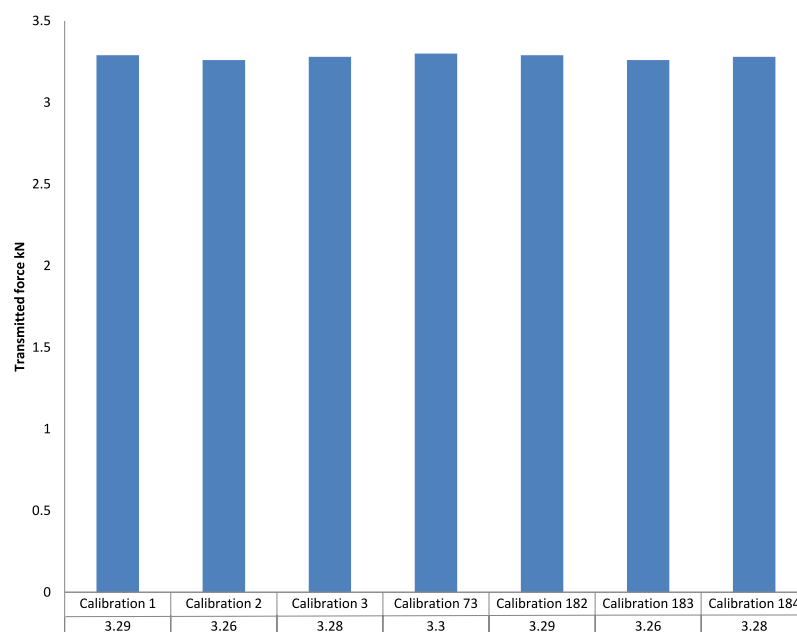
Figure 77 Calibration tests during a program of 200 tests. No hip pad protection in place.

7.2.11 Comparative testing.

After assembly and measurement of the standard value for the unprotected hip, a comparison of open market hip protectors was considered necessary for calibration. Three hip protectors were tested, regarded as current market leaders, the Hip Saver, SafeHip and the newer SafeHip Air X, as well as a new unknown protector provided by Fall Safe. Table 8 shows the average transmitted load for existing protectors. These values formed the performance benchmarks, with the SafeHip Air X being the main focus as the lightest, most breathable and best performing. All the better known products in the open market with some clinical evidence attain a peak transmitted force below the known fracture threshold of 1900N.

Table 8 Product testing, pear transmitted force.

Hip Protector Name	Average Load Cell Value kN
Hip Saver Old	1.84
Hip Saver New	1.92
SafeHip	1.83
SafeHip Air X	1.74
Fall Safe	2.15

The force trace and smoothed trace for SafeHip Air X are shown in Figure 78. These are typical for the dynamic testing for these devices. The undulations at the beginning are due to the mass of the end of the spring, and the

effective contribution of mass in the spring. These are kept to a minimum by reducing this mass as much as possible. The standard specified not more than 1.6kg. The Imperial dynamic drop tower has a mass below the spring of 1.4Kg.

The data has been smoothed using a LOESS regression fit (locally weighted scatter plot smoothing) plotting a Loess curve through the data. It was chosen owing to its simplicity and ability to smooth without the specification of a function. Tests were completed in-line with the draft standard as much as possible, but these results cannot be specified as "standard tests" as the filter is different, and so these results do not comply with the standard and so cannot be claimed as having been tested to the standard.
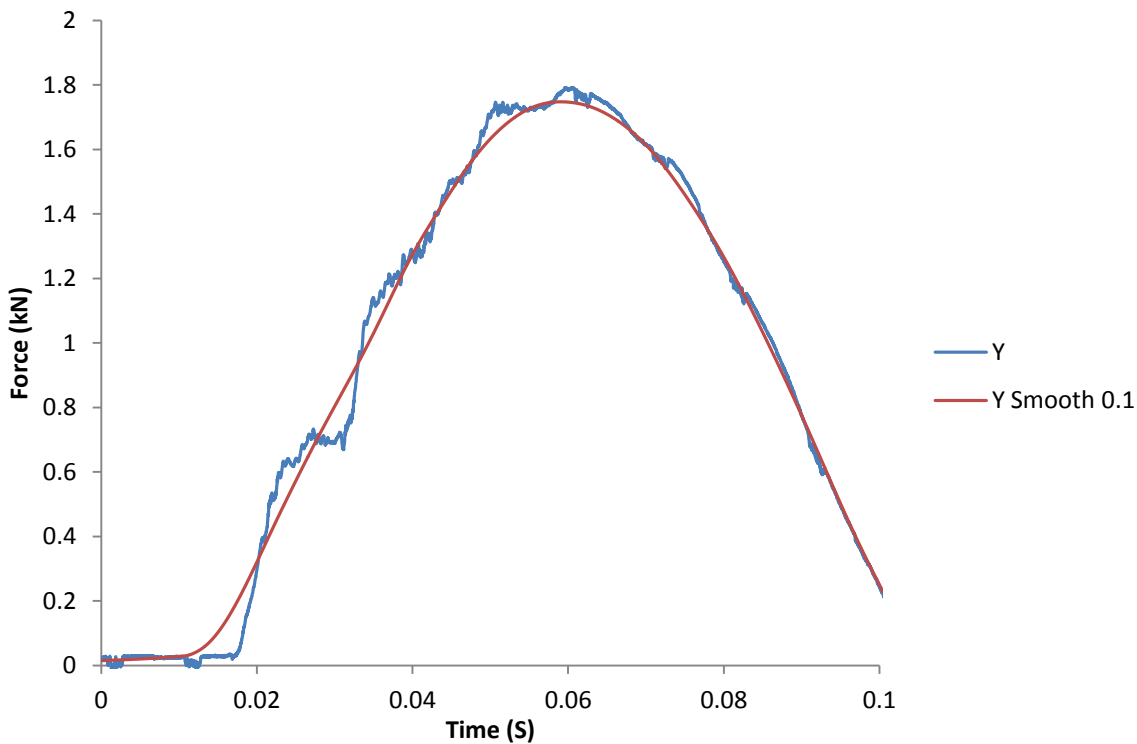
Figure 78 Force trace and smoothed Trace.

7.2.12 Analysis of competitors (fabrics, internal and external construction)

The different hip protectors vary in structure as well as performance. Table 9 below summarises their design features.

Table 9 Design features of commercially available medical hip protectors.

	HipSaver	SafeHip	SafeHip Air X	Fall Safe
Material Manufacturer	HipSaver	Tytex Corp	Tytex Corp	PU foam
Main Material	Closed Cell Foam	Closed Cell Foam		PU Closed Cell Foam with 3% Silicone Dilatant
Casing	Welded Air Bag	Welded Air Bag	Welded Air Bag	None
Fabric	Polycotton	Cheap Felt	Cotton	Cotton
Shape	Circular	Horseshoe	Horseshoe	Teardrop
Depth Shape	Flat	Curved to body	Curved to body	Curved to body
Breathability	Low	Low	Medium	Low/Medium
Max Thickness (mm)	17	18	17	18
Weight (g) One Pad	73	100	46	109

Numerous tests and designs have been developed on the test machine in its current design. The final product has not been produced as the standard for the machine is still being finalised. The standard is currently in draft format and should go for public comment in early 2014. Once the pass level has been set and the drop tower adjusted, the most promising existing prototypes will be retested and the design finalised.
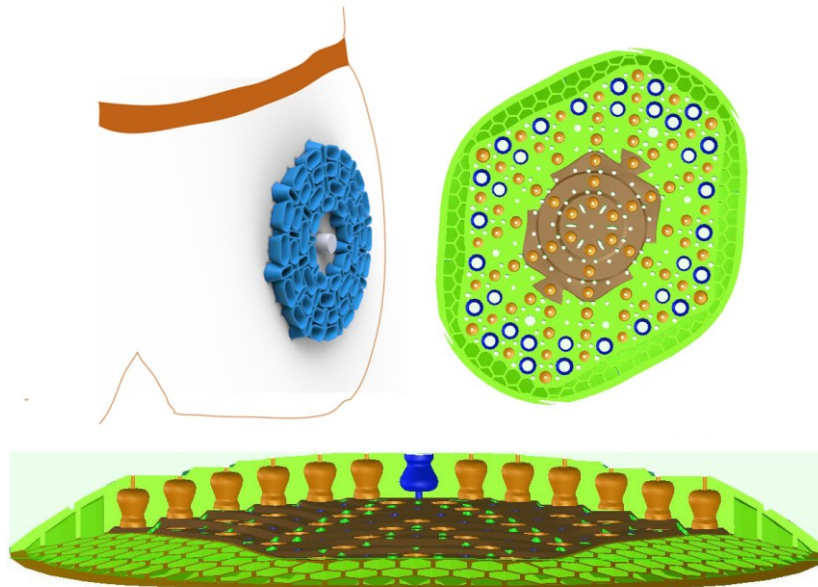
Figure 79 Hip protector concepts

Current concept designs are shown in Figure 79. The top left, in blue, is a current lightweight design using auxetic geometries in two layers (shown without fabric) that are ultrasonically welded together. The other two pictures show a CAD of an S2/S2F hybrid design that has been developed in a radial pattern around the GT.

The radial blue part has been prototyped in a pattern press with a simple tool. Both these parts are less than 11mm thick at the GT and taper off to the edge. The two parts from the pattern press are shown in Figure 80. In production these would be injection moulded in two parts, backed onto textile and then welded together. This is

a development of sample 290 that had been made in rectangle geometry in a test tool. For testing these were referred to as "radial lozenge pad H" or (pad H) and "sample 290" which were their test names.
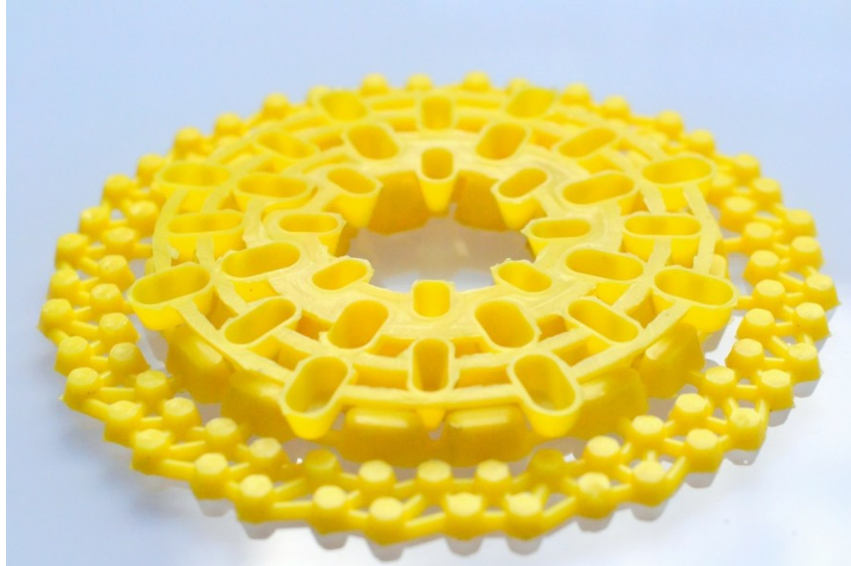
Figure 80 Prototype hip protector no fabric.

7.2.13 Testing results

With the working prototype complete, it was tested against existing products on the market. Accounting for the degradation from impacts, the new protector was impacted dynamically 5 times to replicate the tests that the existing pads had already undergone. As the prototype was made from re-melted pads, the molecular structure is slightly different and this could affect the wear rate.

In the interest of relative testing, all pads were then tested one after the other on the same day. It should be noted that the skin simulant was starting to show some wear after 300 tests and so these tests were off specification, but it was felt that testing on the same day would give relative results.

Table 10 Hip protector Impact testing

Hip Protector	Test 1 (kN)	Test 2 (kN)	Test 3 (kN)	Average (kN)	Rank
SafeHip Air X	1.87	1.8	1.84	1.84	1
New HipSaver	2.02	1.95	2.02	2.00	3
Fall Safe	2.09	2.08	2.12	2.10	4
Radial Lozenge	1.95	1.94	1.94	1.94	2
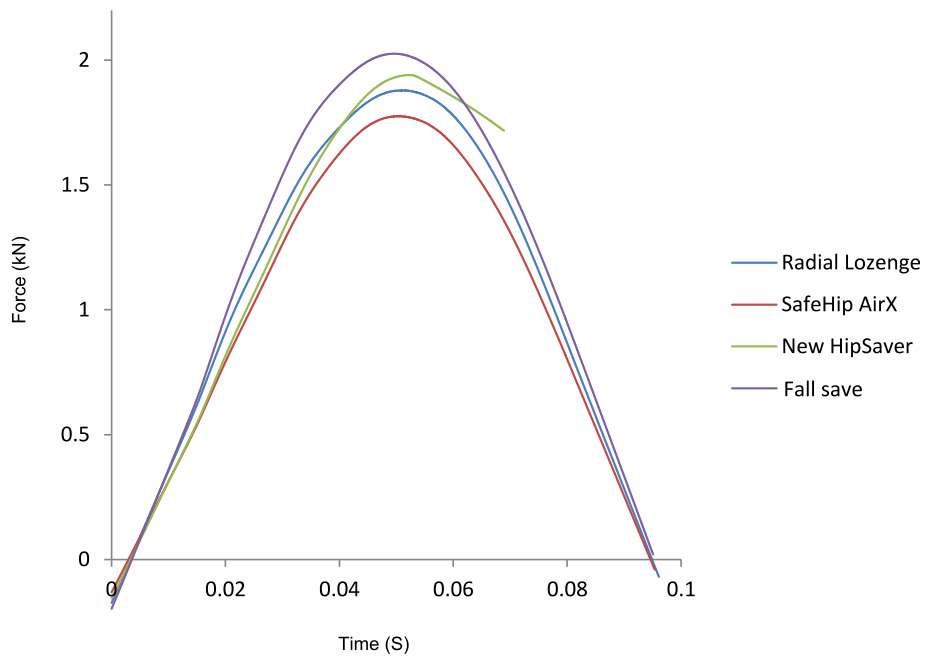
Figure 81 Smoothed Force Plots of 5 Hip Pads.

In this test, only the SafeHip Air X passed the 1.9 kN threshold. However, accounting for degradation after impacts, initial test values would be between 100-200 N lower. Radial Lozenge pad IMDS did not appear to degrade as much as the other pads. However, if moulded from the pelletised material with a superior quality industrial process, an improved result would be expected, taking the design below the threshold. The best values ever achieved by the above pads and original prototype are shown in Table 11.

Table 11 Hip Protector testing

Hip Protector	Best Value kN	% Energy Attenuated
SafeHip Air X	1.74	47
New HipSaver	1.92	42
Fall Safe	2.08	37
Radial Lozenge Pad H	1.94	41
Prototype 290	1.6	52

The rank order is little changed from the tests conducted at the same time, though prototype 290 attained a lower transmitted force. This shows promise for a full production version of the Radial Lozenge Pad, once it has been moulded with textile. Pad H at its thickest point is 12mm and Prototype 290 is 11mm thick. The force trace for Prototype 290 is shown in Figure 82.
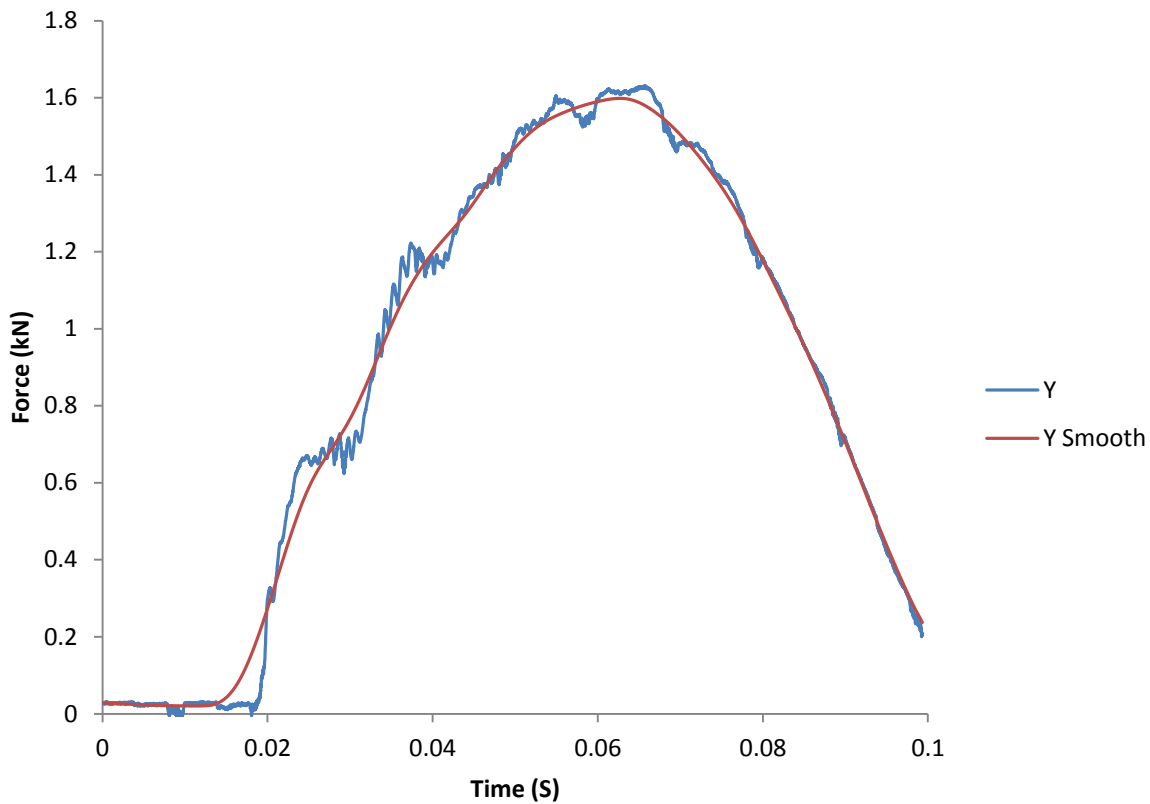
Figure 82 Force trace and smoothed trace for Prototype 290.

7.2.14 *Pressure distribution.*

The peak pressure distribution was measured using Sensor Products "Prescale Film", which gives a red colour code for peak pressure on impact; the brighter the colour the higher the pressure. Figure 81 shows the distribution of peak pressure for Pad H and also the unprotected dynamic test rig.
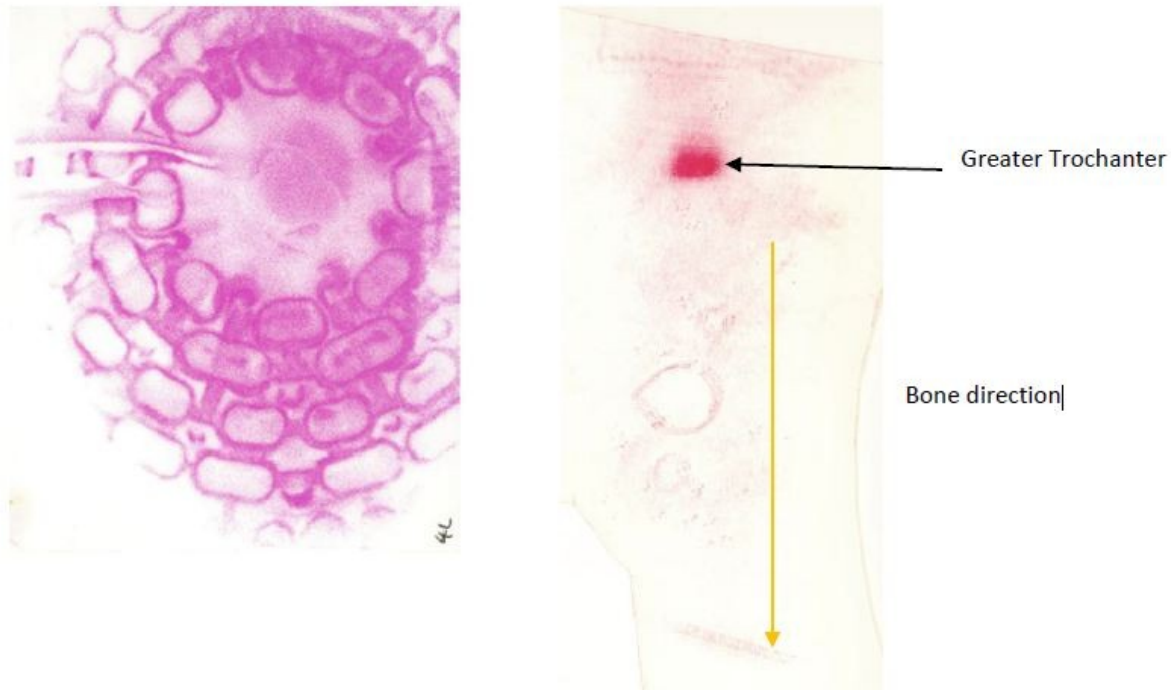
Figure 83 Pressure distribution with "Pre-scale Film".

7.2.15 Low Strain rate development Conclusion

The aim of the project was to design a device that works at low impact speed and corresponding strain rates. This part of the program has deviated a great deal from the initial target, due to the lack of standardised test method. It would have been possible to simply test a protective device at a lower impact speed on a traditional apparatus, but this would not have had relevance to the application. This program set out to develop a part for a specific need, the medical hip protector. The majority of work in this piece was developing the necessary anatomical test apparatus. Indeed this work has helped progress the understanding in this area for improved biomechanical testing. One of the outputs of this work has been to contribute to two pier reviewed papers and undertake a development role for the IHPRG group. The draft standard at time of writing is ready for public comment. It is unfortunate that this was not finalised so that these tests could have been done in exact accordance to that standard.

146

A pre-production prototype that equals the performance of current hip protectors but with improved flexibility and breathability has been produced. There are four key outputs from this section which can be taken forward:

- A working prototype of a hip protector which ranks second in performance.
- The thinnest hip protector that is breathable and flexible.
- Creation of an anatomically correct skin simulant for dynamic and static stiffness around the hip region.
- Calibration and progression of hip protector testing protocol towards forming the basis for a new British standard for hip protector testing.

7.2.16 Further Work

The next steps require validating the testing procedure and skin simulant in different test centres.

After such validation, the creation of an injection moulding tool would be the next step to improve the quality of production, to create samples for testing. Integrating the textile during manufacture should give an improvement in performance, as seen in Chapter 5. Once the tool is made, it would also be possible to produce parts in a few different grades, with different textiles, in order to further optimise the product.

After initial prototype parts have been dynamically tested, an investigation into "*smart pants"* would be the next step, looking at embedding wearable electronics into the smart device which could alarm, or alert either the user or a healthcare service that the user has experienced a fall over a certain magnitude, and therefore medical attention is advisable.

7.3 Medium Strain Rate Development : Motorcycle PPE.

7.3.1 Introduction

This chapter reports on the design and details development of body worn protectors suitable for protecting the wearer whilst motorcycling. The chosen PPE can be considered as two subsets, limb protectors and a back protector. The limb protectors cover the elbows, shoulders, knees and hips.

The limb protectors must meet or exceed the minimum performance requirements set out in the BSI standard for 'Motorcyclists' Protective clothing against mechanical impact –part 1',This has been previously referenced by its standardised code BS EN 1621-1:1998 and is referenced as EN1621-1 in this thesis. The back protectors must also attain the minimum requirements designated in their standard 'Motorcyclists' Protective clothing against mechanical impact –part 2', which will not be references EN1621-2. These standards have become well recognised in the industry and often referenced not only for motorcycle protection, but also skiing, snowboarding and mountain biking as well as a wider use in the sports protection industry. The cited test regimes have been chosen for the medium speed specific development equipment discussed in this chapter of the thesis.

The standard motorcycle tests are conducted with an impact velocity of 4.3m/s, with metal anvils as defined by the standards. Typical impact kinetic energies for these types of motorcycle tests and sporting good protection are $6\text{x}10^6$ J/m^3 ; for comparison, the impact energies resulting from a football tackle are around $5\text{x}10^4$ J/m^3 [72]. The research from Chapters 4 and 5 was completed in order to understand and develop the generic materials and geometry for simple plaque work and to enable initial development samples with auxetic geometry, typically in homogenous sheet form.

To move towards a product, the system needed to be developed to satisfy the specific test templates. In addition, an acceptable anatomical fit needed to be developed. The motorcycle limb protector standard describe

the minimum area coverage and the weighted average impact performance that the tested parts need to pass in order to attain CE accreditation, this to some extent determines the performance level that the protector must reach over the core area of the protector.

7.3.2   Motorcycle PPE Limb protector development to EN1621-1:1997.

This BSI test method defines the test regime and provides templates for the areas to be tested for impact; the anvils and drop tower have already been discussed in Chapter 4.1.1. This section reviews the filtering on the load cell to comply with the BSI standard and also the minimum templates for the protectors.

7.3.3   Force measurement instrumentation

" *The anvil shall be mounted so that during impact testing the whole force between the anvil and the massive base of the apparatus passes through a quartz force transducer, in line with its sensitive axis. The force transducer shall have a calibrated range of not less than 200kN and a lower threshold of less than 1kN. The output of the force transducer shall be processed by a charge amplifier and displayed and recorded on suitable instruments. The measuring system, including the drop assembly, shall have a frequency response in accordance with channel frequency class (CFC) 1000 of ISO 6487*."[55]

The tests also state that the signal should be filtered with a 4th order Butterworth filter. Development tests prior to this were performed with no filter and a lighter anvil, to get more accurate readings. From this point, the tests were performed without the filter and the filter applied to the generated data retrospectively in the software.

7.3.4   Shape and dimensions of templates

"The templates shall comply with the shapes specified in Figure 84 Dimensions for limb protectors EN1621-1, and the dimensions". The manufacturer shall provide sufficient information to the testing laboratory to allow it to select the appropriate size of testing template from the above table". It is worth noting that "The type B protector dimensions are intended to cover the needs of most motorcycle riders. However, for ergonomic

reasons, in certain cases the type B protectors may be unsuitable. In such cases the alternative type A protectors may be chosen by the user."[55] These are shown in the table below and are usually used for smaller sizes and are often a better fit for female riders.
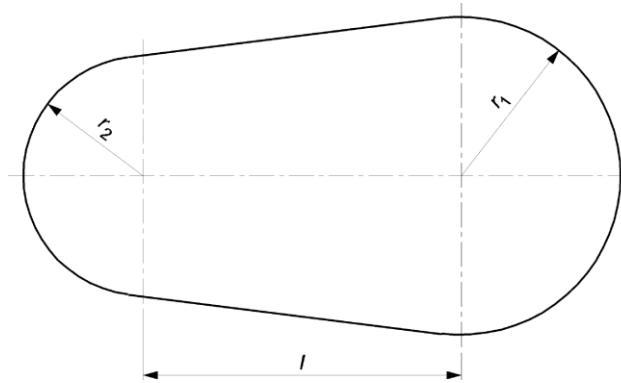
Protector	Type A protector mm			Type B protector mm		
	r_1	r_2	l	r_1	r_2	l
S	55	32	64	70	40	80
E	45	24	118	50	30	150
K	55	24	100	70	30	130
H	35	26	70	44	33	88
L	32	24	64	40	30	80
K + L	55	24	185	70	30	240

Figure 84 Dimensions for limb protectors EN1621-1[55]

The templates define the minimum test area of the protector. Peak transmitted force is to be less that 50kN, the average is 35kN.

7.3.5   Design and Manufacturing development.

The target mass for the limb protectors was 50 grams, which would be 50% of the weight of the lightest commercially available protector, at the time of writing. Level 1 for EN1621-1 can be achieved by a 4mm moulding of S2F backed onto a mesh textile, as described in chapter 6.4. However, when talking to development partners in this field, it was felt that this, although technically viable, would present difficulties for customer

perception, especially as most PU based protectors are normally 20mm thick. The requirement was to develop a 6mm thick protector that would be directly incorporated into a garment. The more flexible the protector the better and the closer the protector can be placed on the body. This would enable a smaller protector in terms of area to be used, as the protector would be located where needed and held next to the skin's surface. Traditionally, protectors are placed in loose pockets and allowed some freedom of movement. This is partly as they are not that flexible, and so cannot be in direct contact with the skin, especially at the elbow joint. By making a very flexible protector, it can be more precisely located with a smaller stand-off distance.   If constrained correctly, this ensures a smaller protector, with less chance of the protector moving away from the protection zone.

A driver for the design was to develop a part that could be stitched directly into the garment. From testing of the 6mm parts, these showed no drop off in performance at this thickness, with repeated impact. Hence the protectors could now be permanently fixed and would not have to be placed in pockets.

7.3.6   Auxetic Cell design.

IMDS S2 had been successfully moulded directly onto a textile (see Chapter 6), but the textile had to be cut into a complex shape, entered into the tool and then inserted onto one half of the pins for subsequent "in tool" moulding. For mass production the geometry was redesigned. Some of the ordinal cells as used in the IMDS S2 geometry were mirrored and a number of different designs were created in CAD, at a reference thickness of 10 mm. This development gave is the part shown in Figure 85. It should be noted that the 'domes' over the top of the cell are not shown in this screen shot. Effectively the roof of the solid part in CAD has been set to transparent so the internal cells can be seen. This gave the test design a mass of 13.21 grams.
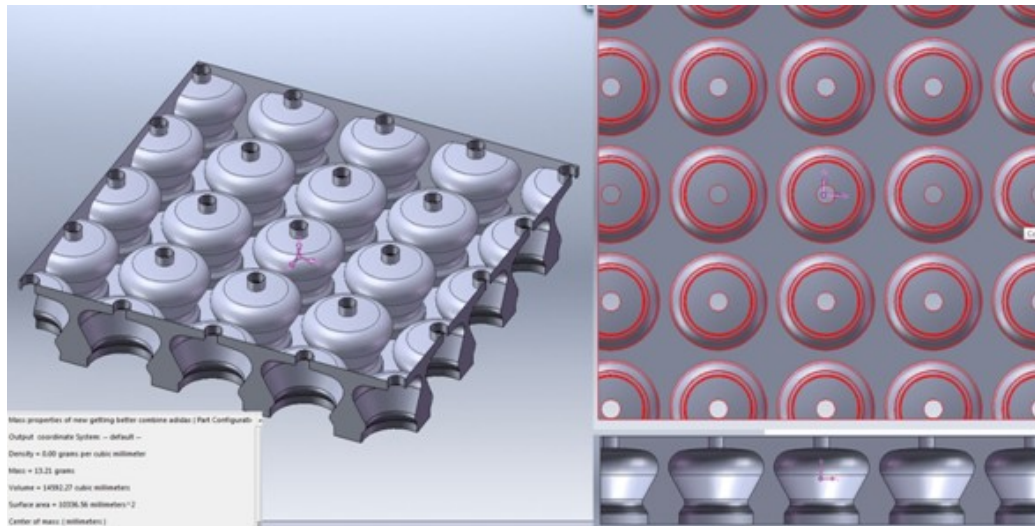
Figure 85 Quad offset CAD

Alternative cell lay-ups were designed. Figure 86 shows the final triangular offset for the auxetic pins. This part was a nominal 12.47 grams, which was 5% lighter than the quad offset design. Although only marginally lighter, this could have some benefits. The minimum distances between the cells are actually larger than for the quad offset cad, which helps with mould flow, and subsequent mould filling. Also the part has the capability to bend easily around three lines of symmetry, which should make for a more flexible part.
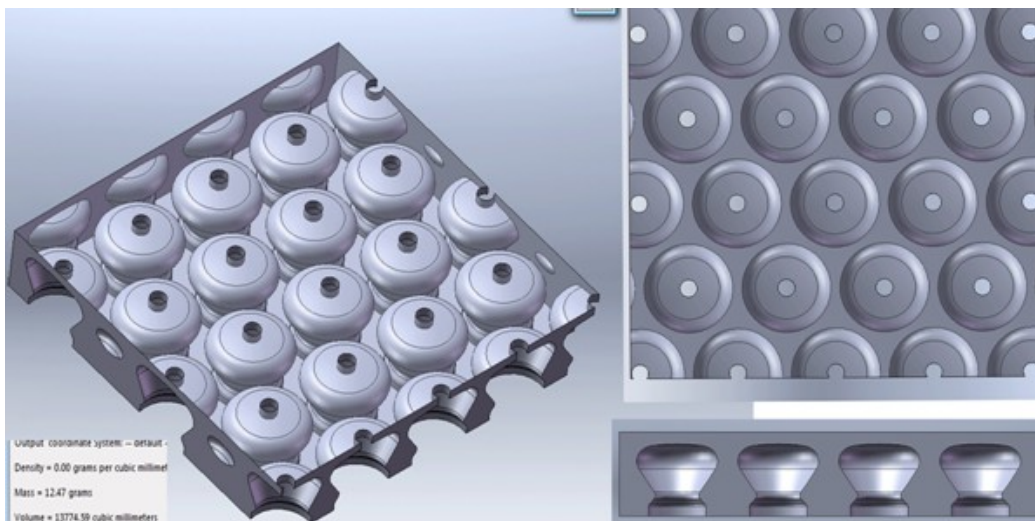
Figure 86 Triangular offset CAD

152

7.3.7   Anatomical form.

The anatomical form of the elbow was considered and the ligaments and fold lines of the skin were drawn onto a stretch thermal shirt. This was completed for different volunteers of different size, one such study is shown in Figure 87. The black lines follow the Humerus (up) and Ulna (down), away from the elbow joint. The thickness of blue marker is approximating the skin thinness at those points. The red marker pen shows the natural folds in the textile when the elbow is flexed. This was then unfolded, to understand how the skin moved, and the design process started.

Figure 87 Anatomical wrap

It was important that the product mimicked the movement of the wearer as much as possible and behaved like a second layer of skin. This part would be moulded onto textile making it possible to separate the edges of the piece from the core, and create a flat tool for easy of manufacture and assembly (stitching). Using this design, the part would 'curl' around the elbow mimicking the skin. The development for these designs is shown in

Figure 88. This shows the development of the main central protector with two islands. The gap between the central body and the islands would be minimised and the islands held in place by the textile.
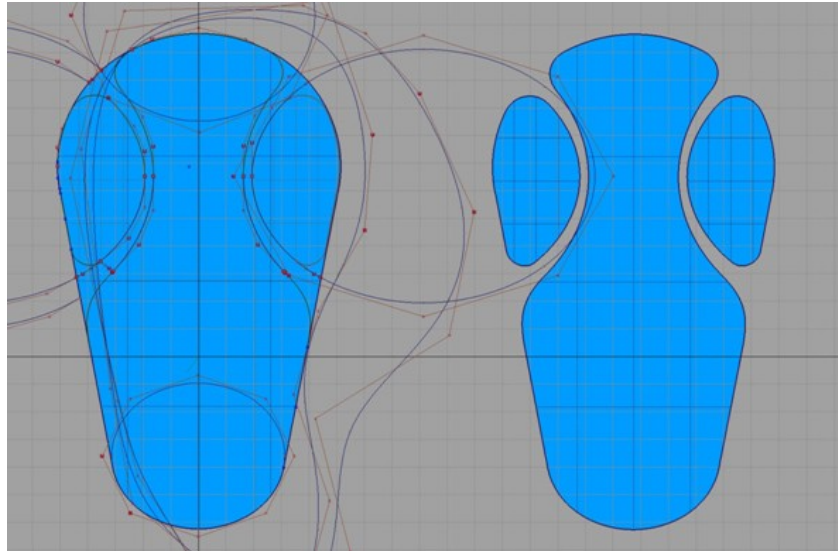
Figure 88 CAD outline of the elbow protector. Traditional (L), 3 piece with Islands (R).

7.3.8   Weight improvement.

To further reduce bulk and weight, the core of the outline, as shown in

Figure 88, was populated in S2F 6mm cells. The peripheral wings and a small part of the perimeter were extruded with a thickness of 4.5 mm and populated with cells; the central protector was made to be 6mm thick. This enabled the target mass of 50 grams to be achieved.

The CAD design was created. Moving from the CAD to the tool was not trivial. There is some considerable know-how in developing a tool with multiple different undercuts to create the auxetic geometry. Suffice to say there are many parts to the tool. A great deal of knowledge and expertise has gone into the design of this tool, the injection points, and some considerable thought as to how to eject the parts. These developments are property of the sponsor and cannot be reported. The surfaces of the tool are shown in Figure 86; left are the pins, right are the domes. There are three injection points, one for each section. The pins were mass manufactured with a form tool and inserted into holes in the parent tool. The textile is placed into the tool on the right, on location pins.

Figure 89 Production tooling

7.3.9 Results Limb Protectors.

The parts were tested to EN1612-1, which specifies conditioning of samples and a set of 8 tests completed and the average taken.
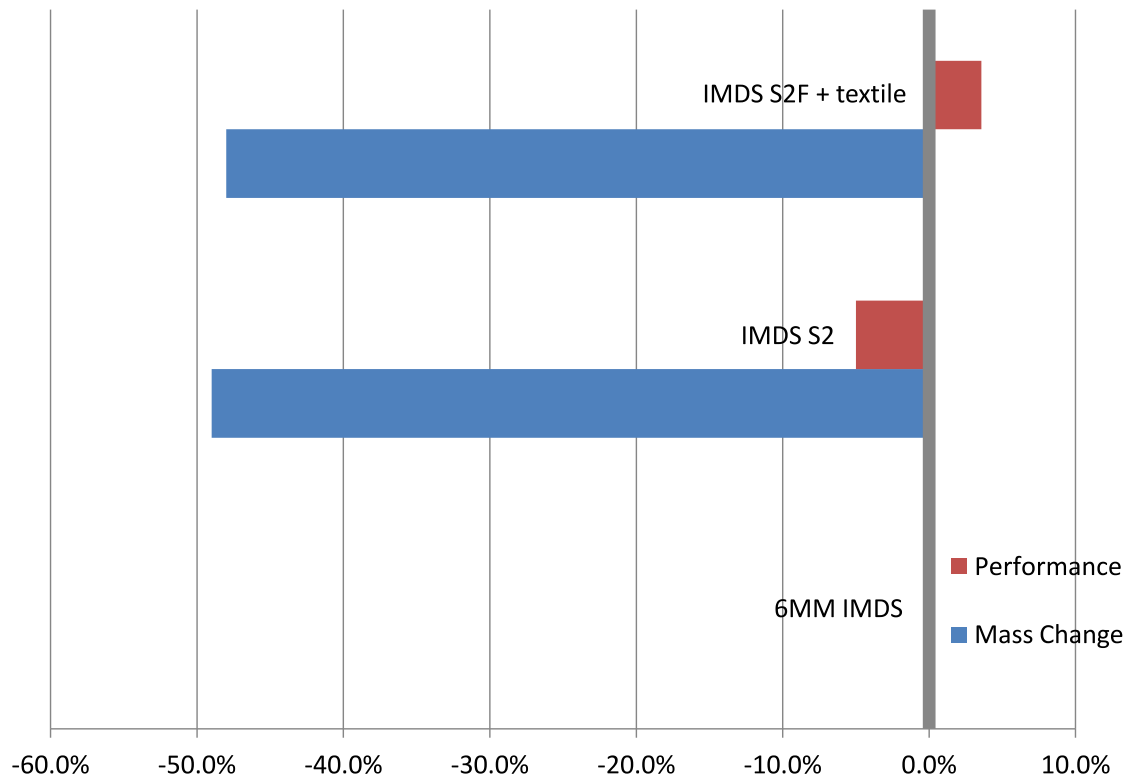
Figure 90 Relative performance of 6mm thick samples EN1621-1

Figure 90 the relative impact performance compared to the weight saving of the samples when compared to solid parts of the same thickness or a control. Mass change is shown in blue, a negative percentage shows a reduction in mass from the control and is expressed as a percentage reduction. Impact performance is again shown in percentage terms, a positive number would express an improvement in performance over the control. Best performance would be a reduction in mass (negative blue), with a performance improvement in transmitted force (positive red). By plotting the results this way we can see if the weight saving surpasses the impact performance change.

For the part mould in auxetic S2 geometry we can see that the reduction in mass out ways the performance reduction in impact performance, showing a 49% reduction in mass and only a 5% performance reduction for impact performance. When combining the auxetic geometry and a textile, the IMDS S2F textile part shows not

only a weight reduction but an impact performance gain. This textile backed part shows a 47.0% reduction in mass while attaining a 3.6% improvement in impact performance.

The performance of the parts was such that they exceed the required of transmitted force in the CE standard, EN1621-1, by 44%. Parts to this design configuration have since been tested and accredited by two external UKAS approved test houses.

7.3.10 Motorcycle PPE back protector development to EN1621-2:2003.

This test method defines the test regime and templates for back protectors to be used in Motorcyclists PPE. The complete standard is available from BSI, but when designing such a device it is important to review the specific templates which define the minimum area that the protectors should cover in order to reach certification. Figure 91 shows the templates that vary with rider size.

Dimensions			
A	B	C	D
72%	29%	44%	29%
All dimensions are referred to waist to shoulder length (100%) of the user			
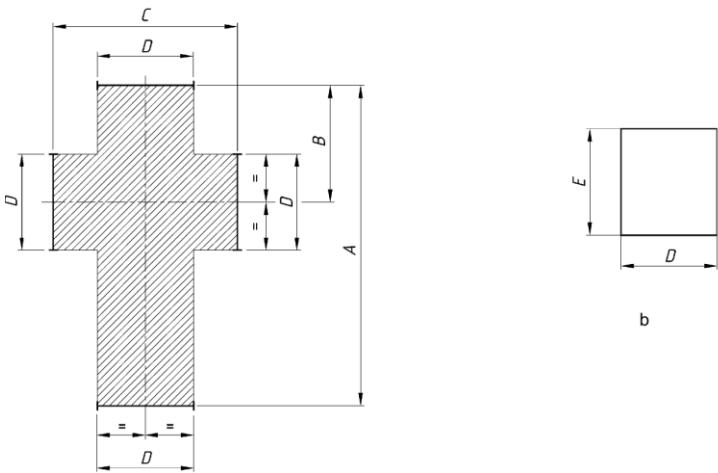
Figure 91 Dimensions for EN1621-2 Back protectors.

157

The back protector development program was carried through in a similar manner to the development strategy for the elbow protector. First, back protector shape outlines were developed with the standard templates and also reviewed in 2D CAD alongside the anatomical form. Maximum performance and comfort were achieved by shaping the part along the spine and anatomically shaping across the width of the product. Initial feasibility studies gave the rough outlines as shown in Figure 92.
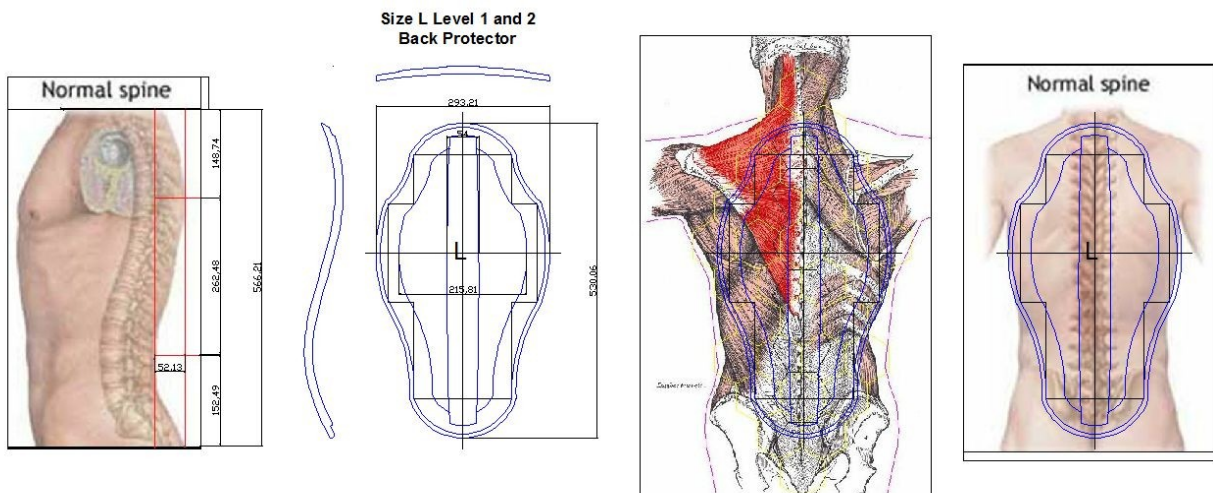
Figure 92 Back protector anatomical development

These anatomical shapes were used for the CAD designs. These were to be launched in the same range as the limb protectors from the previous section. The feel of the parts needed to be the same as well as the look. The CAD models were populated with auxetic cells similar to those in the limb protectors, but this time followed a contoured surface over the tool, in the centre over the spine this was 11mm thick.

These parts have been manufactured and tested. This was a not a trivial task, as the injection mould tool alone had over 1000 parts and is produced on a 1000 ton injection mould machine.

7.3.11   Results Back Protectors.
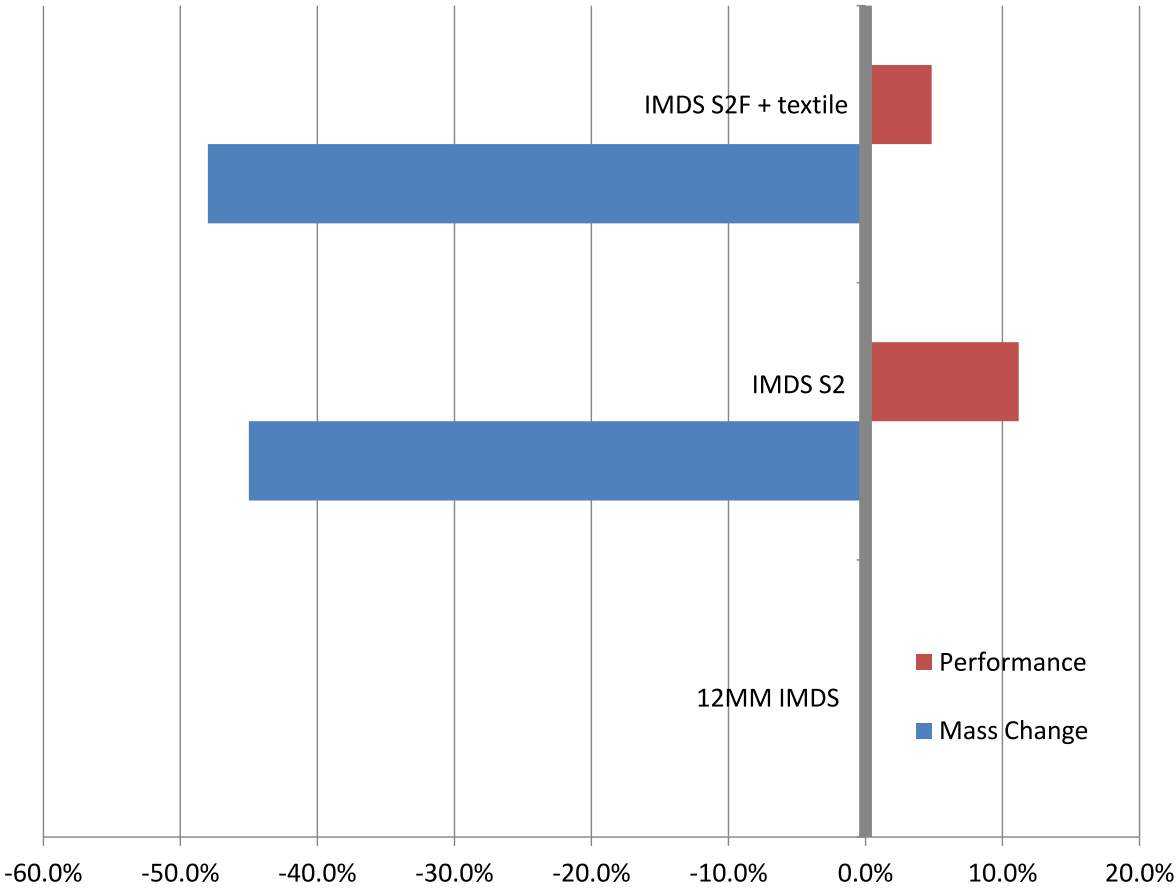
Figure 93 Relative performance of 12 mm thick samples EN1621-2

The relative performance of these parts can be compared to a control in a similar manner to the limb protectors

in the section above. For Figure 93 the control was a 12mm thick sample of solid IMDS, made by stacking two

6mm sheets from section 6. It was felt that this would be a better representation of the control than trying make

an 11mm part in a hot press. The tests were conducted in accordance with the CE standard EN1621-2, which

specifies five tests. The IMDS S2 parts were tested from a 12mm thick moulded sample. S2 samples resulted in a

45% reduction in weight and an 11.2% improvement in impact performance.

The parts with textile were also tested from the design in 8.2.9. Tests were completed on the central section of

the protectors at the thickest point measuring 11mm for these S2F parts, when compared to the comparator a

48% reduction in mass was shown, against a 4.8% impact performance improvement. This is not an ideal comparison as the parts were 1mm thinner than both the control, and the S2. It is not possible to draw too much into comparing the S2 part to the textile backed S2F part because of this 1mm difference. More research would need to be conducted.

The parts have since been accredited by an external test house and exceed the performance requirements of the standard.

7.3.12 Conclusion : Medium strain rate development

The aim of this focused development was to produce finished product for the medium speed strain rate development. Finished parts containing strain rate sensitive auxetic protectors that have been made with an injection moulding process and backed onto textile. The parts are flexible, thin and breathable. The four aims of the thesis have been addressed at this strain rate.

The limb protectors satisfy the pass criterion for the BSI Industry standard, and are currently the lightest and thinnest on the market. The back protectors again exceed the BSI industry standards, but in the opinion of the writer, these parts were still heavier than the target. The mass target could have been met by trimming the part back to the 'cross' shape, as defined by the standard, it was felt that this would give an inferior product with less protective coverage.

The products have been directly incorporated into a wearable garment as shown in Figure 94. This had not been done before as previous systems degraded after the first impact, due to local damage. The resultant product has been awarded two industry awards for innovation.

Images are courtesy of Bliss GmbH.

Figure 94 S2F parts incorporated into garment.

7.4 High Strain Rate Development : Ballistics

7.4.1 Introduction

The military and law enforcement markets for ballistic armour continue to grow. The market for ballistic protection in the United States for law enforcement is worth $140 million. It is estimated that this is about a 1/5 of the total US market [73].

There has recently been more demand for concealable or covert armour that can be worn under normal clothing. The drivers are for thinner, lighter and more comfortable ballistic protection. Today's armours are a compromise between comfort and protection. When rated for higher threat levels, they are usually made of many layers of fabric, as well as containing ballistic ceramic plates to protect vital regions against higher energy rifle rounds, which makes them bulky, heavy and stiff. In addition, the thick fabrics do not allow for good air circulation, which can lead to debilitating heat stress if an effective cooling system is not implemented [74]. Even armour, suited for lower threat levels, such as everyday police use, is regarded as uncomfortable to wear for extended periods.

Currently, lighter weight ballistic protection is possible from a range of materials. Today most these soft armours are manufactured from multilayer high strength fibres, quilted together to for the ballistic pack. Common materials are Ultra high molecular length poly ethylene (UHMWPE) or para-aramid, often referred to as 'aramid' or commonly by one manufacturers trade mark Kevlar®. Advances in high strength fibres are ongoing, but this research looks into reducing the mass of the ballistic pack with the addition of a strain rate sensitive material.

Although para-aramid based personal ballistic armour severely reduces the injuries caused by gunshots, the wearer can still sustain serious injuries, including broken ribs and damage to internal organs. 'Being shot with a .45" calibre round resembles getting hit with a 90mph baseball' [75]. Although the projectile does not pass

through the armour, injuries can be caused by a pressure wave transmitted into the body from the impact. Numerous studies have been carried out to attempt to quantify the energy transferred into the torso of the wearer by this pressure wave and the damage that it causes. When testing to current test methods [76], [29] the energy is transferred through the ballistic pack and on to a "whiteness" medium. In this case, it is a non-work-hardening clay. The depth of impression created into the backing material by the round impact, is representative of the amount of energy which would be transferred to the body of the wearer. If the energy is not sufficiently absorbed or spread out by the fabric, deep impressions will be made which indicate that the armour would still allow the round to cause blunt trauma. The measured perpendicular depth of the signature into the clay is called the Back Face Signature (BFS). This is a very simple test and the clay is easily calibrated. It is believed that by improving the ability of ballistic armour to reduce the BFS you can reduce the injuries the wearer will sustain.

7.4.2   Trends Supporting the Customer Unmet Need

The continued advancement in ballistic armour has led to various innovations which are helping to address the current demands for improved comfort, lower weight, greater flexibility, and most importantly, better ballistic protection. These include new materials, composites, fabric coatings and other unique ideas. Current trends are looking to reduce the BFS of the pack, from the National Institute Justice (NIJ) level of 44mm to the Police Scientific Development Branch (PSDB) level of 22mm. A recent tender was also made by the Japanese military for a reduction to 20mm BSF. This reduction in BFS has led indirectly to an artificial stiffening of the pack, further reducing comfort. It is hypothesised that an active system would keep the low speed flexibility but still significantly reduce BFS when struck by a high speed projectile.

A major gaol of the present research is therefore to show that a strain rate sensitive dilatant material in the ballistic layers can have a positive effect on BFS.

Two earlier studies have investigated the effect on BFS of coating ballistic armour. One used a colloidal shear thickening fluid (450nm silica particles dispersed in ethylene glycol) [4], whilst the other used a dry powder that exhibits dilatant properties [77]. In both studies the modified fabrics showed an improvement in ability to disperse energy and reduce BFS. In the former study, utilizing silica particles, they found that the coated fabric provided equivalent ballistic properties in terms of BFS per unit mass, but a coated armour sample was thinner and more flexible.

7.4.3   Current Test Methods.

A number of standards exist by which to classify ballistic armour. They rate armour on how capable it is of protecting against ballistic threats, ranging from low velocity handguns to armour piercing rifles. Each region and occupation generally requires its own test method, as the most commonly encountered threats vary by geographical location. For example, British police will not usually expect to encounter weaponry more deadly than pistols and shotguns, whilst assault rifles and submachine guns are more common throughout the USA. Furthermore, prison wardens will be considerably more likely to require armour capable of stab resistance than protection against high velocity rounds. Typically, each armour sample is tested for penetration, BFS and ballistic limit. The armour is fitted over a calibrated backing material and shot at specific points, generally not close to a previously tested point of impact or an edge of the material.

The National Institute of Justice (NIJ) standard was designed to establish a minimum performance standard of personal ballistic armour designed to protect the torso. To conform to the standard, armour panels must pass two tests, a BFS test and an ultimate ballistic limit test. Different threat levels in the NIJ tests are shown by the pack's ability to provide the same BFS with different ammunition. The limit for the depth of this impression under the US-NIJ police standard is 44mm (liberal compared to many other standards, for example the British standard specifies 25mm as a maximum depth) [76], [29].

7.4.4   National Institute of Justice NIJ 0101.04

To perform the tests, the armour panel is placed in contact with an open faced wooden or metal tray (610 x 610 x 140, all ± 2mm) containing a homogeneous, non-work-hardening, oil-based modelling clay (specified as Roma Plastillina #1). The clay must have a smooth flat surface level with the top of the tray and no air gaps. For the ballistic limit test, the tray has no back attached (to avoid it getting damaged when the jacket is penetrated). The clay acts as a witness medium so the maximum deformation caused by the test can be measured. Before the clay can be used it must be calibrated by dropping a steel sphere 63.5 ± 0.05mm in diameter, mass 1043 ± 5g onto it, from a height of 2m, 5 times. Impacts must be a minimum of 76mm from the edge of the tray to the edge of the indent and a minimum of 152mm between indent centres. The arithmetic mean depth of the five deformations must be 19 ± 2mm. If the clay does not pass this test then its mechanical properties can be altered by heating or cooling the clay [76]. Different ammunitions are then fired at the armour panel at different velocities, depending on what level of protection the armour is being tested to. There are six different levels, these are;

Type I.   This is the minimum level of protection that any officer should have. Provides protection against 0.22" calibre long rifle lead round nose bullets and 0.380" ACP full metal jacketed round nose (FMJ RN) bullets.

Type IIA.   Provides protection from lower velocity 9mm and 0.40" S&W ammunition.

Type II.   For protection against high velocity 0.357" Magnum and higher velocity 9mm ammunition.

Type IIIA.   The highest level of protection available in concealable body armour. Provides protection from high velocity 9mm and 0.44" Magnum ammunition.

Type III.   Provides protection from rifles, typically 7.62mm full metal jacket bullets at high velocity.

Type IV.   Protects against high powered armour piercing rifle rounds, which are clearly intended for use only in tactical situations when the threat warrants such protection.

For the Type II tests, the two different ammunitions that are fired at the armour panel are;

- 9mm FMJ RN bullet, mass 8g, velocity 367 ± 10m/s
- 0.357" Magnum JSP bullet, mass 10.2g, velocity 436 ± 10m/s

A total of 48 bullets are fired at six identical armour panels in a strict regime, sixteen of which are at an angle of 30 degrees. The maximum allowable deformation into the clay from any impact, as measured from the front face of the clay backing material (the BFS), is 44mm.

Further details about the Back Face Signature test procedure, including detailed specifications for velocity measurements and firing sequence, can be found in the full standard [76].

For the ballistic limit the test's aim is to statistically determine the velocity of bullet that will be stopped 50% of the time.

7.4.5 *PSBD body armour standards for UK police (2003)*[78].

The PSBD standard is very similar to the NIJ standard. According to the PSBD standard, the Back Face Signature test is carried out by placing the armour panel in front of a 450mm x 350mm, 100mm deep steel tray filled with Roma Plastillina #1 modelling clay. Before being used the clay must be calibrated by dropping a 1.030 ± 0.005kg sphere of diameter 63.5 ± 0.05mm onto it from a height of 1.5 ± 0.02m a minimum of two times (ensuring no impact is within 75mm of an edge or another impact) . The arithmetic mean deformation into the clay measured from the top of the steel tray must be 15 ± 1.5mm. If the clay does not pass this test then its mechanical properties can be altered by heating or cooling the clay. Once the backing material and armour are correctly set up, a selection of ammunition is fired at the armour panel at various speeds, depending on the level of protection the jacket is being tested to. There are five levels of protection according to the PSBD standard, these are;

HG1/A   Lightweight flexible armour intended for use by the unarmed officer in very low risk patrolling situations. Suitable for overt and covert use.

HG1   A general duty armour for low risk situations. May be overt or covert.

HG2   Special duty armour intended for use in firearms operations. Can be used in conjunction with RF1 and SG1 plates. Usually overt.

SG1   Offers protection from full length shotguns at close range. Usually used in conjunction with HG2 armour

RF1   Offers protection against soft core ammunition fired from rifles. Usually used in conjunction with HG2 armour.

As with the NIJ standard, each of these levels has different ammunition and impact velocities with which it must be tested. These are designed around the HG1/A tests, for which the two bullets are;

- 9mm FMJ RN Dynamit Nobel, mass 8.0g, velocity 360 ± 10m/s
- 0.357" soft point flat nose Remington, mass 10.2g, velocity 385 ± 10m/s

Six shots are fired at each armour panel being tested, in a specific order, two of which impact at an angle of 30 degrees. The maximum allowable back face signature of any impact for level HG1/A is 44mm, and the maximum for HG1 is 25mm.

It should be noted that these tests were completed before the release of the 2007 HOSDB standard,

'Home Office Scientific Development Branch (HOSDB) publication No. 39/07/C which governs stab resistant body armour performance in the UK' [29].

7.4.6   Overview

This study investigates the effect of coating ballistic material with a shear thickening material, on ballistic properties. The effectiveness of the coating was measured by firing 9mm full metal jacketed rounds at the samples at 360m/s, using a helium powered gas gun, and measuring the Back Face Signature with a clay witness medium, in accordance with reference to PSBD standards (valid at the time of testing). It was possible to test in line with this standards on a gas powered gun under laboratory conditions. These tests have been conducted and form the majority of the high speed testing for this research.

7.4.7   Test Methods.

The high speed tests were completed at Imperial College on the Mechanical Engineering Department's gas gun. Tests can be conducted in a short amount of time without the need of a firearms license, and without the necessity to hire a range.

There were two limitations when using this equipment:

-The barrel of the gas gun is not rifled, so the fact that the round is not spinning may have an effect on the results. However the relative value of the rotational velocity compared to the linear velocity is low, so the effect should not be apparent in BFS terms. The rotation helps to keep the projectile from tumbling and as there was concern that this could occur in flight, the distance from the barrel to the pack was minimised.

- The maximum velocity of the rounds is limited. Depending on the gas used to power the gun, there is a maximum velocity that the rounds will reach. The maximum projectile velocity achieved when using a 9mm round fired with nitrogen is 260m/s, with helium it is 360m/s. For this reason the tests were modelled around NIJ level II and PSDB level HG1/A (the higher levels required higher round velocities). For this reason it was not possible to measure V50, on this equipment.

Following advice from technical experts, tests were only performed with 9mm FMJ rounds, not with the 0.357"

rounds. This was done because the 9mm test is supposedly far harder to pass than the 0.357" test, "if a sample

passes the 9mm test it can be safely assumed that it would also pass the 0.357" test with respect to back face

signature". (Conversation with Dr C. Watson)[].

7.4.8   Gas Gun

The original firing mechanism used a solenoid activated valve on a high pressure air supply to open the main

valve. However, it was found that the solenoid caused an electrical interference that would trip the triggers on

the oscilloscope, making it impossible to measure the speed of the projectile. To overcome this problem this

valve was changed for a manually activated guillotine valve. Figure 95 shows a schematic of the gas gun, which

consists of a barrel, a fast acting valve, a charge tank and a sabot stripper. It was originally setup to run on

nitrogen and used to fire ball bearings into composite panels; to achieve the velocity needed in these tests, the

charge gas was helium. The armour being tested was held against the backing material with an elastic bungee.

The ballistic chamber is not shown in the schematic.

Helium Pressure Gauge

Sabot Stripper

Backing material
Roma plastilina

Charge Tank

Barrel

Fast Valve   Armour
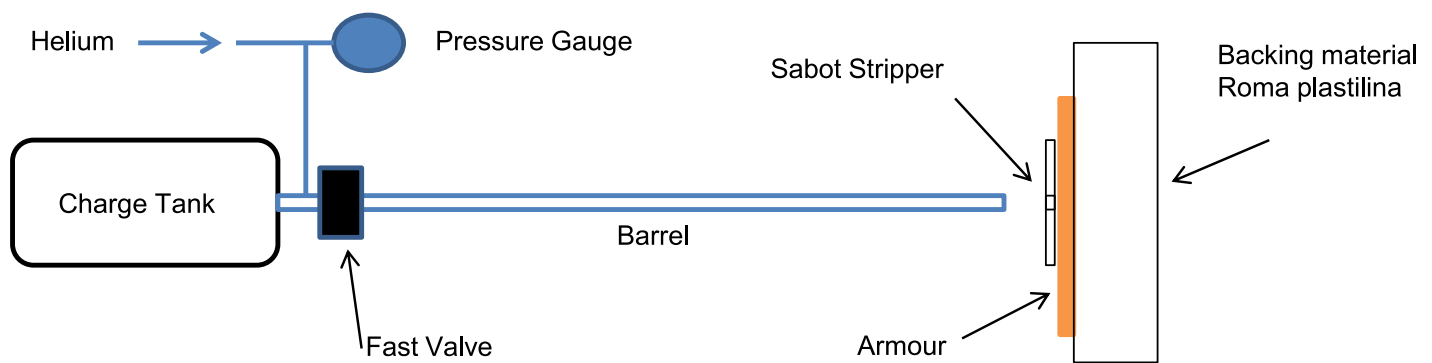
Figure 95 Schematic of Gas Gun

7.4.9   Sabot Making and Preparation

Because the bore of the gas gun is far larger than the diameter of the round, the manufacture of a number of

sabots was required. A sabot is a device that holds the main projectile and fits snugly into the barrel to ensure no

gas escapes down the sides, making a good seal to the bore of the barrel. A sabot stripper was installed at the

end of the barrel. The sabot stripper was used to remove the sabot just before the round impacts the jacket. If

the sabot is removed too early then there is a chance of the round tumbling. A manual injection moulding

machine, was used to manufacture the sabots along with a three piece mould. These were moulded in low

density polyethylene in batches made on the same day to try to reduce any variability in part mass. It was

necessary to prepare the sabots, post-moulding, by trimming away excess polymer around the skirt and back

face surface as shown in

Figure 96.
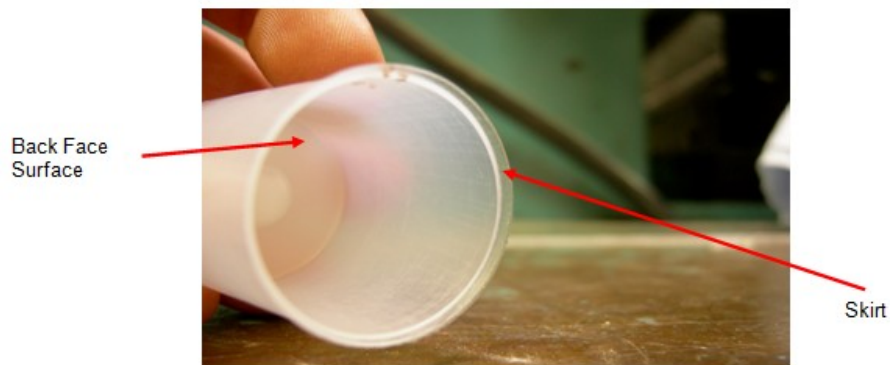
Figure 96 Sabot and Skirt

In order to ensure that all ballistic tests were conducted at a similar speed, it was important that there was

minimal variation between individual sabots. As the sabots were made manually, there were many factors that

could affect a sabot's quality. Their mass was measured, and fell between 6.30g and 6.55g, with the standard

deviation being 0.075g, and the arithmetic mean weight of the sabots being 6.439g. The sabots were then placed

on a mandrel, drilled and prepared for the projectile, as shown in Figure 97 . Prepared projectiles were grouped by mass to help limit speed variation.

Figure 97 Sabot undrilled, drilled and filled

7.4.10 Speed measurement

A speed sensor was implemented to measure the velocity of the rounds. Two sets of light gates were used in order to find the velocity before and after the sabot stripper, as shown in Figure 98.
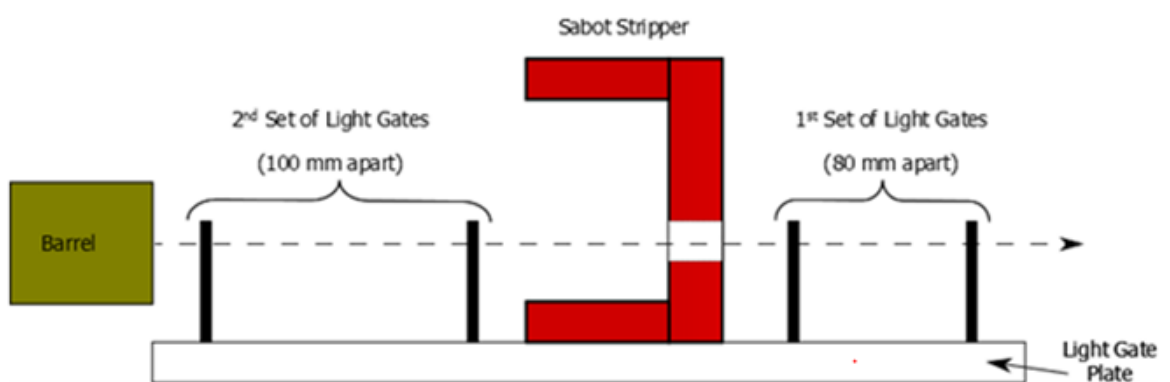
Figure 98 Light gates before and after sabot stripper.

Table 12 shows the threat level according to the HOSDB body armour standards for Police in 2007. The tests that the gas gun apparatus can simulate are highlighted in green. Under the full standard there is a standoff distance between the end of the barrel and the ballistic pack of 5m, for these tests, which will not be possible due to space restrictions and as noted previously the absence of rifling in the gas gun could cause the bullets to tumble with a large stand off distance.

Table 12 Test speeds and rounds for different threat levels.

Threat Level	Caliber	Bullet Description	Bullet Weight [g]	Bullet Velocity [m/s]	Bullet Energy [J]
HG1/A	9mm	9mm FMJ Dynamit Nobel, DM11A1B2	8,0	365 ± 10	533
	0.357" Magnum	Soft Point Flat Nose Remington R357M3	10,2	390 ± 10	776
HG1	9mm Calibre	9mm FMJ Dynamit Nobel, DM11A1B2	8,0	365 ± 10	533
	0.357" Magnum	Soft Point Flat Nose Remington R357M3	10,2	390 ± 10	776
HG2	9mm Calibre	9mm FMJ Dynamit Nobel, DM11A1B2	8,0	430 ± 10	740
	0.357" Magnum	Soft Point Flat Nose Remington R357M3	10,2	455 ± 10	1056

7.4.11 Preparation of Samples.

For this experiment sixty layers of Kevlar ballistic fabric, coated with shear thickening material. The materials were provided by Dr C. Watson and Professor Ian Horsfall of Cranfield University, in the form of ballistic packs. These were separated into individual layers and the para-aramid sheets were coated with active material. This coating material was X3180 from Dow Corning and was diluted in 50% Isopropyl alcohol. This was applied in different coat weights using a modified pad coater. The coat weights were varied by changing the pad pressure, and for the heaviest coat weight a second coating operation was used. The coated para-aramid was hung to dry for 24 hours. The packs were simply layered together and not quilted.

Samples tested are outlined below.

- Plain Kevlar   Set P   12, 16, 20, 24 layers

- Low Coat weight   Set III   12, 16, 20, 24 layers

- Medium Coat weight   Set II   12, 16, 20, 24 layers

- High Coat weight   Set I   12, 16, 20, 24 layers

- Composites   Decided after initial analysis was 8 Plain 8 Heavy.

At a thickness of twelve layers, none of the samples were able to arrest the 9mm FMJ round at 360m/s, and testing was halted. The tests were repeated at a thickness of fourteen layers, but none of the samples were able to stop the rounds at this thickness, so again the tests were halted. Samples at a thickness of 24 layers were then prepared so that there was a spread of results. To test a thickness of 24 layers, the top four layers of the 20 layer pack were simply folded over.

7.4.12 Results

The results of all the tests are shown in the Table 13. There were two discounted tests marked with an asterisk. Due to the limited number of samples and the materials already penetrated at 12 layers and 14 layers, only two shots per pack were measured.

Table 13 Full results High Speed Testing

Material	# Layers	Mass (g/m^2)	BFS (mm)				Penetrated			
			1	2	3	Average	1	2	3	Average
Plain	24	4982	32.3	29.4		30.85	2	3		2.5
I	24	6375	19.2	20.8		20.00	5	5		5.0
II	24	5973	26.0	29.6		27.80	4	4		4.0
III	24	5485	29.1	32.1		30.60	4	4		4.0
Plain	20	4152	27.8*	31.5	33.3	32.40	4	5	4	4.5
I	20	5312	25.7	21.8		23.75	6	6		6.0
II	20	4977	31.1	26.3		28.70	6	5		5.5
III	20	4571	35**	29.8	28.7	29.25	5	3	4	3.5
Plain	16	3322	36.9	36.1		36.50	4	3		3.5
I	16	4250	25.0	31.2		28.10	5	6		5.5
II	16	3982	32.1	29.8		30.95	7	7		7.0
III	16	3657	33.2	33.2		33.20	5	5		5.0
Plain	14	2906	Penetrated							
I	14	3719	Penetrated							
II	14	3484	Penetrated							
III	14	3200	Penetrated							
Plain	12	2491	Penetrated							
I	12	3187	Penetrated							
II	12	2986	Penetrated							
III	12	2743	Penetrated							
Plain + I	8 + 8	3785	29.8	32.0		30.90	3	3		3.0

*Discounted because speed too low
**Discounted because too near edge of sample

The average of these results has been plotted (Figure 99). This shows the number of layers versus the average BFS for the four packs.

174
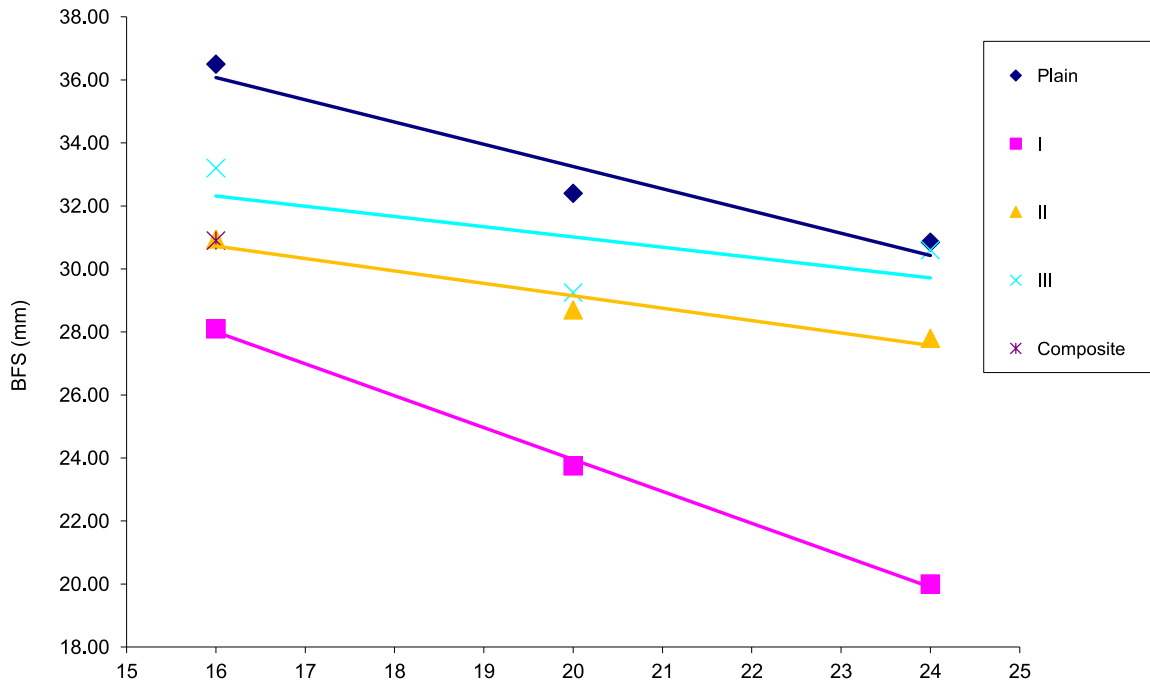
Figure 99 Number of layers versus back face signature

All of the test samples produced a lower Back Face Signature at higher thicknesses. Also, the heavier the dilatant addition, the lower the BFS. Table 14 shows the average percentage reduction in BFS compared to an equivalent thickness, uncoated jacket, for each test sample.

Table 14 Thickness versus back face signature summary

# Layers	Material	BFS (mm)	% reduction compared to plain Kevlar
24	Plain	30.8	-
24	I	20.0	35.2
24	II	27.8	9. 9
24	III	30.6	0.8
20	Plain	32.4	-
20	I	23.7	26.7
20	II	28.7	11.4
20	III	29.3	9.7
16	Plain	36.5	-
16	I	28.1	23.0
16	II	30.9	15.2
16	III	33.2	9.0

These results show that the dilatant material can be effective at lowering Back Face Signature for the same number of layers, providing up to a 35.2% reduction (set I at 24 layers) compared to para-aramid alone. Dilatant material coated para-aramid could be useful for covert jackets (where thickness is the determining factor) but does not take into account the higher mass of the coated fabric.

To start to see if there is any true benefit for coating a para-aramid with dilatant, area mass is plotted against BFS. Figure 100 shows the area mass of the pack in grams per square meter against BFS in mm.
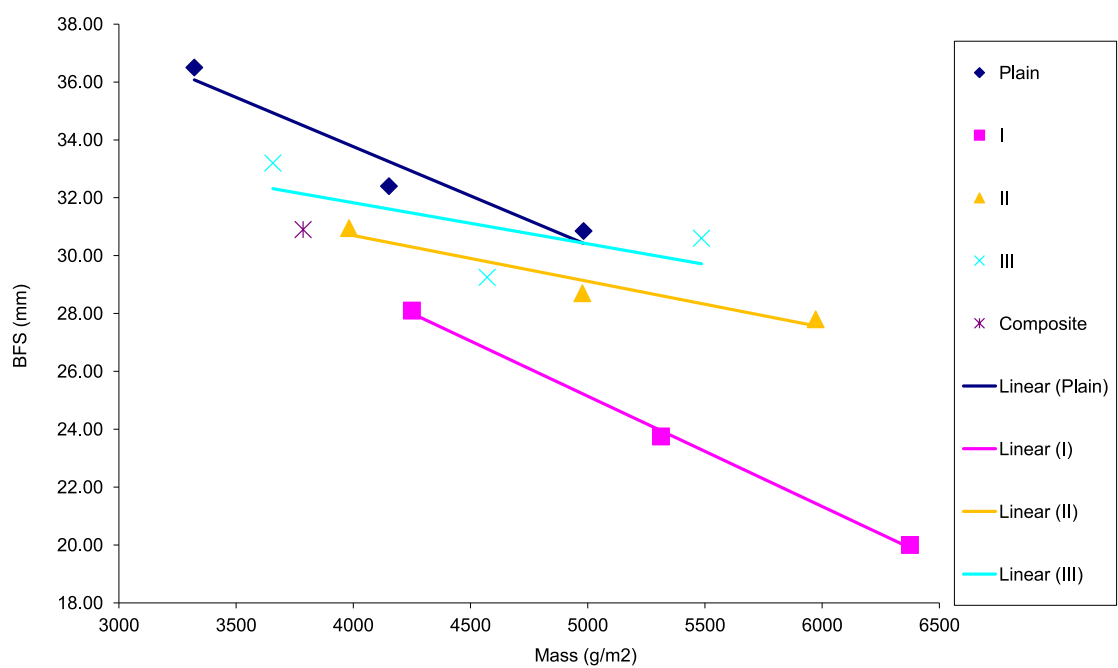
Figure 100 Area Mass versus back face signature

The results can also be considered in terms of pack density, or pack target density. This is achieved by considering a ballistic pack of a certain target area density. If considering a ballistic panel of approximately 4200g/m^2, the calculated theoretical BFS provided by a jacket can be found for plain material, and calculated for each coat weight. The BFS from a pack at a fixed target mass is shown in Table 15.

Table 15 - Summary for 4200g/m^2 armour panel

Material	BFS (mm)	% reduction compared to plain Kevlar
Plain	32	-
I	31	3.1
II	30	6.3
III	27	15.6

This table shows that the shear thickening material is effective at reducing BFS produced by a jacket of a set mass, producing up to a 15.6% reduction in BFS and requiring fewer layers of material.

7.4.13 Penetration

The number of layers of para-aramid that were penetrated by the round in each test was counted. The coated para-aramid showed a disconcerting trend in comparison with the non coated fabrics, as more layers were penetrated. It is not known if this would have an effect on V50, and more research needs to be conducted in this area.
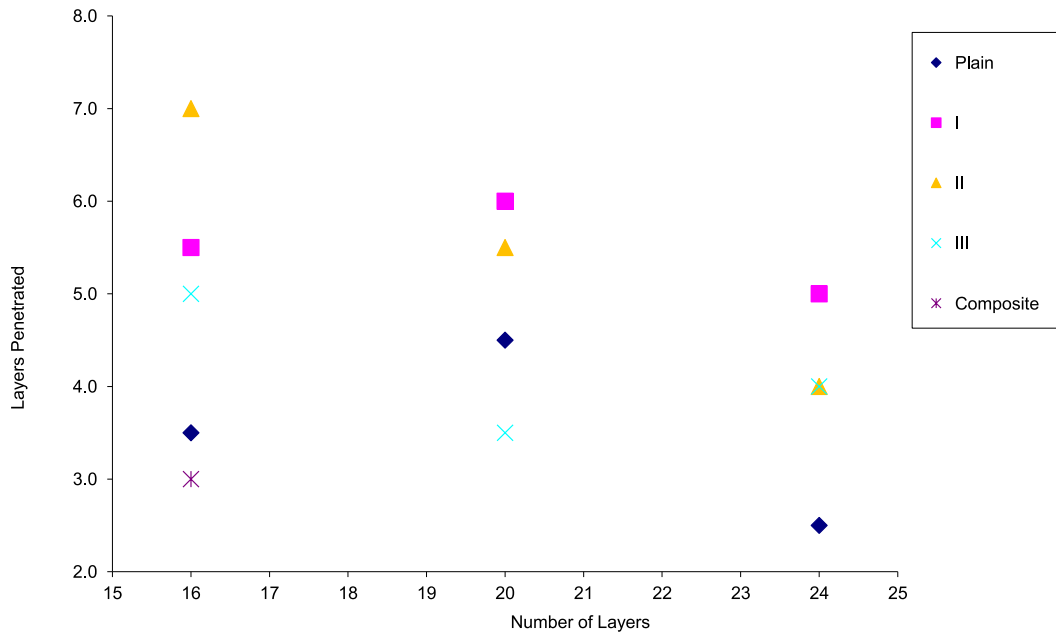
Figure 101 Number of layers penetrated

Although not completely conclusive, there is a slight trend for the heavier coated fabrics to have more layers penetrated before the round was arrested. A possible explanation for this was found by examining the samples after testing.

Figure 102 - First layer of coated sample

Figure 103 - First layer of uncoated sample

In the case of the heavily coated samples it appears that the round passed straight through the first layers of the jacket (very small hole) without be deformed into a mushroom shape, which would have made it easier for the pack to arrest it. It is only after a few layers that significant damage is noticed in the jacket. In the case of the uncoated fabric, it appears that the first layer of fabric was flexible enough to deform as the round struck it and so was able to avoid being penetrated until the round had started to become deformed. Another possible reason for the larger number of layers penetrated could be the inability of the coated fabrics to pull fibres through the pack, instead the fibres are simply being snapped, therefore absorbing less energy. This could possibly be due to the interstitial fibre friction.

Figure 104 - Fibres broken   **Figure 105 - Fibres pulled through**

These two pictures show that the uncoated fabric was damaged over a much larger area. This may have helped to arrest the round before it penetrated as many layers of fabric.

A difference was seen at the final layer that stopped the round, the coated packs seemed to hold their weave better just in front of the projectile as shown Figure 106 below.
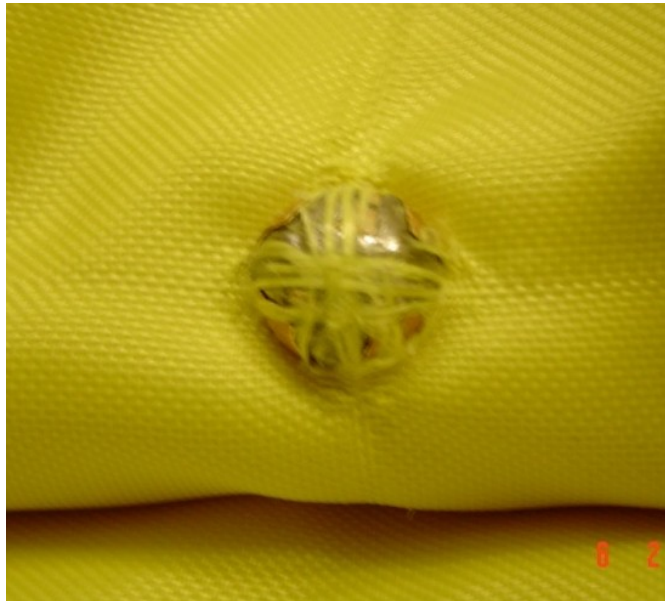
Figure 106 Photograph of hold in coated para-aramid

A composite made of eight layers of uncoated fabric, backed by eight layers of heavily coated fabric was constructed. This point is shown in Figure 100, depicted as a single cross called composite. Due to the limitation in availability of test material it was not possible to try other combinations.

This composite structure provided approximately the same BFS as the medium coat weight fabric of the same thickness. In this test, the composite was able to reduce the BFS by 15.3%, compared to an uncoated sample of the same thickness. From this research, a ballistic panel produced will give the same BFS for a lower thickness (covert use) or mass (everyday use), or a lower BFS for the same mass or thickness.

When mass is plotted against BFS, it demonstrates that there could be a potential benefit over the medium coated sample, as the total mass of the pack is decreased, as shown in Figure 107.
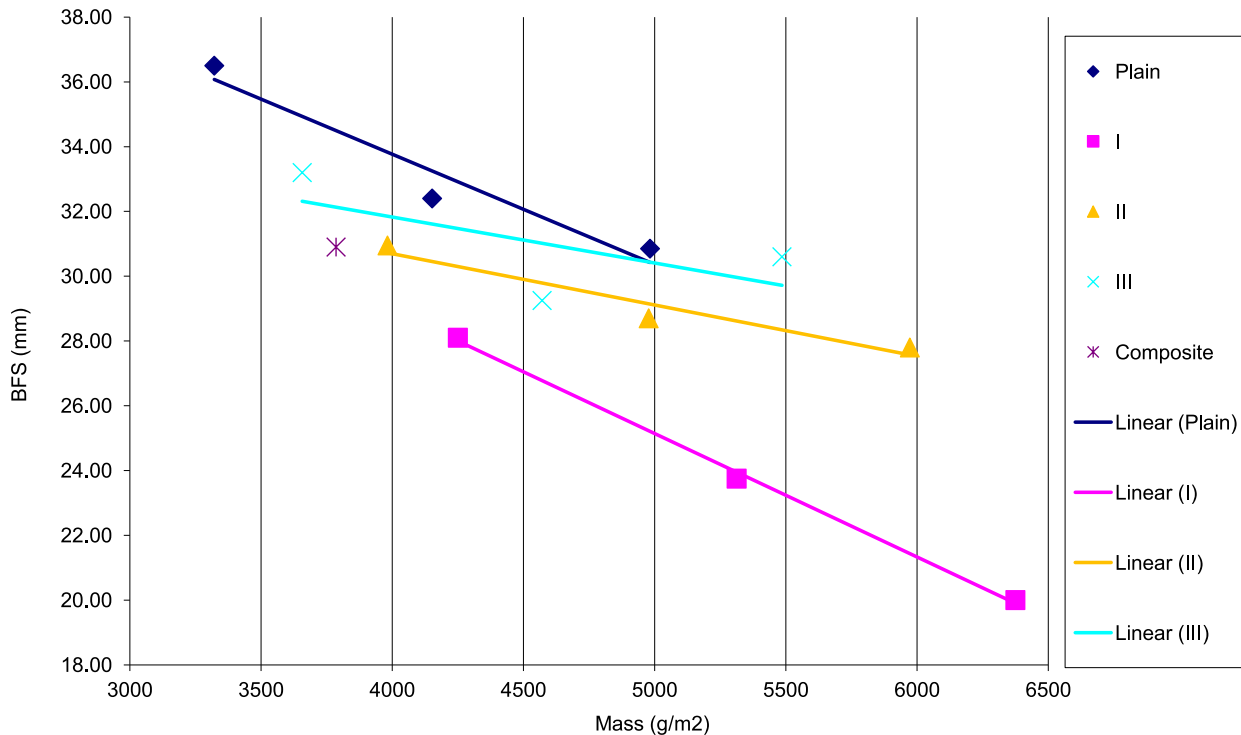
Figure 107 - Mass versus back face signature

Although the composite provides approximately the same BFS as a medium coat weight jacket for the same thickness, it only weighs 587.2g, compared to 617.6g for the medium coating weight jacket (4.9% less). If a jacket of equivalent weight were to be made from uncoated fabric (approximately 18 layers), according to this graph it would produce a BFS of 34.5mm compared to 30.9mm for the composite jacket (a 10.4% reduction in BFS for the same mass). Alternatively if a jacket was produced out of uncoated fabric, designed to provide the same Back Face Signature as the 16 layer composite jacket, it would have to be 24 layers thick and would weigh 772.8g compared to 587.2g (a 24.0% reduction in weight for the same BFS).

According to the above graph the composite jacket appears to have very little benefit over a heavily coated fabric in terms of BFS versus area mass. If you were to continue the pink trend line across towards the y-axis, it would pass below the value plotted for the composite, implying it would give a lower Back Face Signature for the same mass. Unfortunately, to make a jacket of equivalent mass to the composite jacket out of the heaviest

coated material, it would only be 14 layers thick. In the earlier tests it was demonstrated that a 14 layer jacket could not stop the round at these velocities. So V50 would be the limiting factor.

However the composite armour panel may have some potential benefits with regard to penetration over any of the other armour panels, as shown in Figure 101, however more research need to be done in this area. The composite armour sample was able to stop the round with only three layers being penetrated, the lowest penetration of any jacket at sixteen layers thick.

7.4.14 Fibre tests.

Single yarns of fibres that made up the packs were tested in an Instron at low rate to investigate the effects of the coating. Pneumatic Cord and Yarn Grips were used in accordance with ASTM D7269.

The yarns were simply pulled out of the packs by hand. These low speed tests were done at 0.01 s^{-1}. Three tests were carried out on each fibre with a gauge length of 300mm. Test were repeated three times.

The results of the three tests are shown in Table 16.To check for slippage, flags of tape were attached to the ends of the yard and monitored, to make sure there was no relative movement of the flag with respect to the grip.

Table 16 Testing of Para-aramid yarns

Uncoated				Coated		
Extension	Load	strain		Extension	Load	strain
7.595	183.6	0.036		7.195	183.1	0.031
7.106	170.6	0.033		7.735	184.6	0.033
7.116	173	0.033		8.216	188.3	0.036
MEAN	175.7	0.034		MEAN	185.3	0.034
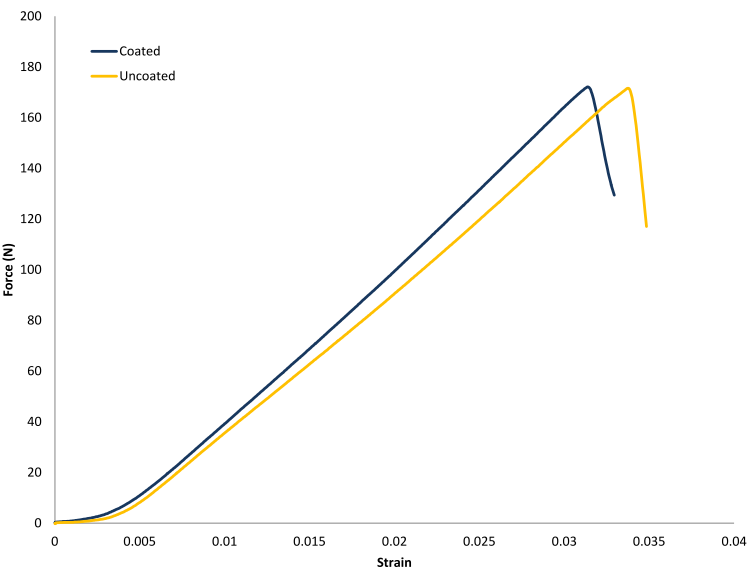
Figure 108 Single Fibre Force versus Strain Tests at 0.01 s^{-1}

Figure 108 shows the mean average of these fibre tests. The graphs show a small but slight increase in the force at failure, but at a lower strain. The increase in force may lead to some of the BFS improvement seen in the high speed tests, but is probably not as important as the potential increase in friction between the fibres, which may be attributed to the coatings.

It should be noted that the samples had been stored for over five years at this point. These tests should be repeated on more samples and newer samples, as the degradation of infused fibres over time could change. The low load at the beginning could be the 'crinkle' coming out of the yarn as it is initially loaded in tension. Further work would need to be done on yarns without this crinkle, to get more accurate values of strain to failure. With current techniques it would be difficult to coat single yarns and get the same infusion as coating a woven pack.

7.4.15 High Strain Rate Development : Conclusion

It would appear that there could be merit in impregnating para-aramid with dilatant mass. This research has demonstrated potential benefits in reduction of BFS with different levels of dilatant coating. These benefits have been shown for packs of the same thickness and also compared using area density. The benefit of using dilatant material with a high tenacity textile as the tensile layer has been shown. Clearly there is information lacking in that it was not possible to test V50.

There would seem to be more merit in adding dilatant mass to the rear of the pack, as was shown by the relative performance of the hybrid composite. It would be interesting in a future trial to test some of the more recent developments in this thesis, such as an additional layer of an auxetic sample behind the ballistic pack help reduce BFS, whilst promoting air flow and cooling. More research needs to be done with these systems to fully understand their benefits, as well as the variability introduced by the choice of test methods.

7.4.16 Future Work.

These tests were carried out on commercially available packs that were deconstructed and coated. It would be interesting to further develop these tests on new materials. However, these experiments did show some reduction of BFS reduction using strain rate sensitive materials, even on a commercially available pack of uncertain history.

The maximum attainable speed on the gas gun was 370m/s. Testing to establish the V50 value was not able to be achieved in this. V50 is clearly an important factor in developing a ballistic panel for a given area mass. More research should be done on this aspect to build up the complete picture of how these coatings could benefit operational packs. With hindsight, 14 layer samples could have been used to test V50 as per PSDB standard specification. However this may still not have been possible because of the amount of damage in the packs while testing and measuring BFS. As the packs were not quilted, the degradation of the packs was considerable, and there were insufficient samples or test areas to conduct a V50 test.

Ballistics Range.

Testing on a range with real ammunition and a rifled barrel might provide different results as the effect of rifling on the round is not known and this work could usefully be repeated on a range along with establishing the V50 limit.

IMDS S2.

The potential benefits of adding dilatant mass to the layers of para-aramid close to the rear of the pack have been shown. Adding a moulded IMDS material that was developed after these tests were completed could be beneficial. A light-weight layer behind the pack could give lead to interesting results, while not changing V50. A trial with an external collaborator is planned. There may also be a benefit of placing these materials between a ceramic plate and the pack, to help reduce the shock wave that travels through the panel.

Quilting

The effect of quilting on these panels was not tested. It could change the BFS. Recent discussions with American test houses have suggested that for single shot tests, differences would be small, but for multi shot impacts the panels would hold up better with quilting.

Unidirectional Fibres.

Future work should look at the effects of interstitial strain rate sensitive films in unidirectional panels.

Recently these tests have been repeated by Marco Petrucci at Cranfield Defence and Security, under the supervision of Professor Ian Horsfall, using a BABT anatomical torso. The damaged panels were reused. Petrucci sees similar trends to this work, but less pronounced benefit in BFS with the coated materials when tested on the anatomical torso. Repeating the work with new untested panels would be beneficial. There was too much damage in the packs to undertake V50 tests.

Thanks to Dr. Celia Watson and Professor Ian Horsfall from Canfield University for their advice and help in carrying out these first simple tests at high speed. Special thanks for supplying the base packs free of charge without which this research would not have taken place.

8 Conclusion

Strain rate sensitive materials which have the ability to change from a low viscosity to a high viscosity state whilst in the solid state, have generated considerable interest in the area of energy absorption systems used in personal body-worn protection. This thesis has explored the need to provide soft armours, which are both lightweight and flexible to improve compliance or wearability. This thesis sets out to explore methods for utilising silicone dilatants as part of a novel energy absorbing system, particularly looking at the synergistic benefit of utilizing these materials with internal geometries and architectures.

1 Materials Development - The primary aim was to develop a highly strain rate sensitive material incorporating silicone based dilatants, and to see if this could be used as 'soft armour' to protect the human body against impact. The main objective of this thesis has been accomplished, in that there is validated benefit in using a highly strain rate sensitive material as 'soft armour' to protect the human body against impact.

2 New Co-continuous blend Developed - The secondary aim was to determine if a new co-continuous blend could be designed that would be suited to the injection moulding process; allowing repetitive preproduction of samples and parts. New co-continuous blends were developed and tested in monolithic form and have been extensively tested to produce a novel blend that can be used for body worn protection; consequently the second aim of the thesis has been satisfied, these results have been validated using the techniques and methods developed in this thesis.

3 Auxetic Structures - The third aim of this thesis was to establish if different architecture and internal geometries could be designed and developed to further the performance of the highly strain rate sensitive materials. Auxetic architectures have been designed and developed. These have been moulded using industrial processes and have been experimentally validated by experiment and round robin tests.

4 Textile incorporation & layering - The final aim was to establish if the strain rate sensitive materials could be combined with a tensile layer and form a basic composite that could further benefit performance., This has been completed and has also helped develop an improved method of incorporating such armour into everyday clothing. Parts have been designed and developed and these are described in chapter 7.2 specifically for an end product. These parts combine a strain rate sensitive co-polymer with an auxetic geometry and a tensile layer. The parts have been validated against alternative systems as well as round robin testing.

5 Strain rate sensitive materials - These have been synergistically combined with auxetic structures to improve overall performance. The energy absorbing mechanisms which occur in such combinations also retain integrity for repeated impacts. This opens up a new methodology for protective equipment design as the protection elements can now be permanently attached to a garment, unlike their previous foam and EPS counterparts.

6 Test Methods and Standards - Development of new techniques and test standards have helped to develop these energy absorbing systems, and have contributed to new CE standards and tests methods.

Optimisation for three different strain rates.

The final output has been to design and engineer an active system for each of three strain rates. Low being in the order of $10^2 s^{-1}$, Medium $10^3 s^{-1}$. and high $10^4 s^{-1}$.

Medical Hip Protectors - Optimised at low strain rates, a system was designed and developed that meets the current impact requirement of the test method, achieves a product that is 36.6% thinner than the thinnest available on the market, with the added benefit of being soft, flexible and breathable.

Motorcycle PPE Protectors - Optimised for medium strain rate application limb protectors that have been design and developed to meet the current motorcycle test method. These injection moulded samples are able to pass the required standard in 4mm; this is currently 42% thinner than the best competing product on the market, as well as being light weight and breathable.

Ballistic Body Armour - The high strain rate focus was ballistics. The silicone based strain rate sensitive material was applied in a coating to existing ballistic packs. There were able to reduce the back face signature by up to 35.2% for the same thickness or by 15.6% for the same mass. It was not possible to test the ultimate ballistic limit and further work needs to be done in this area.

This work has led to the successful commercialisation of a new class of protective apparel. The development of these systems has introduced ten new products into the market place, has been awarded four industry awards, and realised over £500k of seed funding. To date over 100,000 pieces have been produced and global patents have been granted.

Research work in the medical sector is being continued and a proposed research program has gained the benefit of a Royal Academy of Engineering Fellowship, to be started on completion of this work.

The fundamental mechanisms by which energy absorption occurs have been reviewed in the light of the active systems considered. Strain rate sensitive materials have been synergistically combined with auxetic structures to improve overall performance. The energy absorbing mechanisms which occur in such combinations provide a stable system for a variety of environmental conductions, which will also retain integrity for repeated impacts. This opens up a new methodology for protective equipment design as the protection elements can now be permanently attached to a garment.

During the course of this work, the impact surface (in this case the human body) has been considered in detail, and an improved skin simulant, more suitable for low impact speeds, has been developed and tested. Synthetic subcutaneous materials have been developed to allow for improved test methods, and anatomically correct test procedures for low speed impact events have led to a new BSI standard coming into effect. Specifically a new skin simulant was developed for BSI 6366. Furthermore a new standard has been developed for medical hip protection. At the time of writing this is in the final draft as BSI 8575.

Experiments carried out during this research work have introduced high and low temperature tests and a high humidity test for BSI standards for motorcycle protection. BSI 1621, parts 1-4.

Feedback from improved anatomical tests developed from this research has also been incorporated into the development of a new Home Office standard.

References

1   Robinovitch SN, Evans SL, Minns J, *et al.* Hip protectors: recommendations for biomechanical testing--an international consensus statement (part I). *Osteoporosis international : a journal established as result of cooperation between the European Foundation for Osteoporosis and the National Osteoporosis Foundation of the USA* 2009;20:1977–88.

2   Gibson LJ, Ashby MF. *Cellular Solids: Structure and Properties*. Cambridge University Press 1999.

3   Bois P a. Du, Kolling S, Koesters M, *et al.* Material behaviour of polymers under impact loading. *International Journal of Impact Engineering* 2006;32:725–40.

4   Lee YS, Wetzel ED, Wagner NJ. The ballistic impact characteristics of Kevlar® woven fabrics impregnated with a colloidal shear thickening fluid. *Journal of Materials Science* 2003;38:2825–33.

5   Bettin G. High-Rate Deformation Behavior and Applications of Fluid Filled Reticulated Foams, Massachusetts Institute of Technology. *PHD Thesis* 2008;Massachuse:45–67.

6   Budden G, Vazquez F. Silicon technology for intelligent textile protection. *Rubber & plastics news*;36.http://cat.inist.fr/?aModele=afficheN&cpsidt=18476704 (accessed 5 Jan2014).

7   BSI Standards Publication BS 6366:2011 - Specification for studs for rugby football bootsRequirements and test methods. 2012.

8   BSI Standards Publication EN 13277 Parts 1–7 - Protective Equipment for Martial Arts :2000.

9   *BSI Standards Publication EN1621-1 Motorcyclists' protective clothing against mechanical impact Part 1 : Motorcyclists ' limb joint impact protectors — Requirements and test methods*. 2012.

10   *BSI Standards Publication EN1621-2 Motorcyclists ' protective clothing against mechanical impact Part 2 : Motorcyclists ' back protectors — Requirements and test methods. 2012*. 2003.

11   Robinovitch SN, Hayes WC, McMahon TA. Energy-shunting hip padding system attenuates femoral impact force in a simulated fall. *Journal of biomechanical engineering* 1995;117:409–13.

12   Santosa S, Wierzbicki T. Crash behavior of box columns filled with aluminum honeycomb or foam. *Computers & Structures* 1998;68:343–67.

13   Mills NJ, Gilchrist A. Bicycle helmet design. *Proceedings of the Institution of Mechanical Engineers, Part L: Journal of Materials: Design and Applications* 2006;220:167–80.

14   Batchelor GK. *An Introduction to Fluid Dynamics Cambridge Mathematical Library series, Cambridge University Press*.

15   Barnes HA, Hutton JF, Walters K. *An Introduction to Rheology*. Elsevier 1989.

16   Ramachandran M. *Basic Orthopaedic Sciences: The Stanmore Guide*. CRC Press 2006.

17   Wetzel ED, Wagner PNJ, Lee YS. Novel Flexible Body Armor Utilizing Shear Thickening Fluid (STF) Composites.

18   Bettin G, Mckiey GH. Energy Absorption of Reticulated Foams Filled with Shear-Thickening Silica Suspensions. *Massachusetts Institute of Technology* 2005.

19   Wetzel E, Lee Y, Egres R. The effect of rheological parameters on the ballistic properties of shear thickening fluid (STF)-Kevlar composites. *AIP Conference …* 2004;:1–6.

20   Coleman PCPMM, Coleman PCP. *Fundamentals of polymer science : an introductory text*. Lancaster, Pa.: : Technomic 1997.

21   Rinde JA. Poisson's ratio for rigid plastic foams. *Journal of Applied Polymer Science* 1970;14:1913–26.

22   Choi JB, Lakes RS. Fracture toughness of re-entrant foam materials with a negative Poisson's ratio: experiment and analysis. *International Journal of Fracture* 1996;80:73–83.

23   Alderson A, Alderson KL. Auxetic materials. *Proceedings of the Institution of Mechanical Engineers, Part G: Journal of Aerospace Engineering* 2007;221:565–75.

24   Stott P, Mitchell R, Alderson K, *et al.* A growth industry. *Materials world* Published Online First: 2000.http://cat.inist.fr/?aModele=afficheN&cpsidt=1519280 (accessed 25 Jan2014).

25   Alderson A, Alderson KL. Auxetic materials. *Proceedings of the Institution of Mechanical Engineers, Part G: Journal of Aerospace Engineering* 2007;221:565–75.

26   Friis EA, Lakes RS, Park JB. Negative Poisson's ratio polymeric and metallic foams. *Journal of Materials Science* 1988;23:4406–14.

27   Yang W, Li Z-M, Shi W, *et al.* Review on auxetic materials. *Journal of Materials Science* 2004;39:3269–79.

28   Standard NIJ. 0101.04 (2001). *Ballistic Resistance of Personal Body Armor NIJ* 2001.

29   Croft J, Longhurst D. HOSDB Body Armour Standards for UK Police (2007) Part 2: Ballistic Resistance. *C) Crown Copyright* 2007.

30   Adelphi USARL. *Department of Defense Test Method Standard (1997). MIL-STD-662. V50 Ballistic Test for Armor.*

31   Jr RE, Lee Y. Liquid armor: protective fabrics utilizing shear thickening fluids. *Safety and Protective Fabrics October 26-27* 2004.

32   Kalman D, Schein J. Polymer dispersion based shear thickening fluid-fabrics for protective applications. *Proceedings of SAMPE 2007 Baltimore, MD 3-7 June* 2007.

33   Rosen B, Laufer CN. Multi-threat performance of kaolin-based shear thickening fluid (STF)-treated fabrics. *Proceedings of SAMPE 2007 Baltimore, MD 3-7 June* 2007.

34   HowStuffWorks "Liquid Body Armor: Shear-thickening Fluids".
      http://science.howstuffworks.com/liquid-body-armor1.htm (accessed 25 Jan2014).

35   Duan Y, Keefe M, Wetzel ED, *et al.* Effects of friction on the ballistic performance of a high-
      strength fabric structure. ;49.

36   Stronge WJ. *Impact Mechanics*. Cambridge University Press 2004.

37   Jain. *Textbook Of Engineering Physics, Part 1*. PHI Learning Pvt. Ltd.
      http://books.google.com/books?id=DqZlU3RJTywC&pgis=1 (accessed 10 Jan2014).

38   Bennett CO, Myers JE. *Momentum, heat, and mass transfer*. McGraw-Hill 1982.

39   Hibbeler RC. *Engineering Mechanics: Statics (12th Edition)*. Prentice Hall 2008.

40   Young HD, Freedman RA. *University Physics*. Addison Wesley 2003.

41   Serway RA, Jewett JW. *Physics for Scientists and Engineers*. Cengage Learning 2013.

42   Stuhmiller J. Blast injury. *United States Army Medical Research and Materiel … *Published Online
      First:
      2008.http://citeseerx.ist.psu.edu/viewdoc/download?doi=10.1.1.188.1833&rep=rep1&type=pdf
      (accessed 6 Jan2014).

43   Foster JK, Kortge JO, Wolanin MJ. Hybrid III-A Biomechanically-Based Crash Test Dummy. 1977.
      doi:10.4271/770938

44   Enoka RM. by the nervous system. 2013;:2339–46.

45   Pintar F, Yoganandan N, Eppinger R. Response and tolerance of the human forearm to impact
      loading. Published Online First: 1998.http://trid.trb.org/view.aspx?id=514601 (accessed 25
      Apr2014).

46   Dejeammes M. *Lower abdomen and pelvis: kinematics, tolerance levels and injury criteria.* 1984.

47   Schueler F, Mattern R, Zeidler F, *et al.* Injuries of the lower legs - foot, ankle joint, tibia; mechanisms, tolerance limits, injury-criteria evaluation of a recent biomechanic experiment-series (impact-tests with a pneumatic-biomechanic-impactor). In: *Proceedings of the 1995 International IRCOBI Conference on the Biomechanics of Impact*. 1995. http://wbldb.lievers.net/10096886.html (accessed 25 Apr2014).

48   Kressta, Snider JN, Porta DJ, *et al.* Human femur responses to impact loading. In: *Human femur responses to impact loading. Proceedings of the 1993 International IRCOBI Conference, Eindhoven, Netherlands. pp 93 – 104. 1993*. 1993. http://trid.trb.org/view.aspx?id=389929 (accessed 25 Apr2014).

49   Brun-Cassan F, Leung Y c., Tarriere C, *et al.* Determination of knee-femur-pelvis tolerance from the simulation of car frontal impacts. *Proceedings of the International Research Council on the Biomechanics of Injury conference* 1982;10:101–15.

50   Snyder RG. Human Impact Tolerance - American Viewpoint. 1970. doi:10.4271/700398

51   Yang JK, Rzymkowski C, Kajzer J, Development and validation of a mathematical breakable leg model. In: *Proceedings of the 1993 International IRCOBI Conference, Eindhoven, Netherlands. pp 175 – 186. 1993.* 1993. http://trid.trb.org/view.aspx?id=389935 (accessed 25 Apr2014).

52   Corporation DC, Road SS, Liquid V. Dow Corning Corpertation 3179 DILATANT COMPOUND Material Safety Data Sheet. 2013;:1–8.

53   BS EN 1621-1:2012 Motorcyclists' protective clothing against mechanical impact. Motorcyclists' limb joint impact protectors. Requirements and test methods.

54   Choi, J. B. and Lakes RS. "Nonlinear properties of polymer cellular materials with a negative Poisson's ratio", J. Materials Science, 27, 4678-4684 (1992). Cover issue.

55   BSI. BS EN 1621-1:2012 Motorcyclists' protective clothing against mechanical impact. Motorcyclists' limb joint impact protectors. Requirements and test methods View details Status: Current.

56   Corporation ©C 2004 I. Instron Dynatup Model 8200 Drop Weight Impact Testing Instrument Original Instructions © Copyright 2004 Instron Corporation.

57   Magazine C. Auxetic materials: stretching the imagination. *soci.org*http://www.soci.org/Chemistry-and-Industry/CnI-Data/2011/2/Auxetic-materials-stretching-the-imagination (accessed 14 Jan2014).

58   Plant D. ENERGY ABSORBING SYSTEM. *EP Patent 2,361,023* Published Online First: 2011.http://www.freepatentsonline.com/EP2361023.html (accessed 14 Jan2014).

59   Soldier Survivability Propelling the Market for Body Armor and Persona | ASDReports. https://www.asdreports.com/news.asp?pr_id=707 (accessed 17 Feb2014).

60   Wu G., Xue S. Portable preimpact fall detector with inertial sensors. IEEE Trans. Neural Syst. Rehab. Eng. 2008;16:178–183.

61   Lauritzen JB, Petersen MM, Lund B. Effect of external hip protectors on hip fractures. *Lancet* 1993;341:11–3.

62   O'Halloran PD, Murray LJ, Cran GW, *et al.* The effect of type of hip protector and resident characteristics on adherence to use of hip protectors in nursing and residential homes--an exploratory study. *International journal of nursing studies* 2005;42:387–97.

63   Bentzen H, Forsén L, Becker C, *et al.* Uptake and adherence with soft- and hard-shelled hip protectors in Norwegian nursing homes: a cluster randomised trial. *Osteoporosis international : a journal established as result of cooperation between the European Foundation for Osteoporosis and the National Osteoporosis Foundation of the USA* 2008;19:101–11.

64   Robertson J. 2nd Report, 2013 (Session 4): Demographic change and an ageing population. Published Online First: 2013.http://scottish.parliament.uk/parliamentarybusiness/CurrentCommittees/59613.aspx (accessed 17 Jan2014).

65   Viceconti M, Ansaloni M. The muscle standardized femur: a step forward in the replication of numerical studies in biomechanics. *Proceedings of the … Published Online First: 2003.http://pih.sagepub.com/content/217/2/105.short (accessed 17 Jan2014).

66   Prevention I. HIP PROTECTOR BIOMECHANICAL EFFECTIVENESS : THE INFLUENCE OF HIP REGION SOFT TISSUE STIFFNESS Andrew C . Laing , Connor Gillan , Stephen N . Robinovitch RESULTS : HIP PROTECTOR TESTS. ;:15.

67   Derler S, Spierings A, Schmitt K. Anatomical hip model for the mechanical testing of hip protectors. *Medical engineering & physics* Published Online First: 2005.http://www.sciencedirect.com/science/article/pii/S1350453305000330 (accessed 17 Jan2014).

68   Laing AC, Robinovitch SN. The force attenuation provided by hip protectors depends on impact velocity, pelvic size, and soft tissue stiffness. *Journal of biomechanical engineering* 2008;130:061005.

69   Suzuki T, Yoshida H, Ishizaki T. Compliance in use of external protectors for hip fractures among the community elderly in Japan]. *Nihon Ronen Igakkai …* Published Online First: 1999.http://www.ncbi.nlm.nih.gov/pubmed/10332193 (accessed 17 Jan2014).

70   Ross P, He Y, Yates A, *et al.* Body size accounts for most differences in bone density between Asian and Caucasian women. *Calcified tissue …* Published Online First: 1996.http://link.springer.com/article/10.1007/s002239900137 (accessed 17 Jan2014).

71   Laing a C, Robinovitch SN. Effect of soft shell hip protectors on pressure distribution to the hip during sideways falls. *Osteoporosis international : a journal established as result of cooperation*

between the European Foundation for Osteoporosis and the National Osteoporosis Foundation of the USA 2008;19:1067–75.

72   Zhao S, Zhang M, Ren Y. Impact Resistance of Shear Thickening Fluid (STF)/Kevlar Composites for Body Armor Application. *Advanced Materials …* Published Online First: 2014.http://www.scientific.net/AMR.834-836.241.pdf (accessed 21 Jan2014).

73   http://media.msanet.com/www/PDFs/MSAPoliceLine/MSA_Enters_Ballistic_Market.pdf.

74   Http://defense-update.com/features/du-2-07/infantry_armor_cooling.htm. Physiological and Physical Challenges of Body Armor. http://defense-update.com.

75   Lee I, Kosko B, Anderson W. Modeling gunshot bruises in soft body armor with an adaptive fuzzy system. *Systems, Man, and Cybernetics, …* Published Online First: 2005.http://ieeexplore.ieee.org/xpls/abs_all.jsp?arnumber=1542283 (accessed 25 Jan2014).

76   Office J. Balllistic Resistance of Personal Body Armour NIJ Standard-0101.04. 2001.

77   Patent US5776839 - Dilatant powder coated fabric and containment articles formed therefrom. http://www.google.co.uk/patents?hl=en&lr=&vid=USPAT5776839&id=jE0jAAAAEBAJ&oi=fnd&dq=5776839&printsec=abstract#v=onepage&q=5776839&f=false (accessed 25 Jan2014).

78   Croft J. PSDB Body Armour Standards Ballistic Resistance. *Police Scientific Development Branch, Publication* 2003.